AD A130402

AFWAL-TR-83-4023

THE APPLICATION OF A NONLINEAR FRACTURE MECHANICS
PARAMETER TO DUCTILE FATIGUE CRACK GROWTH

University of Dayton
Research Institute
300 College Park Avenue
Dayton, Ohio 45469

December 1982

Final Report for Period September 1978 - December 1982

Approved for public release; distribution unlimited.

JUL 1 0 1983

A

Materials Laboratory
Air Force Wright Aeronautical Laboratories
Air Force Systems Command
Wright-Patterson Air Force Base, Ohio 45433
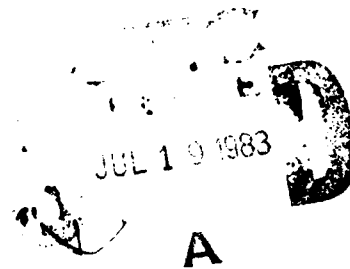
NOTICE

When Government drawings, specifications, or other data are used for any purpose other than in connection with a definitely related Government procurement operation, the United States Government thereby incurs no responsibility nor any obligation whatsoever, and the fact that the government may have formulated, furnished, or in any way supplied the said drawings, specifications, or other data, is not to be regarded by implication or otherwise as in any manner licensing the holder or any other person or corporation, or conveying any rights or permission to manufacture, use, or sell any patented invention that may in any way be related thereto.

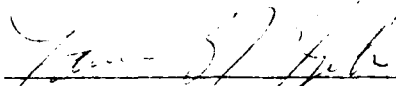This technical report has been reviewed and is approved for publication.

JOHN P. HENDERSON, Chief   THEODORE NICHOLAS
Metals Behavior Branch   Project Engineer
Metals and Ceramics Division   Metals Behavior Branch

FOR THE COMMANDER:

LAWRENCE N. HJELM, Asst Chief
Metals and Ceramics Division
Materials Laboratory

"If your address has changed, if you wish to be removed from our mailing list, or if the addressee is no longer employed by your organization please notify AFWAL/MLLNW-P AFB, OH 45433 to help us maintain a current mailing list".

Copies of this report should not be returned unless return is required by security considerations, contractual obligations, or notice on a specific document.

REPORT DOCUMENTATION PAGE		READ INSTRUCTIONS BEFORE COMPLETING FORM
1. REPORT NUMBER AFWAL-TR-83-4023	2. GOVT ACCESSION NO. A130402	3. RECIPIENT'S CATALOG NUMBER
4. TITLE (and Subtitle) The Application of a Nonlinear Fracture Mechanics Parameter to Ductile Fatigue Crack Growth		5. TYPE OF REPORT & PERIOD COVERED Final Report Sept. 1978 - December 1982
		6. PERFORMING ORG. REPORT NUMBER
7. AUTHOR(s) G. A. Hartman, III A. M. Rajendran D. S. Dawicke		8. CONTRACT OR GRANT NUMBER(s) F33615-78-C-5184
9. PERFORMING ORGANIZATION NAME AND ADDRESS University of Dayton Research Institute Dayton, Ohio 45469		10. PROGRAM ELEMENT, PROJECT, TASK AREA & WORK UNIT NUMBERS Program Element 676100, Proj. # 2418, Task # 03, Work Unit 11
11. CONTROLLING OFFICE NAME AND ADDRESS Materials Laboratory (AFWAL/MLLN) Air Force Wright Aeronautical Laboratories, AFSC Wright-Patterson AFB, OH 45433		12. REPORT DATE December 1982
		13. NUMBER OF PAGES 114
14. MONITORING AGENCY NAME & ADDRESS(if different from Controlling Office)		15. SECURITY CLASS. (of this report) Unclassified
		15a. DECLASSIFICATION/DOWNGRADING SCHEDULE

16. DISTRIBUTION STATEMENT (of this Report)

Approved for public release; distribution unlimited.

17. DISTRIBUTION STATEMENT (of the abstract entered in Block 20, if different from Report)

18. SUPPLEMENTARY NOTES

19. KEY WORDS (Continue on reverse side if necessary and identify by block number)

20. ABSTRACT (Continue on reverse side if necessary and identify by block number)

This report describes the methodology for predicting fatigue crack growth rate response of cracked structural components wherein the assumptions of linear elastic fracture mechanics are violated. Fatigue crack growth rate tests were conducted on copper specimens using compact tension (CT), center-cracked panel (CCP), and radial-hole cracked (RHC) geometries. The CT and CCP specimens provided baseline fatigue crack growth rate data that were utilized to predict both the fatigue crack growth rate and the crack growth life behavior of the RHC test specimens.

DD FORM 1473 1 JAN 73   EDITION OF 1 NOV 65 IS OBSOLETE

- The nonlinear fracture mechanics parameter chosen for extensive study on this program was the J-Integral. Crack growth rate correlations were based on J_{max}, i.e., the J-Intetral evaluated at the maximum loading condition, rather than the more traditional ΔJ associated with the range of load. Three calculations of J_{max} were made; two were based on numerical results, the other on experimental results. The numerical J_{max} values were based on (a) the line integral calculated using nonlinear finite element results and (b) the Shih estimating scheme which assumes power law hardening behavior. The experimental J_{max} values were based on the method for measuring the change in the potential energy of deformation using load displacement data recorded during a fatigue test.

Crack growth rate correlations were actually developed using a pseudo maximum stress-intensity factor parameter ($\sqrt{J_{max} \cdot E}$) based on the elastic plane stress conversion relationship between J_{max} and K_{max} (the maximum stress-intensity factor). Such correlations allow for direct comparisons with correlations based on linear elastic fracture mechanics parameters. For the data generated herein, the crack growth rate correlations based on the numerical J_{max} values were shown to be similar to that achieved by the elastic K_{max} parameter. When life predictions of the RHC test specimens were made, it appeared that the numerical J_{max} analyses were slightly improved over the typically non-conservative predictions based on the elastic K_{max} parameter. The Ratwani et al., methodology was discussed and it was shown to lead to basically conservative life predictions.

As a result of symmetrical plasticity that occurred on both sides of the hole, it was not possible to accurately calculate the driving factor associated with the radial crack condition using the experimental load-displacement results. The experimental J_{max} for the CT and CCP test geometries did, however, correlate the fatigue crack growth rate data obtained from these configurations.

FOREWORD

TABLE OF CONTENTS

LIST OF FIGURES

LIST OF FIGURES
(Continued)

LIST OF FIGURES
(Concluded)

LIST OF TABLES

SECTION 1
INTRODUCTION

1.1 BACKGROUND

In 1974, Dowling and Begley[1] presented results on correlating fatigue crack growth rate behavior with an elastic-plastic parameter based on the J-integral[2,3]. Subsequently, a substantial number of investigators have directed their attention toward further developing this J-integral parameter as well as other elastic-plastic parameters all for the purpose of aescribing crack growth behavior for those conditions where plasticity can be expected to occur. Recent reviews of past work are provided by References 4, 5, and 6.

To date, no single elastic-plastic fracture mechanics (EPFM) type parameter has achieved universal acceptance for its correlation capability. Most organizations continue to utilize the linear elastic fracture mechanics (LEFM) parameter K, the stress-intensity factor, to correlate crack growth rate behavior even though the conditions of LEFM are sometimes violated by the presence of plasticity. Possibly, one of the reasons for this choice is that the stress-intensity factor can be directly related to stress and geometry (structure and crack size), typically without regard to material properties. Another reason could be that the K correlations of crack growth rate behavior from different geometries and at different stress levels are (a) reasonably good or (b) sufficiently conservative for those conditions where plasticity occurs. One current concern, however, is for the localized plasticity that occurs in the region of a stress concentration or notch which is a site for crack growth.

1.2 OBJECTIVE OF RESEARCH

The general objective of the program was to develop methodology for predicting the fatigue crack growth rate (FCGR) response of cracked structural components wherein the assumptions

1

of LEFM might be violated. The methodology was to be developed and demonstrated for two-dimensional (planar) cracks subjected to constant amplitude loading conditions.

To accomplish the general objective in a systematic and logical fashion, we considered three specific but interrelated objectives:

a. To establish a structural parameter (P*) that controls fatigue crack growth (FCG) response.

b. To use this parameter to correlate fatigue crack growth rate (FCGR) data collected in the laboratory so that the data can be used independent of geometry and stress level.

c. To predict the behavior of cracks in typical structural components as a function of applied loading.

1.3 SCOPE OF RESEARCH

The efforts involved conducting a combined analytical-experimental program using a ductile copper alloy. The initial focus was on defining candidate structural-material parameters that could correlate FCGR behavior when the assumptions of LEFM are apparently violated. The philosophy behind the approach was based on the similarity concept; that is, when the calculated parameter "P*" is the same for two different structures, each having a crack, then the fatigue crack growth rate at the instance of the occurrence of similar P* will produce equal fatigue crack growth rates (da/dN). Hence, the FCGR should be represented by the empirical relationship:

$$\frac{da}{dN} = f \ (P^*) \tag{1}$$

where the controlling parameter, P^*, is influenced by the structural geometry, crack configuration, crack length, and stress level.

2

The derived crack driving parameter P^* was evaluated for its independence of crack geometry, global geometry, and the level of constant amplitude loading. Baseline data were generated using center-cracked panel (CCP) and compact (CT) type specimen geometries. Blind predictions of FCG behavior were made for a different structural crack geometry, the radial hole cracked (RHC) geometry.

SECTION 2
EXPERIMENTAL PROGRAM

2.1 MATERIAL

The material utilized in this investigation was ETP Bus
Bar copper with a 101 mm (4 inch) width and thicknesses of 9.5 mm
(0.375 inch) and 12.7 mm (0.50 inch). This material was chosen
for its high degree of ductility. Most of the tests utilized the
material in the as-received condition. In the as-received
condition, the material exhibits a negligible amount of strain-
hardening. One test was conducted using the material in a fully-
annealed (400°C - 1.5 hr.) condition to evaluate the effect that
increased strain-hardening had on the behavior.

The monotonic material properties of the as-received
material were modeled as an elastic-perfectly plastic material for
finite element calculations. The elastic modulus (E) was taken
as 17.0×10^3 ksi and the yield point (σ_o) as 39 ksi. For calcu-
lations involving the J-integral estimation scheme, the material
was modeled using the Ramberg-Osgood stress-strain relationship:

$$\frac{\varepsilon}{\varepsilon_o} = \frac{\sigma}{\sigma_o} + \alpha \left(\frac{\sigma}{\sigma_o}\right)^n \qquad (2)$$

where

$n = 36$

$\sigma_o = 39$ ksi

$E = 17.0 \times 10^3$ ksi

$\alpha = 0.002/\varepsilon_o$

$\varepsilon_o = \sigma_o/E$

2.2 TEST SPECIMEN GEOMETRIES AND LOADING CONDITIONS

Three different types of fatigue crack growth rate specimens
were employed in this investigation: the center-cracked panel (CCP)
specimen, the compact (CT) specimen and the radial hole cracked
(RHC) specimen. The geometries are illustrated in Figure 1.

4

W
101.6

L
559

GAGE
LENGTH
101.6

2a

a) CENTER CRACK PANEL (CCP)

W
101.6

L
559

GAGE
LENGTH
203

25.4

a

b) RADIAL HOLE CRACK (RHC)

2H
63.5

27.6

A
B

a

W 50.8

95.2

ALL DIMENSIONS IN
MILLIMETERS (1mm=.0394 in.)

c) COMPACT TENSION (CT)
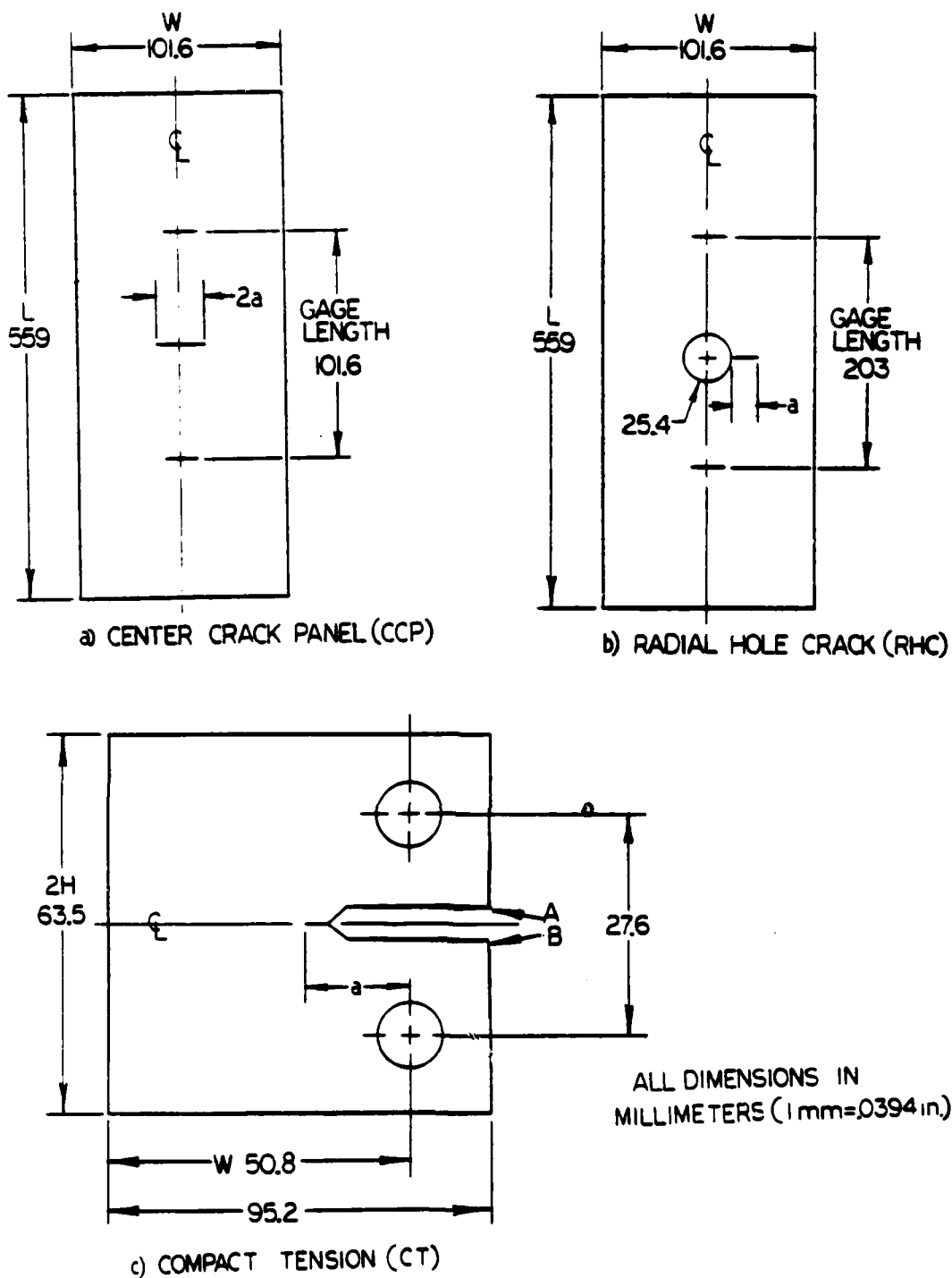
Figure 1.   Specimen Geometries Employed in this Investigation.
(See Table 1 for Thicknesses).

5

The fatigue test conditions were chosen so that the maximum stress levels induced a sufficient amount of plasticity to create localized conditions where it was expected that linear elastic fracture mechanics parameters would fail (see Figure 2). All three geometries were subjected to a stress ratio (R) of 0.1. In addition, some CCP and CT specimens were subjected to 0.5 stress ratio conditions.* One CCP specimen was subjected to a zero stress ratio condition. The test conditions, initial and final crack lengths, and specimen lives are summarized in Table 1.

2.3 EXPERIMENTAL PROCEDURES

The tests were conducted following the procedures outlined below. Generally, the specimens were first precracked according to ASTM Standard E647[7] until a predetermined crack length was achieved. The test was then conducted such that crack length, cycle count, and load-displacement hysteresis loops were periodically recorded whenever the crack grew a predetermined increment (Δa).

All tests were conducted using a sinusoidal waveform under the load control mode in a servo-controlled electrohydraulic test system. Figure 3 illustrates a RHC test in progress. As shown by Figure 3, CCP and RHC specimens were loaded using hydraulic grips. Loads were measured with a 220 KN (50 kip) load cell calibrated to an NBS standard. The load cell was placed in series with the specimen. Cycle counts were determined from a mechanical cycle counter.

Crack lengths were measured optically with a traveling microscope. Surface crack lengths could be reliably determined within ±0.025 mm (±0.001 inch). The crack increments were chosen to give 20 to 40 data points per test. Typical Δa ranged from 0.254 mm (0.010 inch) to 0.635 mm (0.025 inch).

---

*These tests are not described herein because they were preliminary tests performed to evaluate extensometry and crack measurement techniques.

```
|——————————|
   1 inch
  (25.4mm)
```

Figure 2.   A Photograph of a CCP Specimen in Test Showing
Substantial Plastic Deformation Near the Crack
Tip as the Crack Grows.

TABLE 1

TEST CONDITIONS SUMMARY

Specimen ID	Thickness (mm)	Max. Load (KN)	Min. Load (KN)	Stress Ratio	Frequency (hz)*	a_o (mm)	a_f (mm)	N (cyc)
CCP1	12.7	200.0	0.0	0.0	0.5/.01	6.35	19.79	15980
CCP2	12.7	189.5	18.95	0.1	0.5/.01	12.62	19.94	5531
CCP3	12.7	222.4	22.24	0.1	0.5/.01	6.63	17.48	11088
CCP4	9.5	89.0	0.0	0.0	0.5/.01	6.99	20.65	27811
CCP5	9.5	166.8	16.68	0.1	0.5/.01	7.16	19.02	24920
CCP6	12.7	222.4	22.24	0.1	0.5/.01	5.74	15.57	9510
CCP7	9.5	124.5	12.45	0.1	10/.01	3.25	25.55	104500
CT1	12.7	7.50	0.750	0.1	9/.1	13.67	32.26	140047
RHC1	9.5	146.8	14.68	0.1	0.5/.01	0.89	13.77	7441
RHC2	9.5	146.8	14.68	0.1	0.5/.01	0.86	13.79	6241
RHC3	9.5	161.5	16.15	0.1	0.5/.01	1.14	9.32	2661
RHC4	9.5	161.5	16.15	0.1	0.5/.01	1.57	9.42	
RHC5	9.5	146.8	14.68	0.1	0.5/.01	0.20	15.39	12600

*First Frequency/Second Frequency
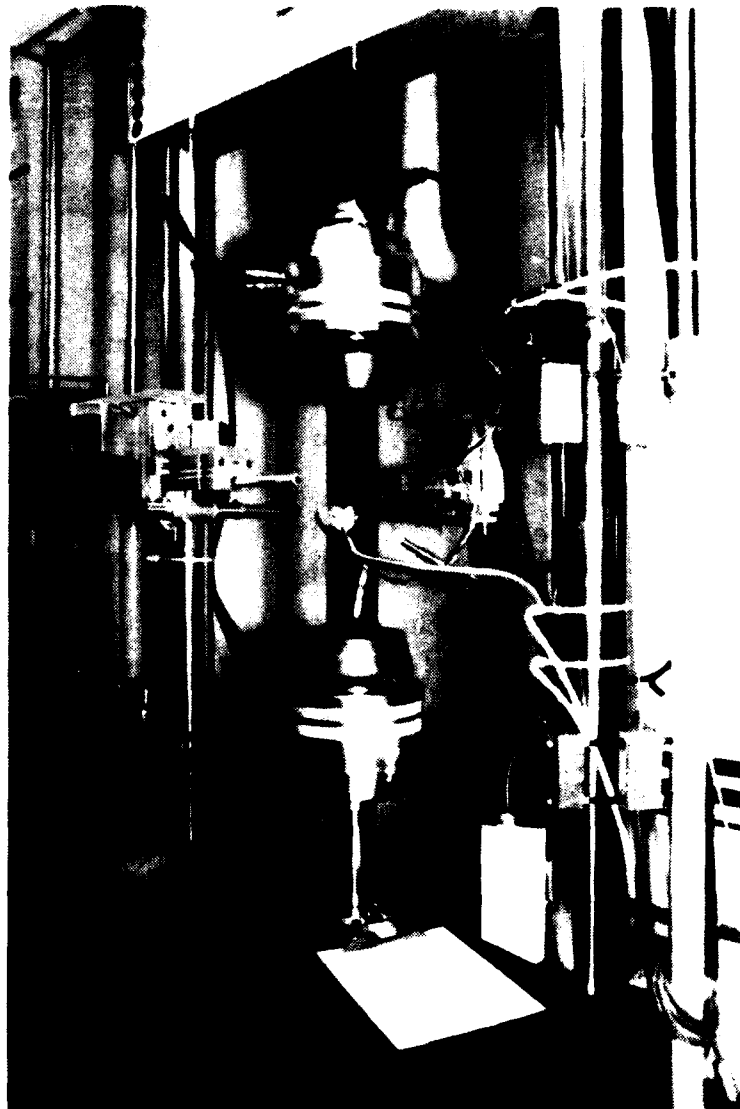
Figure 3.   RHC Test in Progress with Early Style
Clip On Gage.

The displacements for the CT specimen were measured along the axis of loading with an ASTM Standard E399[8] style clip-on gage. These displacements were measured at points A and B shown in Figure 1c.

Displacements on the CCP and RHC specimens were measured in several different ways. Initially, LVDT transducers were used. These produced substantial nonlinearity and were deemed unacceptable. The second method was using an ASTM 300 style clip-on gage and extension arms bolted to the specimen (see Figure 3). This method provided accurate measurements; however, when the gage length was extended to 203 mm (8 inch) the total displacements were beyond the range of this gage. The method finally used the custom built extensometer with a 203 mm (8 inch) gage length illustrated in Figure 4. This extensometer provided accurate measurements, but the measurements were made on one side of the specimen only. This introduced the possibility of inaccuracies due to specimen bending. Additional tests comparing load-displacement data collected from both sides of sample CCP-3 showed this error to be small.

Figure 5 illustrates typical load-displacement data recorded during a test of a CCP specimen (CCP-3). These data were used in conjunction with the potential energy definition of the J-integral to establish values of the operational J-integral discussed in Section 3.
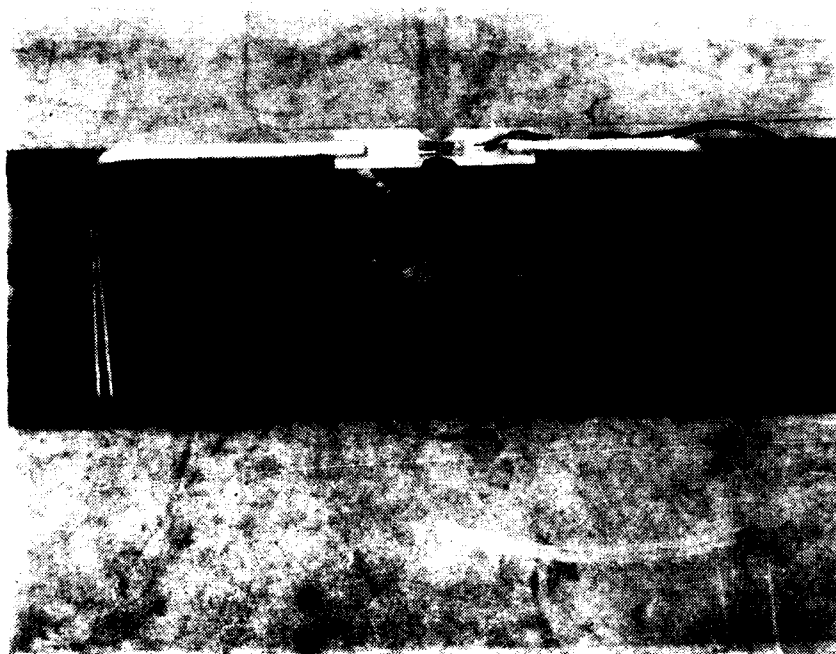
Figure 4. RHC Specimen with 203mm (8 inch) Gage Length Extensometer Attached.

DEFLECTION (MM)
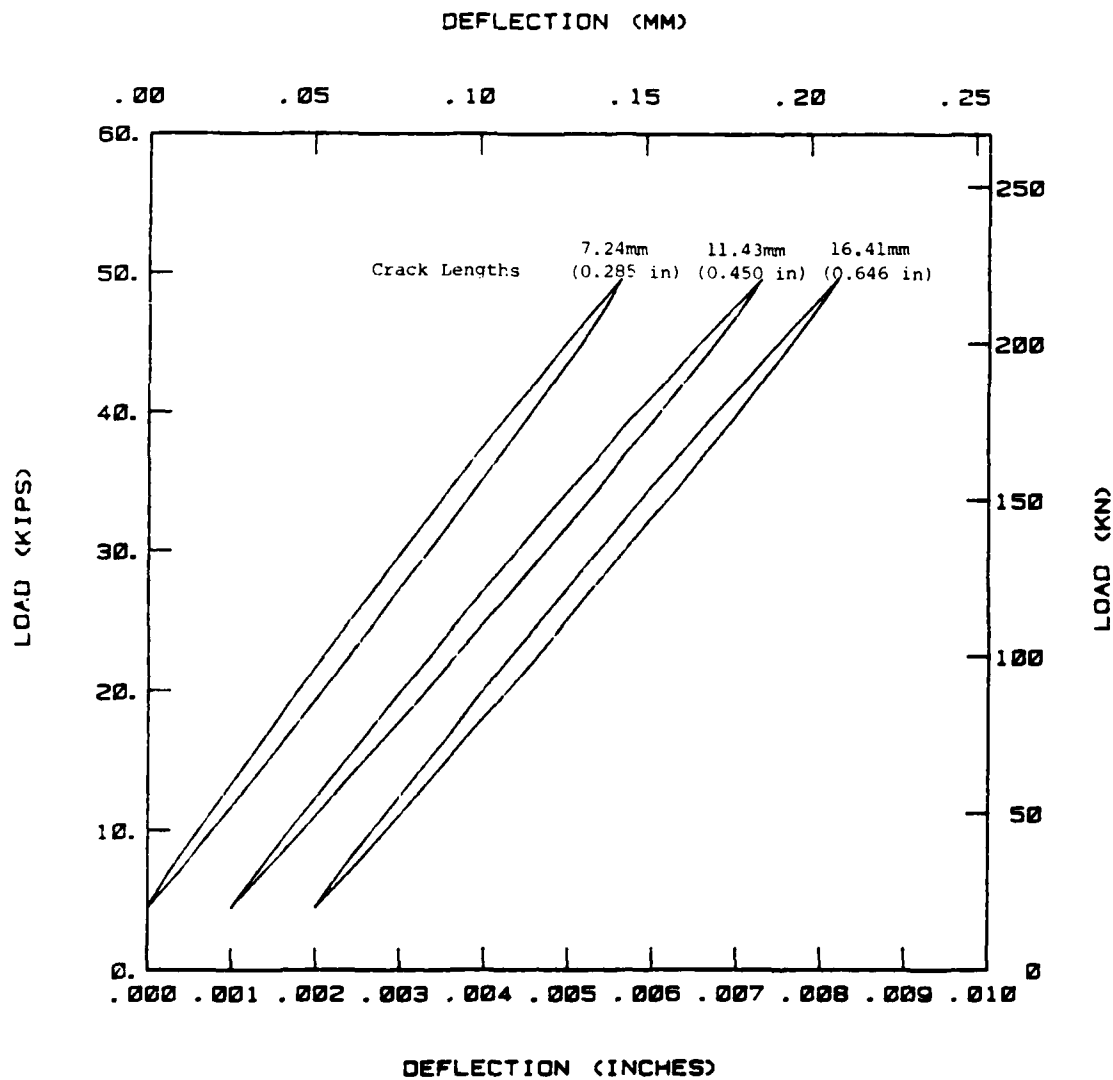
Figure 5. Load-Displacement Diagram for a CCP Specimen Subject
to a Load that Ranged Between 4.5 Kips (20kN) and
50.0 Kips (222.4 kN).

12

SECTION 3
PARAMETER DESCRIPTIONS

Two correlation parameters were chosen for characterizing the fatigue crack growth rate (FCGR) behavior of ETP copper. One parameter is the linear elastic fracture mechanics (LEFM) parameter - the stress-intensity factor (K) and the other is a fracture mechanics parameter that has been extended into the nonlinear range - the J-integral (J). The subsections below outline the methods employed to obtain the values of these two parameters for the three specimen geometries of interest.

3.1 THE STRESS-INTENSITY FACTOR

For the standard test specimens, i.e., the center-crack panel (CCP) specimen and the compact (CT) specimen, the stress-intensity factor solutions are available from ASTM Standard E647[7]. The stress-intensity factor used to describe the magnitude of stress in the crack tip region of the CCP specimen is:

$$K = \sigma \sqrt{\pi a \, \sec \frac{\pi a}{W}} \tag{3}$$

(σ = stress, a = half crack length, and W = panel width) while that of the compact specimen is:

$$K = \frac{P(2 + \frac{a}{W})}{B\sqrt{W}(1 - \frac{a}{W})^{3/2}} [0.886 + 4.64 \, (\tfrac{a}{W}) - 13.32 \, (\tfrac{a}{W})^2 + 14.72 \, (\tfrac{a}{W})^3 - 5.6 \, (\tfrac{a}{W})^4] \tag{4}$$

(P = load, a = crack length, B = thickness, and W = width).

The evaluation of the stress-intensity factor for non-standard test geometries requires the solution of an elasticity problem in which the geometry and boundary conditions are appropriately modeled. This type of evaluation normally requires the use of numerical analysis procedures based on either the

finite element method or the boundary integral equation method. For the case of the radial hole cracked (RHC) specimen geometry utilized for this investigation, the stress-intensity factor was obtained by modeling the specimen with the finite element method. Specifically, the MAGNA[9] finite element code was selected to perform the stress-strain calculations. Several additional routines[10] were developed to calculate the stress-intensity factor based on the elastic properties of Rice's path-independent line integral, i.e., the J-integral[2]. [See subsection 3.2 for a description of the integral and how it is calculated.]

The finite element results for the RHC geometry were obtained for a number of crack lengths and the stress-intensity factor values were computed from the elastic plane stress relationship[2]

$$K = \sqrt{JE} \tag{5}$$

where E is the elastic modulus. These stress-intensity factor results are described in Figure 6 along with a least squares determined curve that describes the finite element results. The equation that describes this curve is:

$$K = \sigma \left[0.1164 + 30.99a - 164.8a^2 + 458.7a^3 - 619.4a^4 + 329.9a^5 \right]^{1/2} \tag{6}$$

where σ is the applied stress and a is the length of the radial crack. Equation 6 is valid in the range $0.01 \leq a \leq 0.65$ inch. For comparison purposes, the Bowie infinite plate radial hole crack results[11] as described by Grandt[12], i.e.,

$$K = \sigma \left(0.6762 + \frac{0.8733}{0.3245 + \frac{a}{R}} \right) \sqrt{\pi a} \tag{7}$$

are also presented in Figure 6.

14

CRACK LENGTH (MM)

CRACK LENGTH (INCHES)
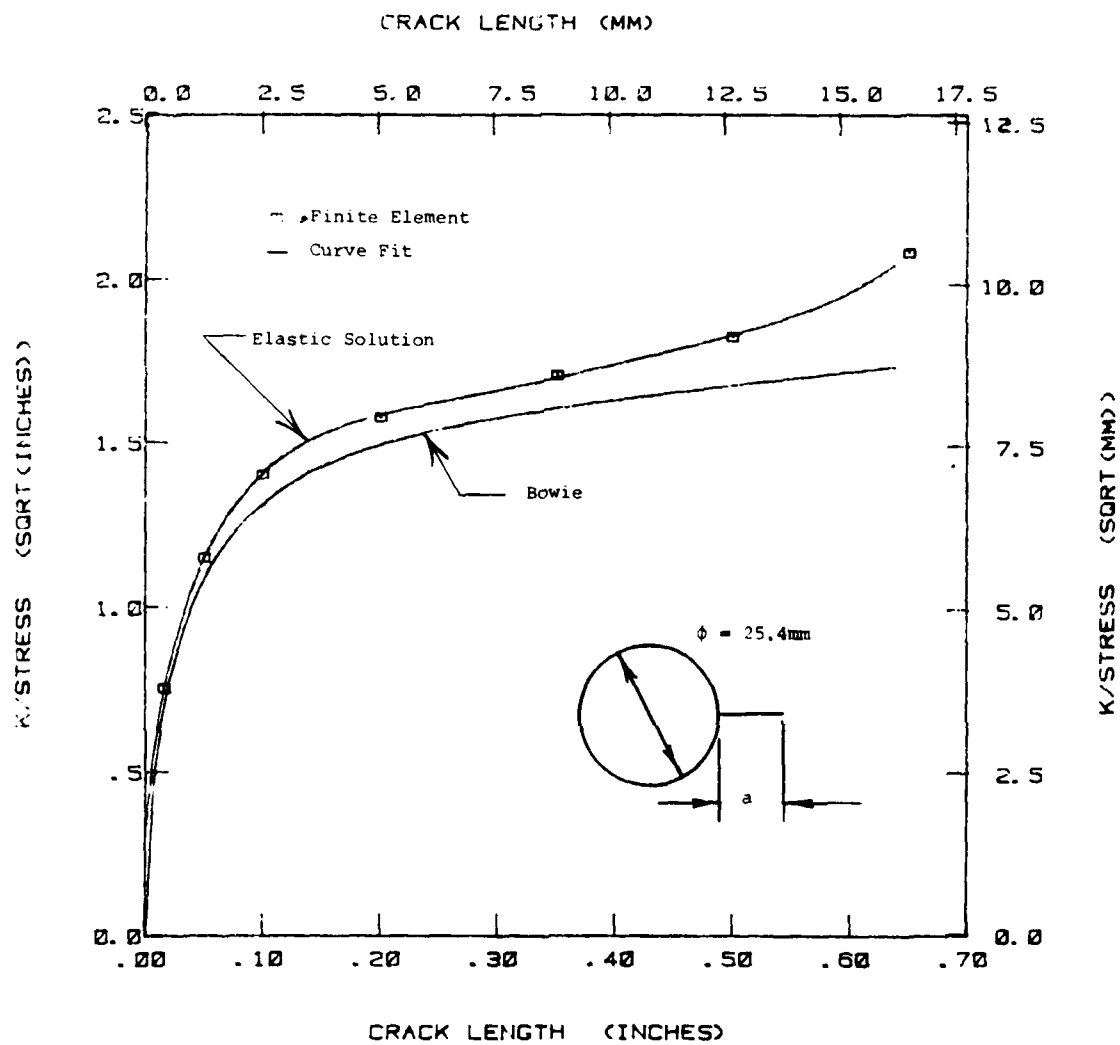
Figure 6.   Comparison Between Finite Element, Finite Width Results
             and Bowie Radial Hole Crack Results. (Elastic Conditions
             Exist for Loads Below 15 kips (66.7 KN).)

15

3.2 THE J-INTEGRAL

Past work has shown that there are several procedures available to obtain values of the J-integral as a function of load and crack length (see References 4, 5, and 6). The procedures chosen for evaluation were based on: (a) the finite element method used in conjunction with a direct evaluation of the line integral, (b) the Shih et al.[13-15] estimation schemes, and (c) the use of experimental load-displacement data in conjunction with the operational definition of the parameter. In this subsection, the various procedures utilized to evaluate the J-integral parameter for the three test geometries are discussed.

3.2.1 Line Integral Evaluation

A series of values for the J-integral were computed as a function of crack length from the direct evaluation of the line integral given by Rice[2], i.e., from

$$J = \int_{\Gamma} (w dy - T_i \frac{\partial u_i}{\partial x} ds) \qquad (8)$$

where

$$w = \int \sigma_{ij} d\varepsilon_{ij} \qquad (9)$$

is the strain energy density and Γ is any contour surrounding the crack tip, transversing in a counter clockwise direction, as described by the path in Figure 7. The figure further defines the parameters in Equation 8, i.e.,

ds = Increment of distance along the contour,

T_i = Traction vector on the contour,

u_i = Displacement vector on the contour, and

x,y = Rectangular coordinates.

To compute the value of the J-integral for a given load and crack length condition, Equation 8 has to be integrated along any path that circuits the crack tip. The integrand parameters are then based on the stresses, strains, and displacements

$$W = \int \sigma_{ij} d\varepsilon_{ij}$$

$\hat{n}$, outward unit normal vector

$\vec{T}$, traction (stress) vector

$\vec{u}$, displacement vector

ds

y

x

Crack Tip

Crack

Γ, path
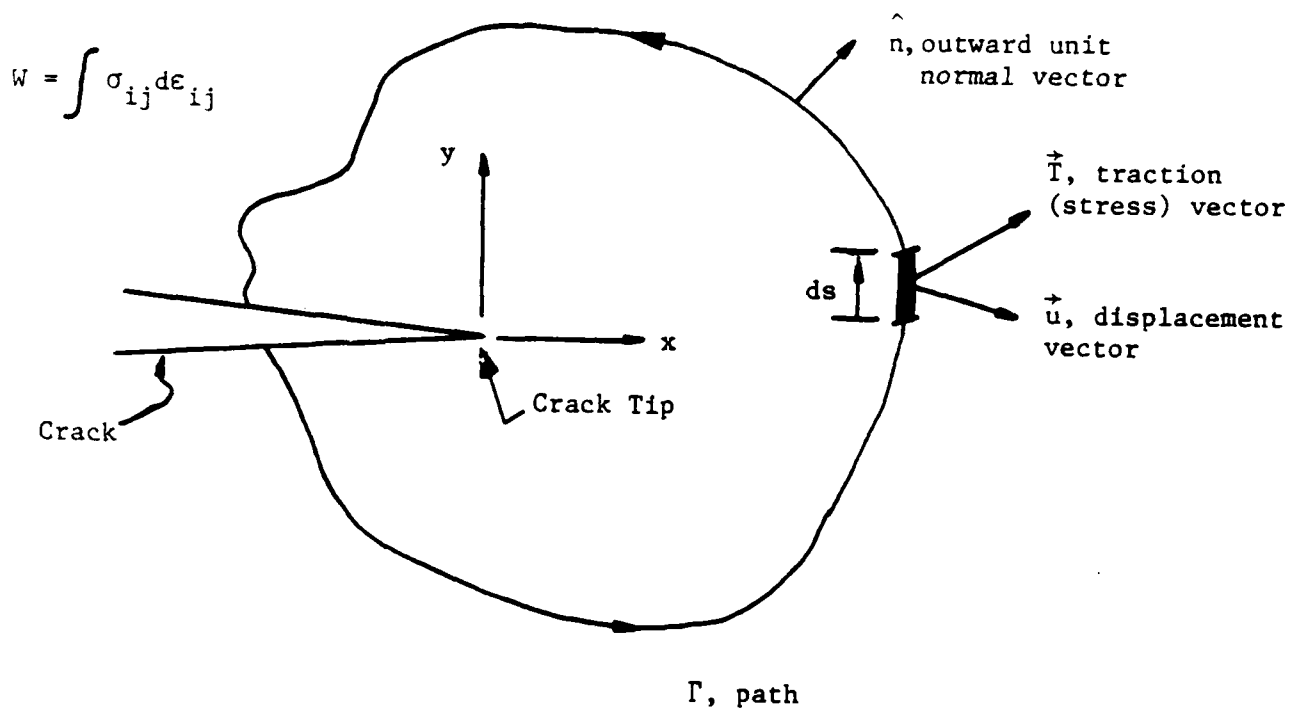
Figure 7.   J-Integral Path and Associated Parameters.

evaluated for the specific path chosen. For the purpose of obtaining these mechanical parameters, the MAGNA[9] finite element code was employed.

There are several ways that the line-integral path can traverse the finite elements. In the formulation added to MAGNA[10], the J-integral paths were made to pass through the middle of each element, where smooth stress and strain data can be obtained more easily than along the element boundaries (See Figure 8 for an example illustrating three separate paths chosen for a study to evaluate path independence for the CCP geometry). The accuracy and validity of the J-integral routines in MAGNA were recently evaluated by Rajendran[16] who compared the numerical results from MAGNA with those generated previously by Kumar et al.[15], by Yamada and Yoshimura[17] and by Ashbaugh and Ahmad[18].

The finite element mesh formulations utilized for the CCP and RHC geometries are illustrated by Figures 8 and 9, respectively. These meshes were generated by an automatic mesh generator program which provides relevant mesh patterns for notch cracks as small as 0.13 mm (0.005 inch). The crack tip element sizes were always less than a/6, where a is the half crack size for the CCP geometry and the radial crack length for the RHC geometry. As a check on the suitability of the mesh shown in Figure 8, a second mesh with a larger number of degrees of freedom was generated and used in the analysis of RHC-1. The results from the second mesh differed by less than 2% from the results obtained using the mesh in Figure 8. For cost effectiveness, the mesh in Figure 8 was used in subsequent RHC analyses.

In the present study, the J-integral was calculated for the CCP and RHC geometries using the elastic-perfectly-plastic stress-strain model described in subsection 2.1. The results obtained for the RHC geometry compared reasonably well with the experimentally obtained load-displacement results. Figures 10 and 11 summarize some of the results for displacements measured on opposite sides of the hole along the axis of loading. The curves in these figures are from sample RHC-2.

18
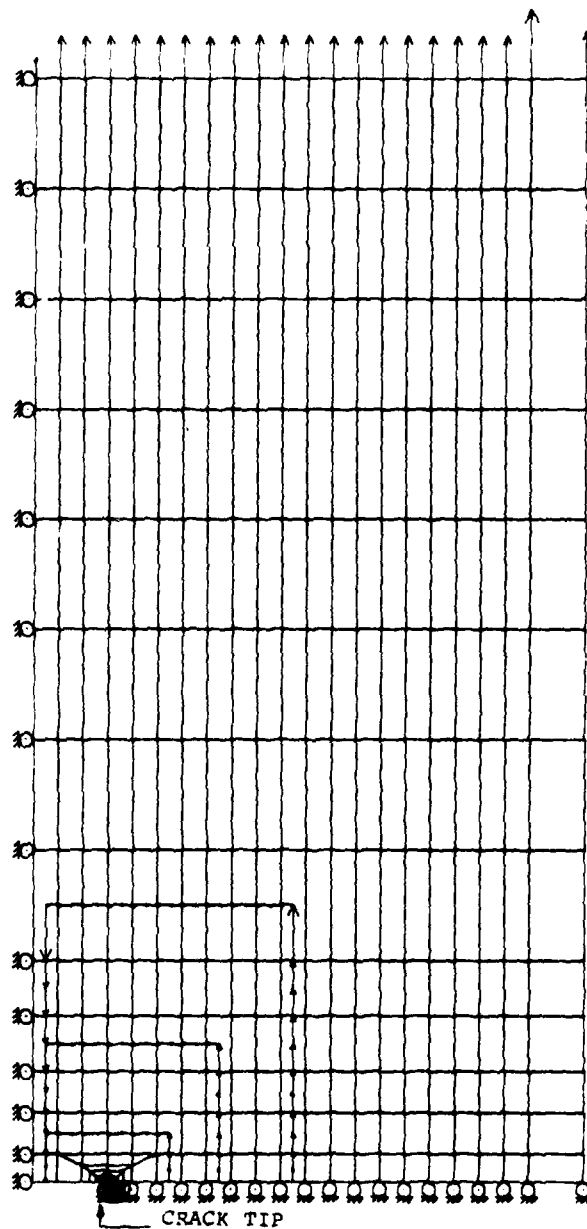
Figure 8. Three J-Integral Paths Shown Relative to the Finite Element Mesh Describing the Upper Right Quarter of the CCP Geometry and Loading.

CRACK TIP
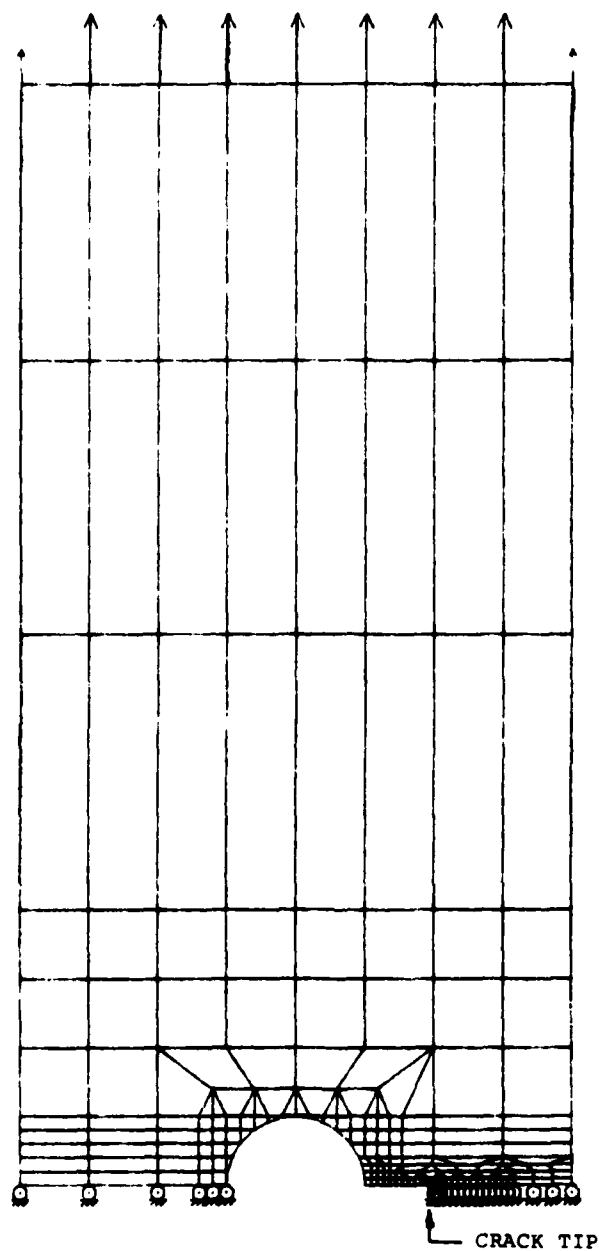
Figure 9.   Upper Half Panel RHC Specimen Finite Element Mesh Used
in Calculation of the J-Integral with the MAGNA Code.

20

CRACK LENGTH   (MM)

0.0   2.5   5.0   7.5   10.0   12.5   15.0   17.5
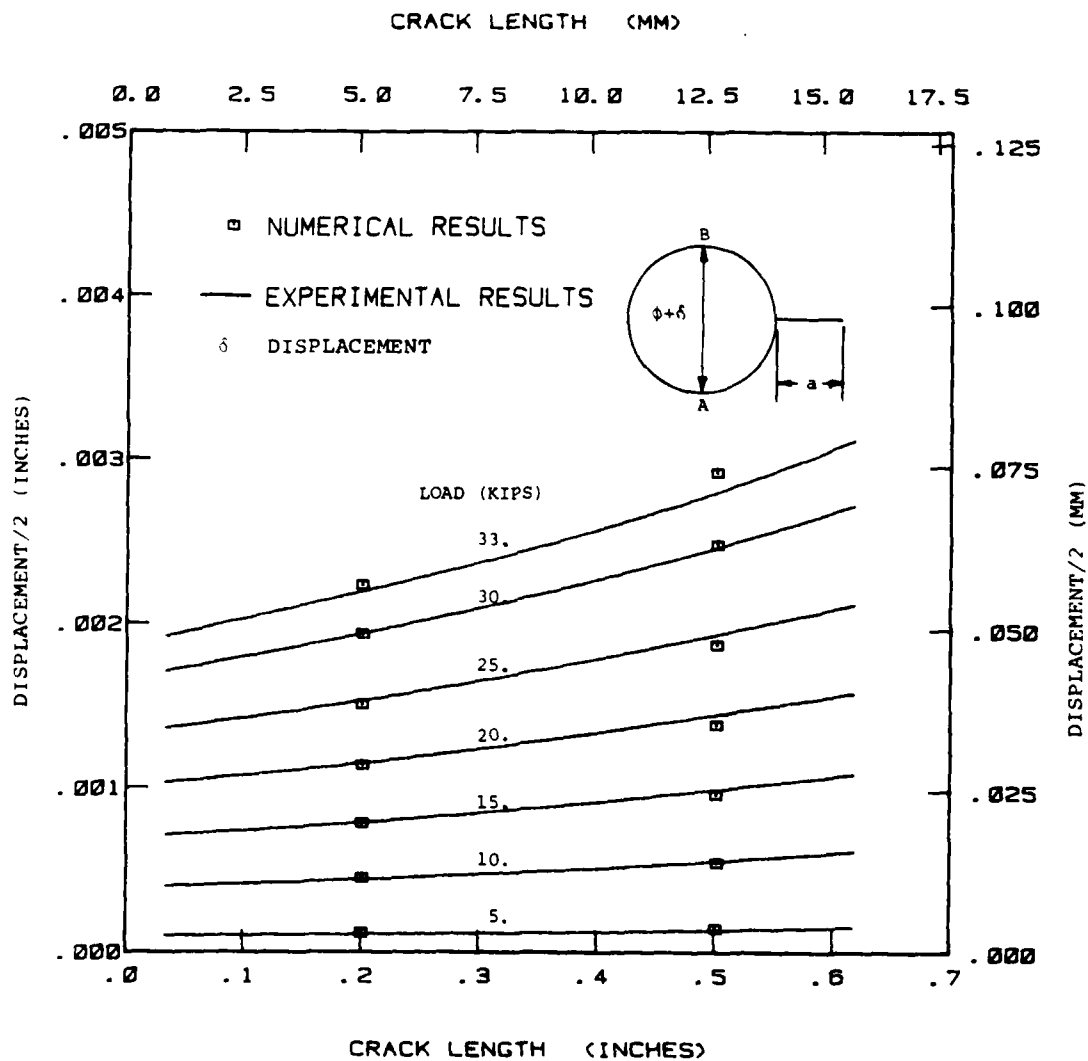
Figure 10.   Comparison of Deflection Across the Hole
             Vs. Crack Length Between the Test and
             Numerical Results for Radial-Hole-Crack
             Specimens for Various Load Levels.

21
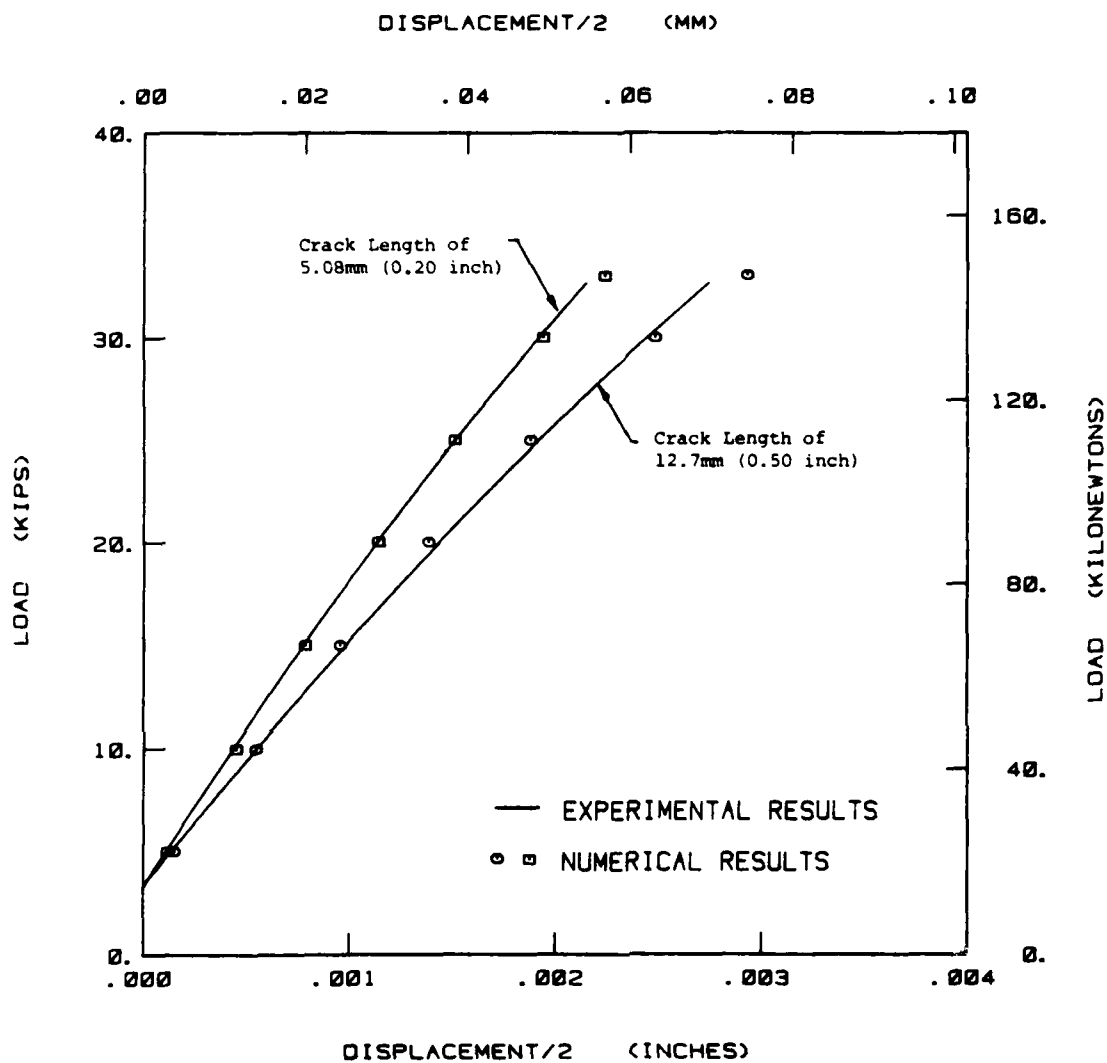
Figure 11. Comparison of Load Vs. Displacement Curves Obtained
Through Experiments and Numerical Simulations for Two
Different Cracks of Radial-Hole-Crack Configuration;
Experimental Results from RHC-2.

The J-integral values obtained for three paths are plotted for several crack lengths in Figure 12 for a CCP specimen. It can be seen from Figure 12 that the path independent property of J-integral is well demonstrated for the crack length region of interest.

To evaluate the ability of the J-integral for correlating the fatigue crack growth rate data obtained from the CCP and RHC specimens, it was necessary to determine the values of this parameter at the specific test load levels. Figures 13 and 14 present the J-integral results for the CCP and RHC specimens, respectively, in the same format that was previously used to express the stress-intensity factor results, i.e., in terms of the ratio of stress-intensity factor (K) to stress (σ). The J-integral results obtained from the elastic-plastic finite-element analysis were converted to psuedo stress-intensity factors using Equation 5. For comparison purposes, the elastic stress-intensity factor results are also portrayed in Figures 13 and 14. We note from Figures 13 and 14 that as the load increases (and thus introduces more material nonlinearity) the psuedo stress-intensity factor is no longer linearly related to load. This is better illustrated in Figures 15 and 16 where the $\sqrt{JE}$ results have been normalized to the elastic stress-intensity factor. Figures 15 and 16 are provided to directly show the effect that increasing the amount of plasticity has relative to the elastic result.

3.2.2 Estimated J

The J-integral can also be calculated using an estimation scheme suggested by Hutchinson, Shih, and their coworkers[13-15, 19-20]. The estimating scheme calculates the intensity of the HRR (after Hutchinson[21] and Rice and Rosengren[22]) stress-strain field at the crack tip for an elastic-plastic material. A recent study of the estimating scheme and its implementation in terms of a computer program (EST) was reported by Weerasooriya and Gallagher[23]. The equations involved in the J-estimation scheme by program EST are briefly described below.

HALF CRACK LENGTH   (MM)
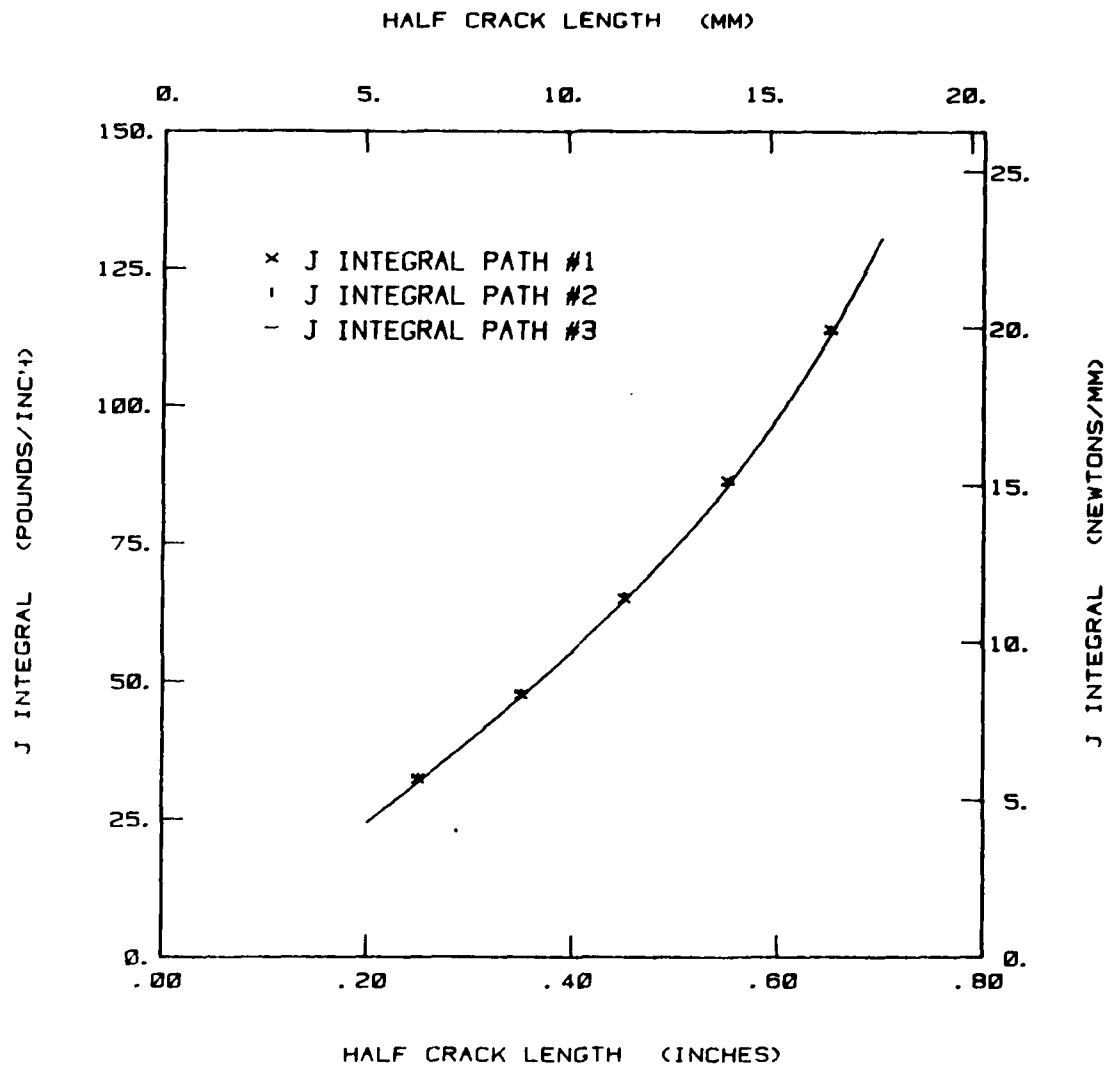
Figure 12.   Elastic-Plastic J-Integral Results for the CCP
             Specimen Based on Finite Element Results for
             Three Different Paths of the Type Illustrated in
             Figure 8.   The results presented are for a load
             of 50.0 Kips (222.4KN).
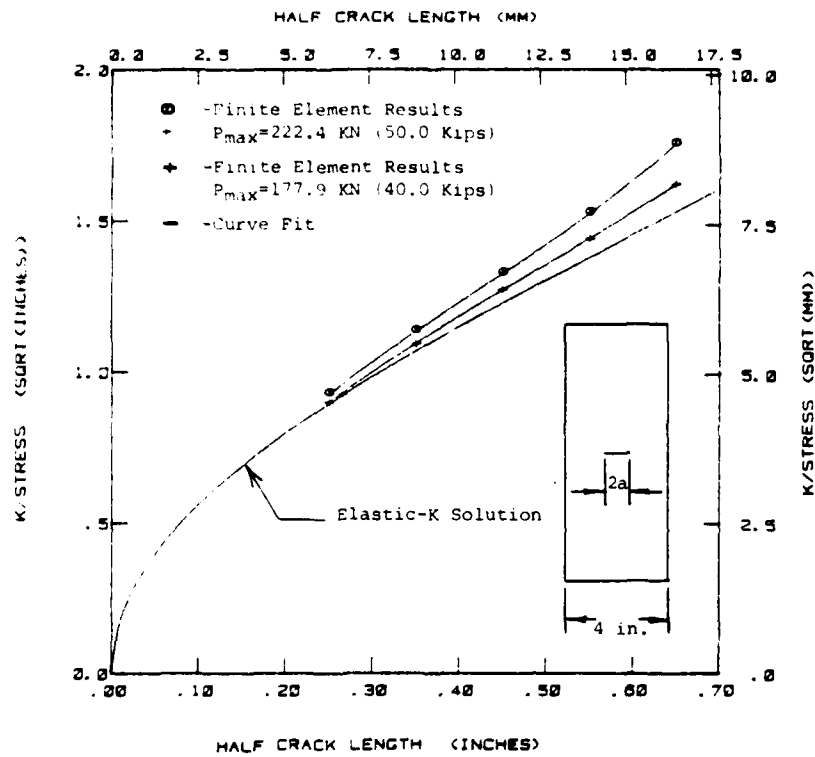
Figure 13. Comparison Between the Elastic and Elastic-Plastic Stress Intensity Factor Coefficient Results for the Center Crack Panel Tests.
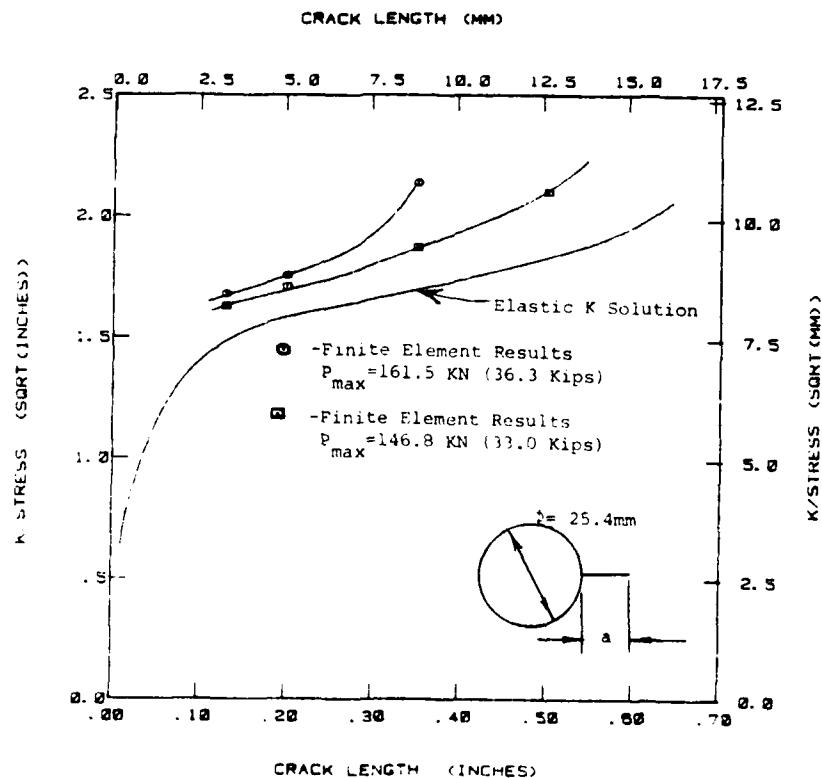
Figure 14. Comparison Between the Elastic and Elastic-Plastic Stress Intensity Factor Coefficient Results for the Radially-Cracked Hole Crack Tests.
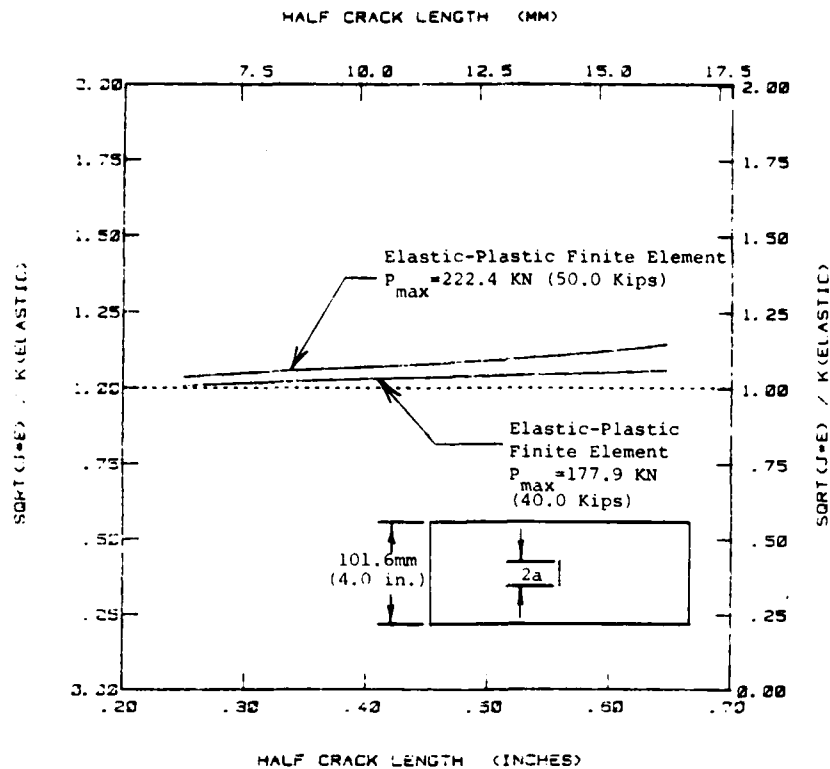
Figure 15. Impact of Including the Plastic Component in a Stress-Intensity Factor Analysis for the Center Cracked Panel Test Conditions.
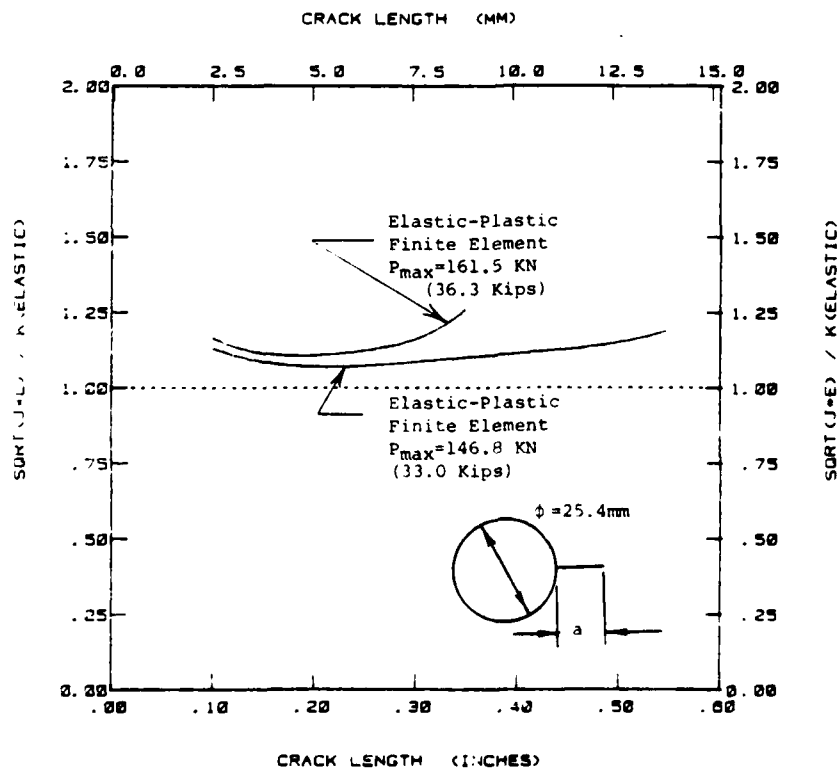
Figure 16. Impact of Including the Plastic Component in a Stress-Intensity Factor Analysis for the Radially Cracked Hole Test Conditions.

26

For elastic-plastic materials, the parameter J can be approximated by summing contributions due to the linear elastic and plastic parts[13,14]

$$J = J^e + J^p . \tag{10}$$

Superscripts e and p denote the elastic and plastic components, respectively. The elastic J parameter appearing in the above equation can be expressed in the form:

$$\frac{J^e}{\sigma_o \varepsilon_o a} = (\frac{\sigma}{\sigma_o})^2 \hat{J}^e (a/b) \tag{11}$$

where σ is the remotely applied stress, and σ_o and ε_o are reference stresses and strains related by the expression $\sigma_o = E\varepsilon_o$. Function $\hat{J}^e$ depends only on the ratio of crack length to width (a/b). This function can be found in the literature for various finite width crack geometries.

The plastic contribution J^p can be expressed as:

$$J^p = \alpha \, \sigma_o \, \varepsilon_o \, a \, f_1 \, (\frac{a}{b}) \, h_1 \, (\frac{a}{b}, n) \, (\frac{P}{P_o})^{n+1} \tag{12}$$

where P and P_o are the applied and limit loads per unit thickness, respectively. f_1 is a function only of geometry and crack length while h_1 depends on geometry, crack length, and the strain hardening exponent (n) which appears in the Ramberg-Osgood stress-strain model (see Equation 2). Shih and coworkers[13,15] have tabulated the functions f_1 and h_1 for a number of geometries.

The report by Weerasooriya and Gallagher[23] discusses the limitations and conditions under which the estimation procedure used for our calculations is valid.* In the current work, J-integral values were obtained for both the CCP and CT specimens using the estimation program EST[23] for different crack lengths.

---

*The Program EST was modified to include tabular f_1 and h_1 values for strain hardening exponents (n) up to 36.

An indepth comparison between the CCP specimen
finite-element results reported in subsection 3.2.1 and the
estimation scheme results were conducted to verify the validity
of the estimation scheme and the material model on which it was
based. The analytical estimates of the psuedo stress-intensity
factor results created through the conversion of elastic-plastic
J to K using Equation 5 are compared to the elastic-plastic
finite element results at a maximum load of 222 KN (50 kips) for
the CCP specimen in Figure 17. The maximum load condition of
222 KN is the largest load that the test machine could apply and
it is seen that the estimation scheme provides a close approxi-
mation to the elastic-plastic finite element results shown in
Figure 17. At lower load levels, the correlation was even better.

Additional comparisons were also made between the
load-displacement results obtained using the EST computer code
and those obtained both by finite element calculations and by
experimental measurements. These comparisons showed that we
could rely on the estimation scheme to calculate the J-integral
as a function of load level and crack length for the two
geometries used to collect the baseline crack growth rate data.
The psuedo stress-intensity factor for the CT specimen is
presented in Figure 18 for the load level used in the test of
this specimen. The estimation scheme is numerically more
efficient and thus more economical for calculating J-integral
values than the finite element method. However, it must be
noted that the functions embedded within the estimation scheme
typically are based on finite element results; so, unless these
functions are already available, the finite element method would
be the most efficient method for developing the J-integral values.

3.2.3   Experimental J Definition

In Rice's original formulation of the J-integral,
it was shown that the line integral definition (Equation 8) was
equivalent to the negative rate of change of potential energy
with respect to crack area[2,3]

HALF CRACK LENGTH (MM)
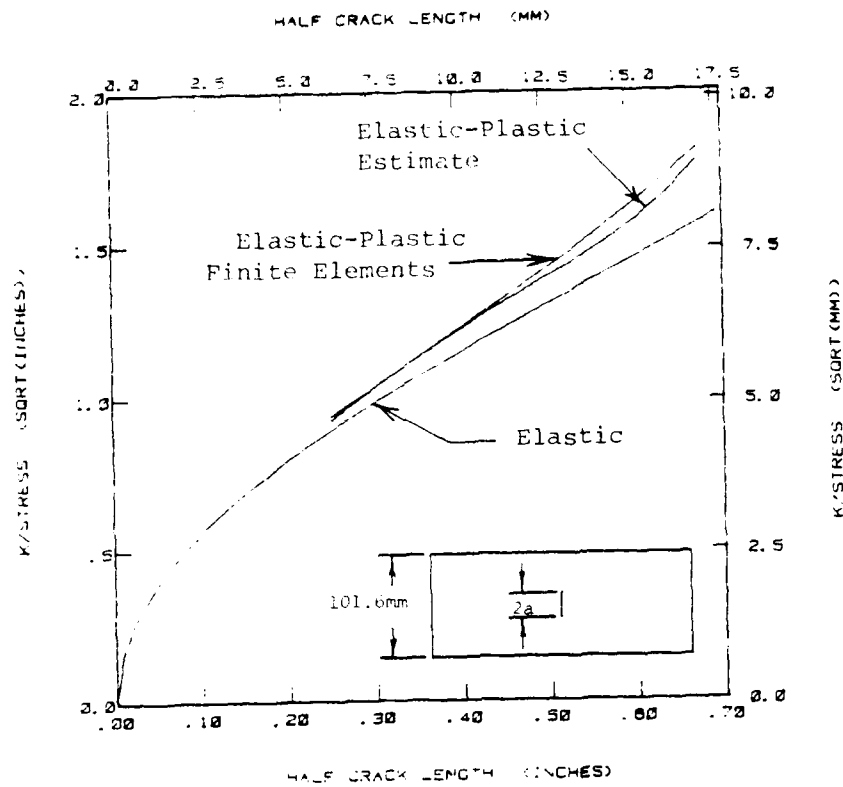
Figure 17. Comparison of Elastic-Plastic Finite Element, Elastic-Plastic Estimated and Elastic Results for a Center Crack Panel (CCP) Subjected to a Maximum Load of 50 Kips (222.4 kN).

CRACK LENGTH (MM)
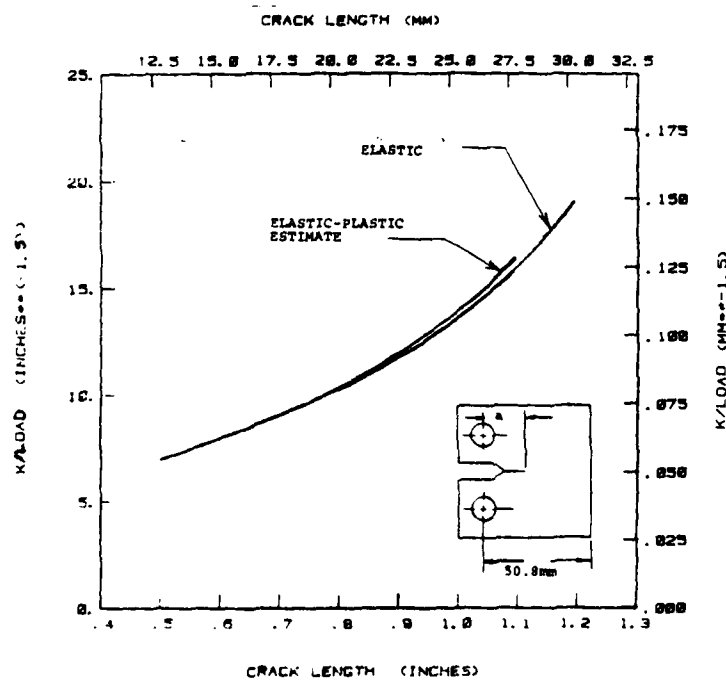
Figure 18. Comparison of Elastic-Plastic Estimated Results with the Elastic Solution for a Compact (CT Specimen Subjected to a Maximum Load of 1.69 Kips (7.5 kN).

29

$$J = -\frac{1}{\alpha} \left. \frac{\partial U}{\partial A} \right|_\Delta = \text{constant} \tag{13}$$

for a condition of fixed load point displacement. The parameter α is equal to 1 for the CT and RHC crack geometries (one crack tip) and is equal to 2 for the CCP geometry (two crack tips); the parameter A is the crack area typically taken as the product of crack length (a) and thickness (B). Experimentally, estimates of the J-integral are obtained by evaluating the area between two load-displacement curves obtained for different crack lengths, such as illustrated in Figure 19.

There are a number of potential problems that arise when the procedure suggested by Equation 13 and Figure 19 is applied to a propagating fatigue crack. One class of problems is associated with utilizing the load-displacement curves to obtain estimates of the potential energy available for cyclic crack growth while the other class is associated with experimental technique and measurement capability.

3.2.3.1 Definition of Crack Driving Factor

In attempting to define the major source of the driving factor, we considered the approaches suggested by Dowling and Begley[ ] and Sadananda and Shahinian[24] who described two methods for correlating load-displacement data for non-zero minimum load conditions (See Figure 20). Each method is based on the use of the load range (maximum load minus minimum load) and allows investigators to obtain an experimental "ΔJ" parameter. In those cases where the crack closed prior to reaching the minimum loading, an effective load range (maximum load minus closing, or opening, load) can be utilized. Initially, we attempted to utilize the Sadananda-Shahinian method described in Figure 20c. An evaluation of this ΔJ parameter was conducted using load-displacement data obtained from finite element calculations for the center crack panel geometry. When the ΔJ results were compared to the line integral results presented in subsection 3.2.1, the ΔJ results were shown to consistently predict levels of the driving force that were lower than the line integral.
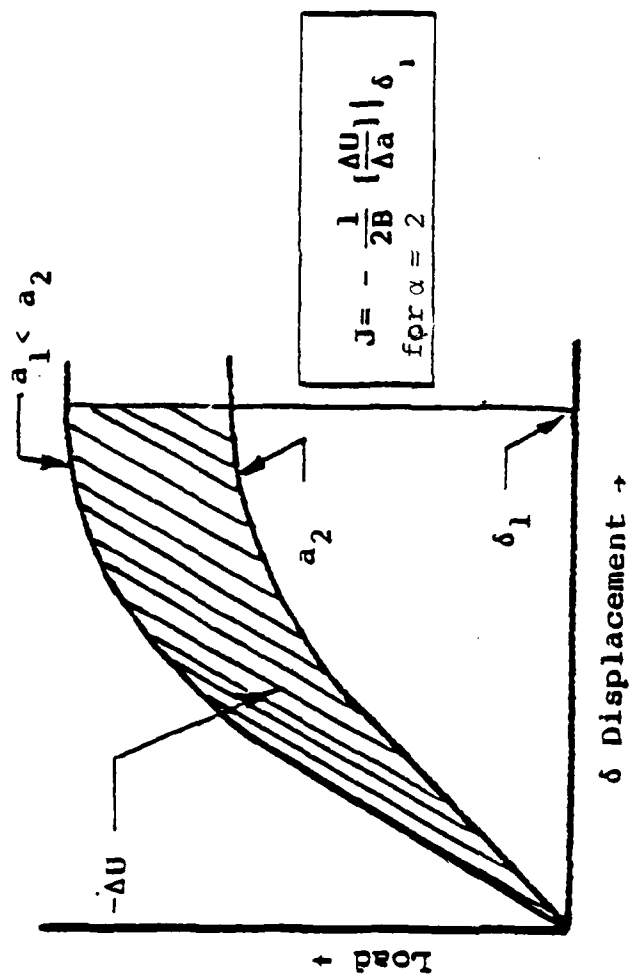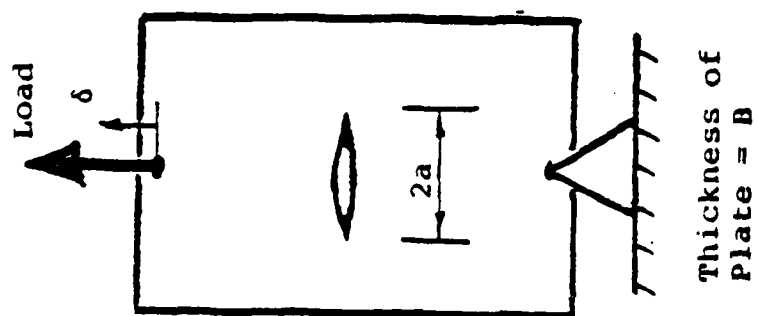
Figure 19. Procedure for Calculating Operational Values of the J-Integral.

$$J = -\frac{1}{2B}\left[\frac{\Delta U}{\Delta a}\right]|_{\delta_1}$$

for $\alpha = 2$

$a_1 < a_2$

Thickness of Plate = B

31
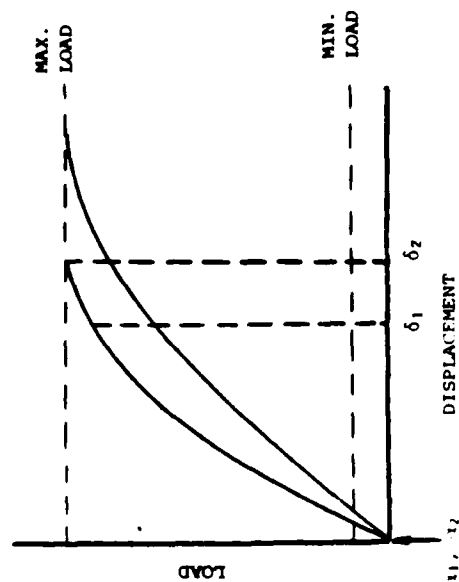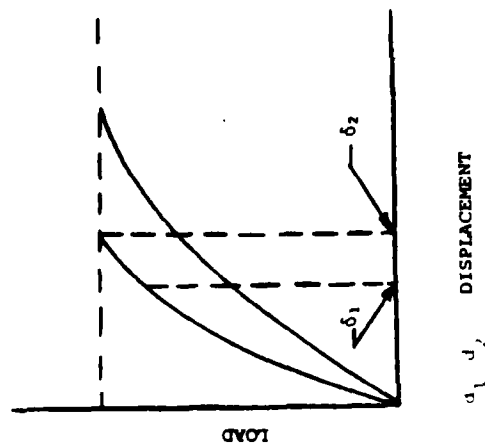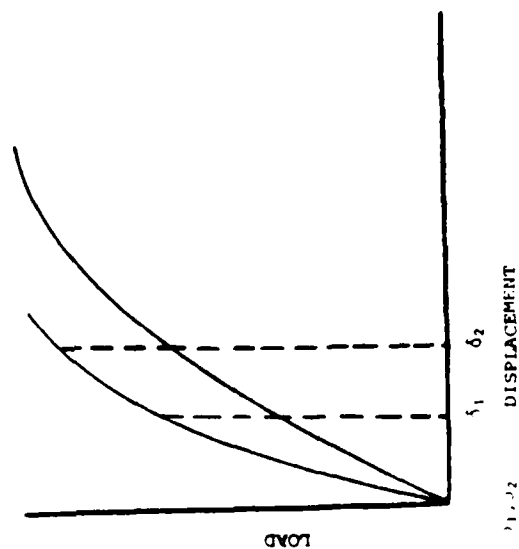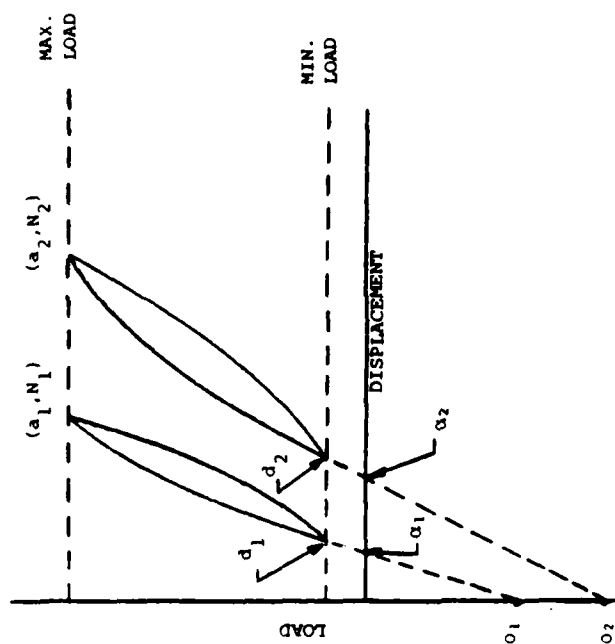
Figure 20. A Schematic Description of Approaches Used to Determine Experimental Values of the J-Integral.

32

HALF CRACK LENGTH (MM)
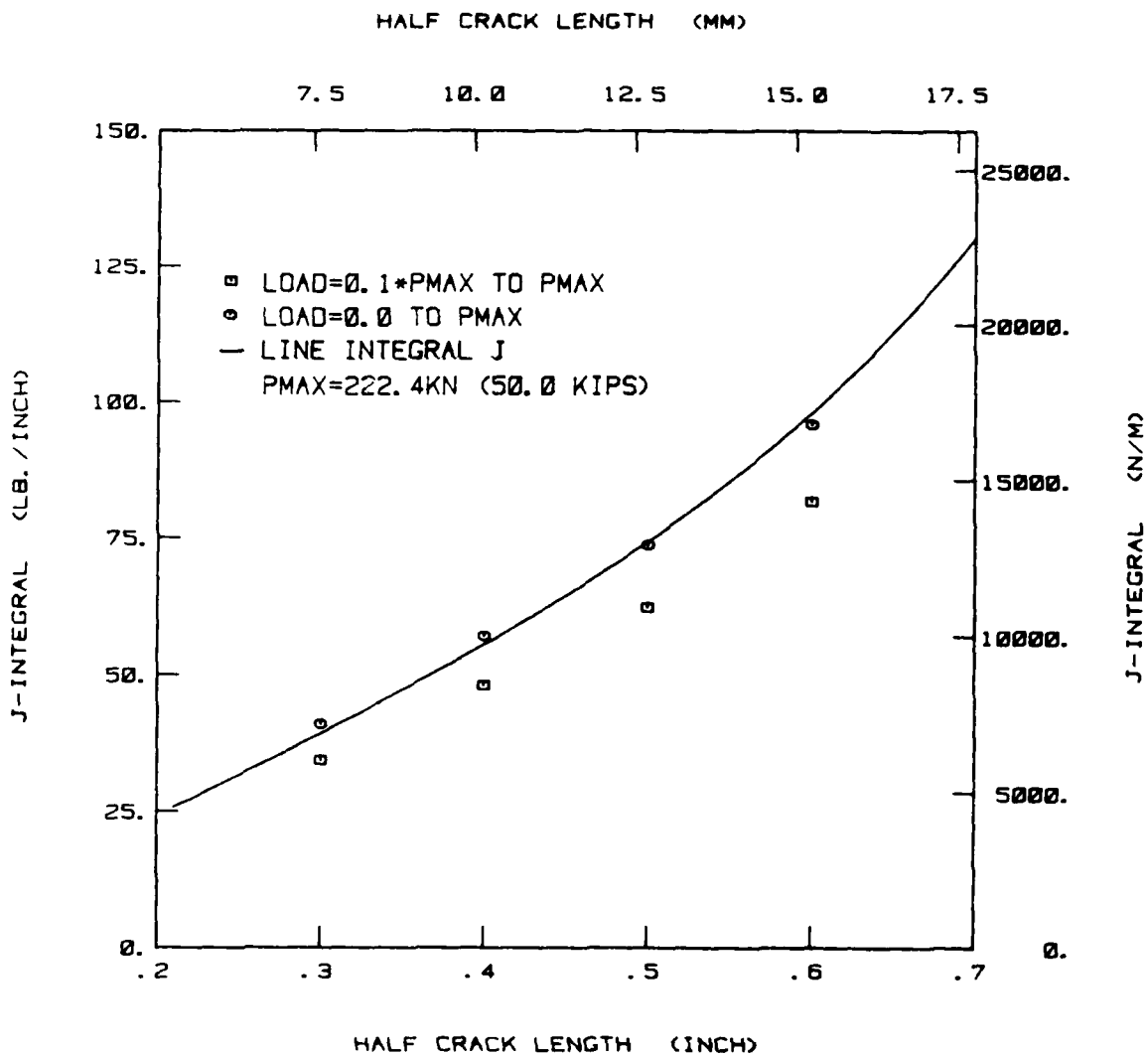
Figure 21. Comparison of J-Integral Calculations Based on Finite Element Results. The Direct Line Integral Calculation is Compared to the J-Integral Calculated Via Equation 13 wherein the Load-Displacement Data were Processed Using the Schemes Illustrated in Figure 20c and 20d.

33

The ΔJ results shown in Figure 21 might have been anticipated since the ΔJ parameter is based on the load range whereas the line integral results are based on the maximum load. In fact, when the zero-tension area under load-displacement curve (ala Figure 20d) was chosen for input to calculations based on Equation 13, it was found that these J-integral values (J_{max}) compared favorably with the line-integral results (See Figure 21).

It can be shown that the Sadananda-Shahinian ΔJ parameter is related to the J_{max} parameter by

$$\Delta J = J_{max} (1-R)^2 \tag{14}$$

under elastic conditions and not to the difference between the maximum and minimum J-integral values (J_{max} and J_{min}, respectively) obtained by evaluating the line integrals at the maximum and minimum load as might initially be suspected. The ΔJ definition provided by Sadananda-Shahinian is directly related to the pseudo elastic stress-intensity factor given by the inverse of Equation 5, i.e.,

$$\Delta J = \frac{\Delta K^2}{E} = \frac{\Delta \sigma^2}{E} (\frac{K}{\sigma})^2 \tag{15}$$

where the range of stress-intensity factor and of stress are given by ΔK and $\Delta \sigma$, respectively.

Unfortunately, we were not able to develop evidence that ΔJ is directly related to J_{max} by Equation 14 when the load-displacement curves exhibit nonlinear behavior. It also appears that the relationship is sufficiently complicated such that it might be difficult to relate line-integral calculations of J_{max} to the ΔJ parameter. We therefore decided to employ the J_{max} calculation based on the experimental data evaluated using Equation 13 according to the procedure identified in Figure 20d.

3.2.3.2 Modification of Load-Displacement Data

Relative to the problems associated with experimental technique, there are two important factors: (1) the displacement (δ) changes (increases) as a function of crack length for a constant load condition, and (2) the displacement (δ) given in Equation 13 is associated with the point of loading and is measured in the direction of loading. One major experimental difficulty lies in measuring the displacement accurately enough so that the displacement change can also be accurately determined. This problem is better realized when the displacement is decomposed into two parts, δ_{NCK} and δ_{CK}, associated with the displacement of the structure without a crack and only with the crack, respectively, i.e.,

$$\delta = \delta_{NCK} + \delta_{CK} \tag{16}$$

(Note that the differences in areas under successive load-displacement curves, which are used to obtain J values, depend directly on the increase in δ_{CK} as the crack grows.)

In many structural geometries, the no crack component (δ_{NCK}) which does not change as a function of crack length, is many orders of magnitude larger than the δ_{CK} component. Thus, to assure appropriate displacement sensitivity throughout the crack length range of interest, it is important to design experiments so that the no crack contribution to the displacement is minimized relative to δ_{CK}. This means that for remotely loaded structural geometries, such as the center cracked panel and the radial hole cracked geometries, the displacement should be measured as close to the crack as possible to minimize the δ_{NCK} component.

However, the potential energy utilized in Equation 13 must be evaluated such that the displacement measurements meet other conditions. For the case of a point loading, such as for the CT geometry, the displacements must be associated with the point of loading and be in the direction of

35

loading. For the case of remote uniform loading such as for the CCP and RHC geometries, the displacement must be measured along the direction of loading and at a sufficient distance from the crack so that the displacement field is approximately uniform. Strictly speaking, the stresses and displacements in a remote location should be measured completely across the width of these geometries and then integrated to sense the potential energy of deformation. Thus, by approximation, the stresses are taken as the applied load divided by the area (width x thickness) and the displacement at a point is assumed representative of a uniform displacement applied across the width of the CCP and RHC geometries.

For the CT geometry, the displacements were measured at the front face of the specimen. The results reported by Hudak et al.[25] were utilized to transfer the measured displacements at the front face of the specimen to the center line of loading. If δ_{LL} and δ_{ff} represent the displacements along the loading line and at the front face, respectively, then

$$\delta_{LL} = \delta_{ff} \quad \frac{\dfrac{x_o}{W}}{\dfrac{x_o}{W} + 0.275} \tag{17}$$

where

$$\frac{x_o}{W} = \frac{0.0924}{1 - V_1/V_o} - 0.25 \tag{18}$$

and

$$\frac{V_1}{V_o} = \frac{\left(1 + \dfrac{0.1576}{a/W}\right)}{\left(1 + \dfrac{0.250}{a/W}\right)} x \tag{19}$$

$$\frac{\left(2.537 + 3.904\left(\frac{a}{W}\right) + 22.44\left(\frac{a}{W}\right)^2 - 91.53\left(\frac{a}{W}\right)^3 + 107.4\left(\frac{a}{W}\right)^4 - 40.7\left(\frac{a}{W}\right)^5\right)}{\left(1.614 + 12.68\left(\frac{a}{W}\right) - 14.23\left(\frac{a}{W}\right)^2 - 16.61\left(\frac{a}{W}\right)^3 + 35.05\left(\frac{a}{W}\right)^4 - 14.49\left(\frac{a}{W}\right)^5\right)}$$

The use of these elastic formulas was justified on the basis that the load-displacement curves for the CT specimen were primarily linear. Figure 22 describes the relationship given by Equation 17 as a function of crack length.

For the CCP and RHC geometries, gage lengths were selected such that the displacement fields contained a sufficiently high level of δ_{CK} relative to δ_{NCK} (See Equation 16) and the displacement was reasonably uniform across the specimen width. Initially, we attempted to utilize the load-load point displacement curves generated in the experiments without giving adequate consideration to the assumption of uniformity in the displacement field. Further consideration of this assumption lead us to evaluate exactly, via finite element calculations, the displacements completely across the specimen width at the gage length associated with the measurement site along the center line of the specimens. Figure 23 describes the finite element displacement results for the CCP geometry with a half crack length (a) of 0.55 inch. As can be seen from the exaggerated scale the displacements are not exactly uniform and the measurement location yields the maximum displacement for the cross-section. Comparisons were made between the line-integral results presented in subsection 3.2.1 and J-integral values obtained using Equation 13. The Equation 13 (single value) load point displacement was approximated by the measurement site (maximum) displacement and by the average displacement across the specimen width at the gage length distance. A comparison is shown in Figure 24 for the maximum load condition for the test gage length (4 inch/101mm).

In evaluating the effects that the various displacements had on the J-integral results, it was determined that it would be better to utilize the average displacement at the gage length than that of the measurement point. Figure 25 provides the transfer function, developed on the basis of finite element results, in order to convert displacements at the measurement site to the average displacement across the width. The transfer function presented in Figure 25 was found

37

CRACK LENGTH (MM)
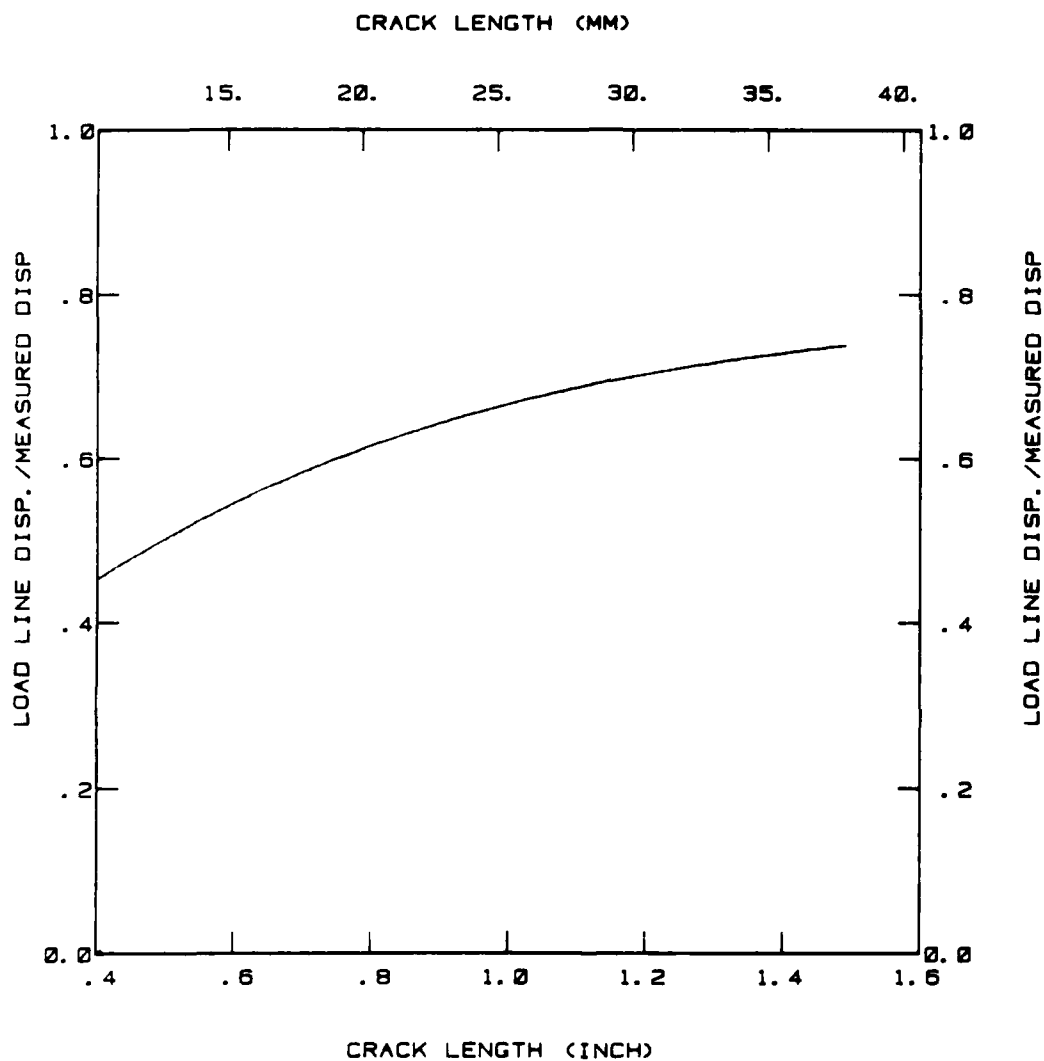
Figure 22.   Factor Used to Convert the Measured Displacement
to the Load Line Displacement for the CT Specimen.
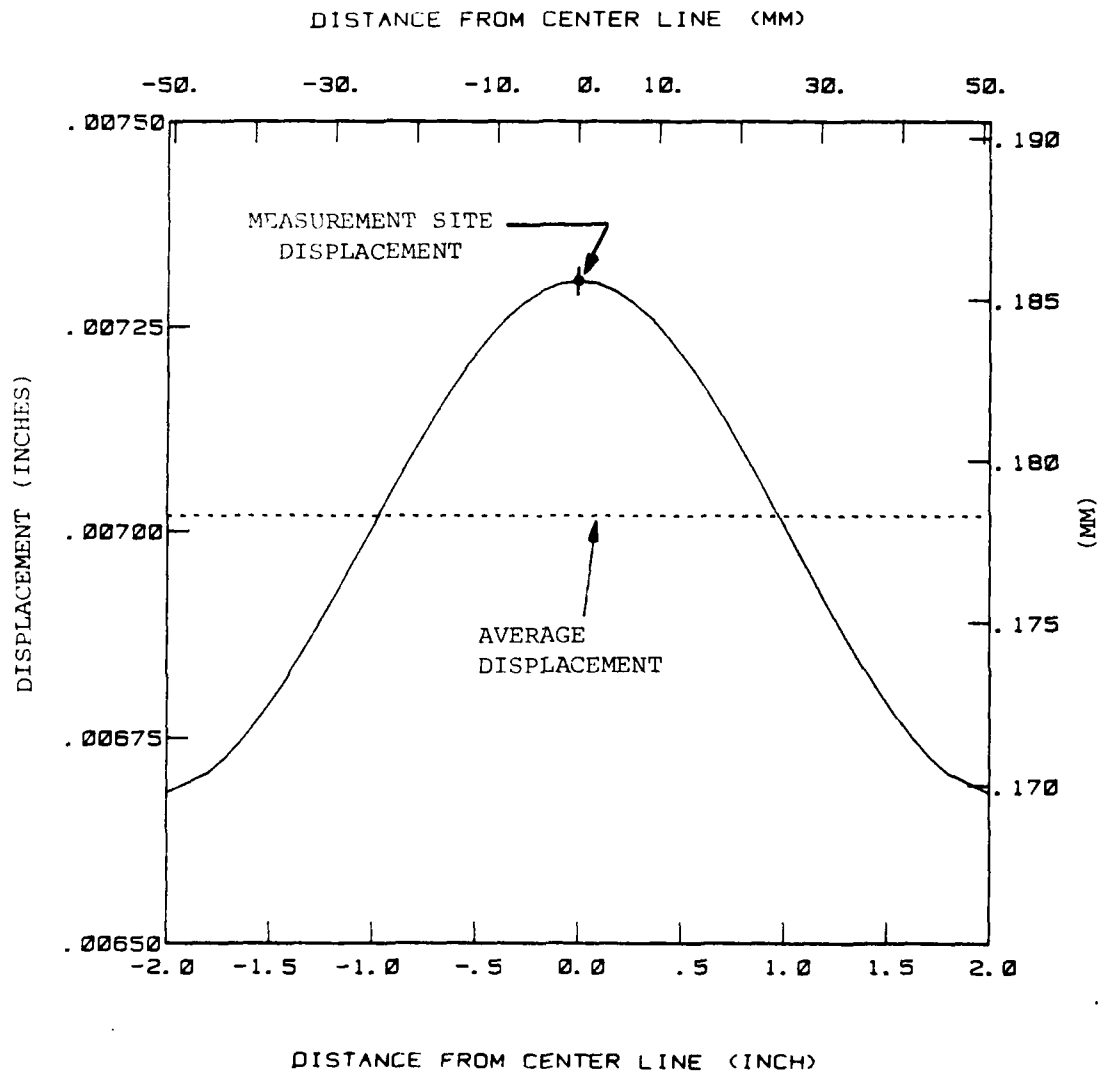
Figure 23. Variation in Displacement Across the CCP Specimen at a Distance of 2 inch (51mm) from the Crack Plane. Displacements Based on Finite Element Results for a Stress of 50.0 Kips (222.4 KN) and a Crack Length of 0.55 inch (14mm).

39

HALF CRACK LENGTH (MM)
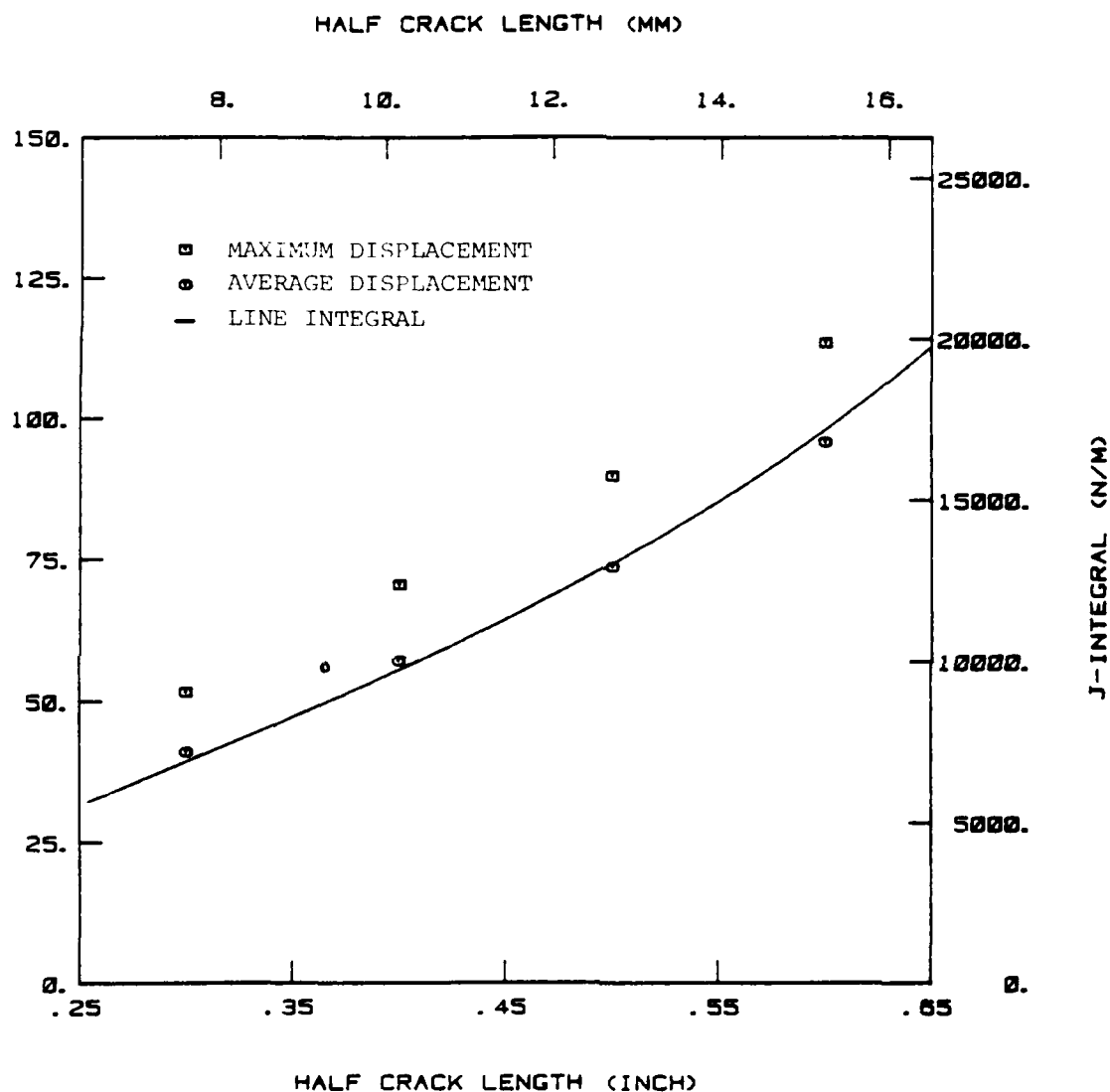
Figure 24.   J-Integral Values Based on a Potential Energy
Calculation Using Finite Element Load-Load Point
Displacement (Gage Length = 4 inch).   Results
Compared to Line Integral Calculation.

40

HALF CRACK LENGTH (MM)
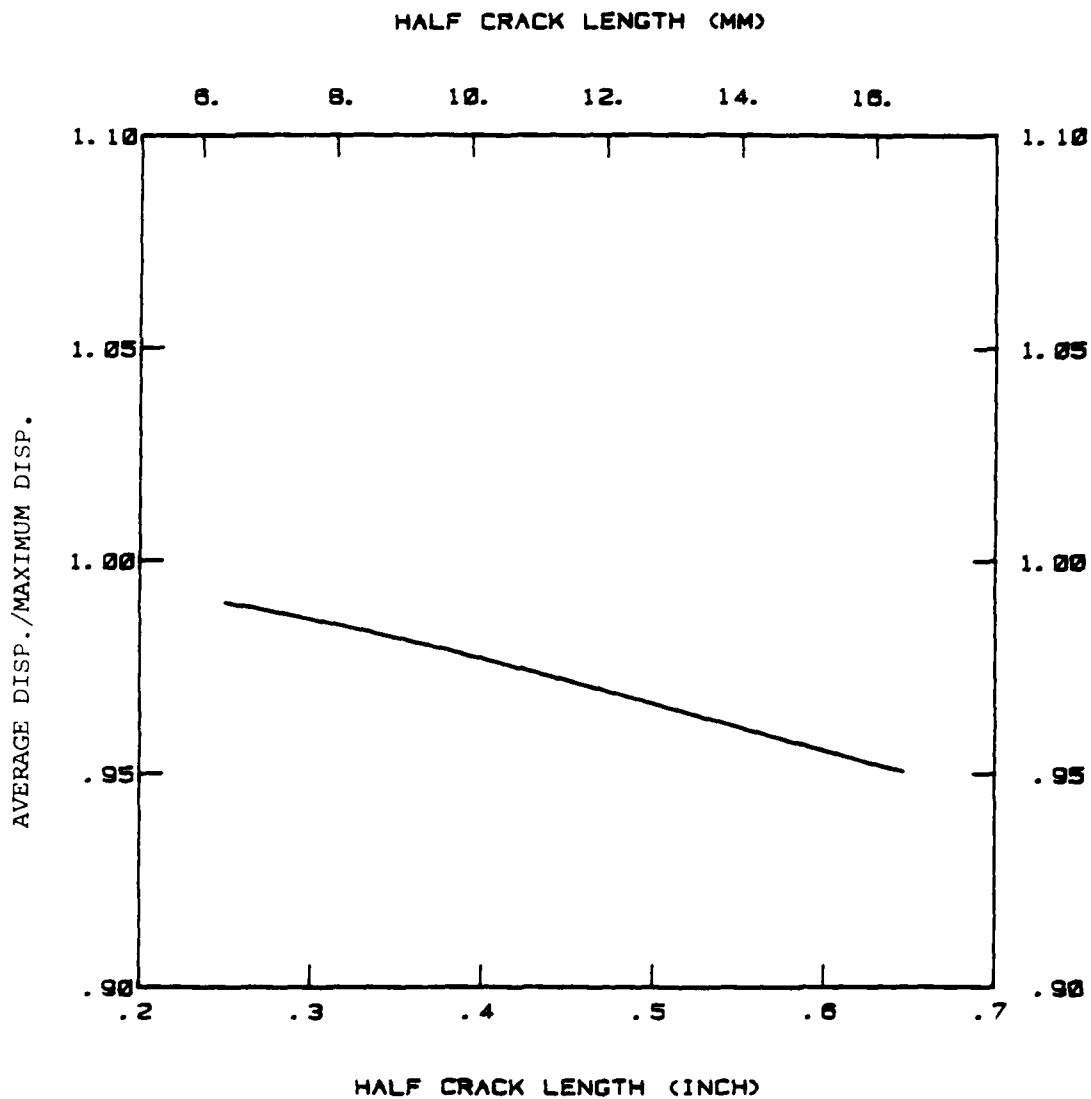
Figure 25.   Correction Factor to Convert Measured Point
Displacement of the CCP Specimen to the Average
Displacement (Based on Finite Element Results
for a Maximum Load Condition).

41

to be relatively independent of load (maximum differences were less than 5 percent from that shown).

A study similar to that described above was also conducted on the RHC specimen geometry. Unfortunately, due to the lack of displacement symmetry across the specimen width, it was not possible to derive a similar meaningful transfer function. For all crack lengths considered in the RHC geometry, the measurement site location gave displacements larger than at other locations across the specimen width. Thus, the displacement used to evaluate the J-integral based on Equation 13 were as measured for the RHC specimens.

3.2.3.3 Summary of Procedures and Results

As described in the above paragraphs, a certain amount of preconditioning of the load displacement information obtained during the tests was required before Equation 13 would provide meaningful results. To summarize, for the CP and CCP tests, the displacements were made compatible with the theoretical assumptions associated with Equation 13 using the transfer functions described in Figures 22 and 25, respectively. No displacement transfer function was used for the RHC test results. The transfer functions were directly applied to computer compatible displacement data obtained by digitizing the experiment load-displacement curves from the X-Y plots taken during the tests.

A linear extrapolation of these load-displacement results was utilized to obtain an estimate of displacement at zero load. Each set of load-modified displacement results for a given crack length was then described with a third order polynominal obtained using least squares results. Figure 26 shows a typical set of load-modified displacement points (obtained from the compact specimen CT-1) described by the least squares determined third order polynominal curve.
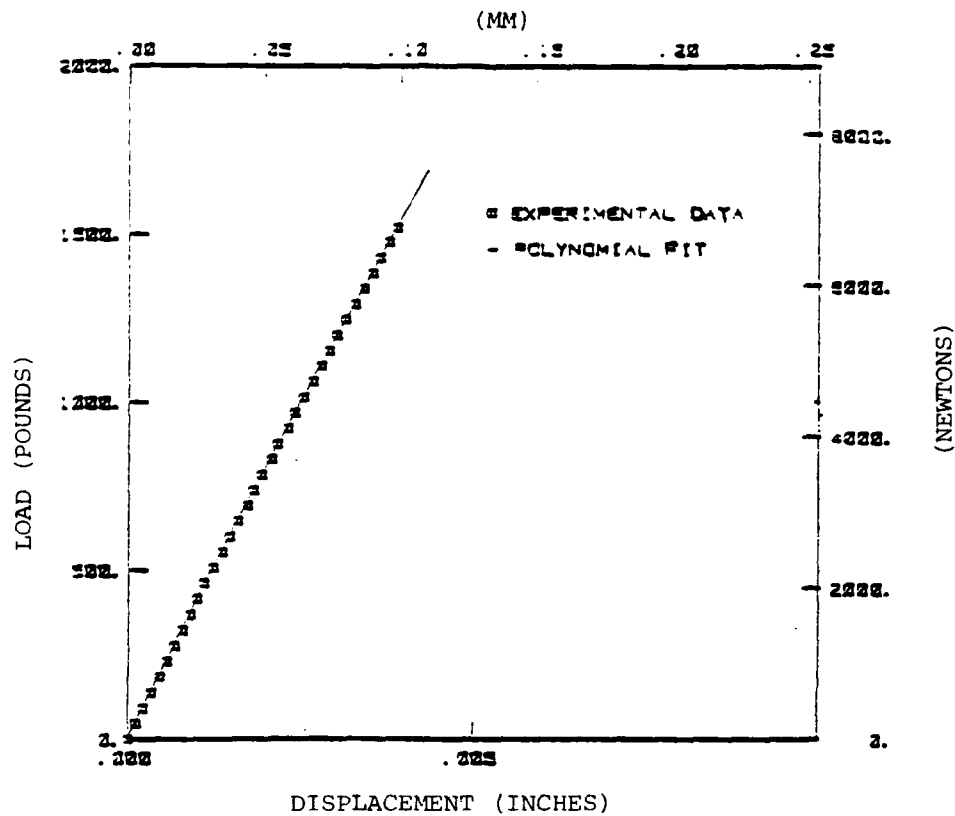
Figure 26. Load Versus Displacement Data and A Least Squares Established Curve (Compact Specimen CT1, Crack Length 13.7mm (0.538 in.).

The resulting load-displacement curves were integrated between the appropriate displacement limits to produce the potential energy (U) for each curve.

Figure 27 presents the calculated potential energy (U) for CT-1. In Figure 27, the symbols represent the data obtained by integrating the area under the load-displacement curves for the defined values of displacement (δ). The curves illustrated in Figure 27 are obtained from least square polynomial fits to the data points shown. The leftmost point of each curve in Figure 27 corresponds to the maximum applied load at each deflection. By determining the slopes of the fitted curves at the left end, it is possible to generate J values for constant (maximum) load as a function of crack length as shown in Figure 28.

The procedure described above was applied to the load-displacement data collected on CCP, CT, and RHC specimens. The resulting J-integral values which are referred to as experimental J values, were again converted to pseudo stress-intensity factor values through the use of Equation 5. Figures 29, 30, and 31 present the experimental J-integral based values for the CCP, CT, and RHC specimens, respectively; each figure compares the experimental J based value to the elastic numerical values presented earlier in this section. It should be noted that the experimental J value differs significantly from the numerical elastic-plastic results for the CCP and RHC specimens.
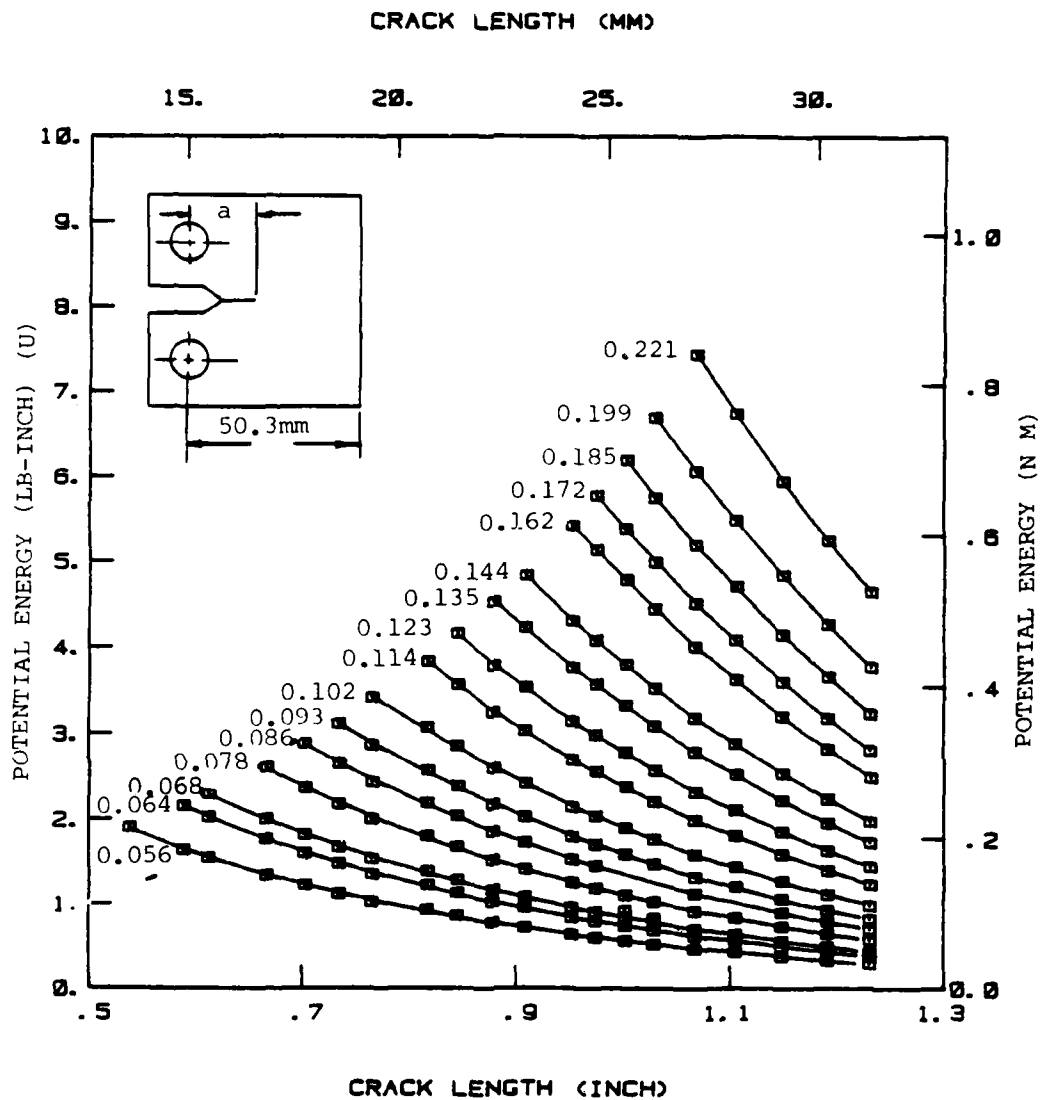
Figure 27. The Potential Energy (U) Based on the Area Under the Load-Displacement Curve up to Defined Values of Displacement (δ) as a Function of Crack Length for Specimen CT1.
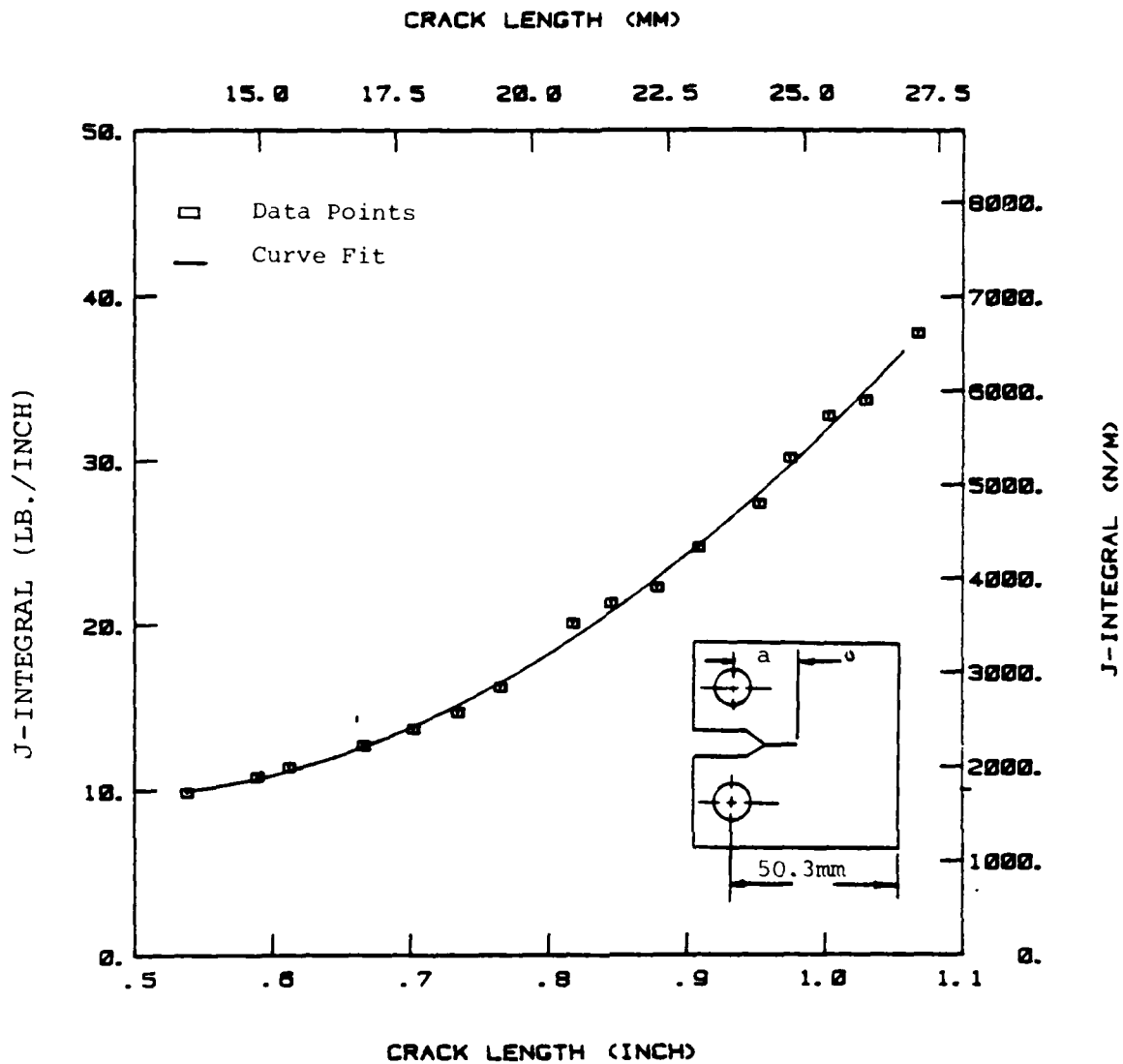
Figure 28. Experimental J-Integral for Compact (CT1) Specimen with an Applied Maximum Load of 1.686 Kips (7.5 KN) and a stress Ratio of 0.1.

HALF CRACK LENGTH (MM)
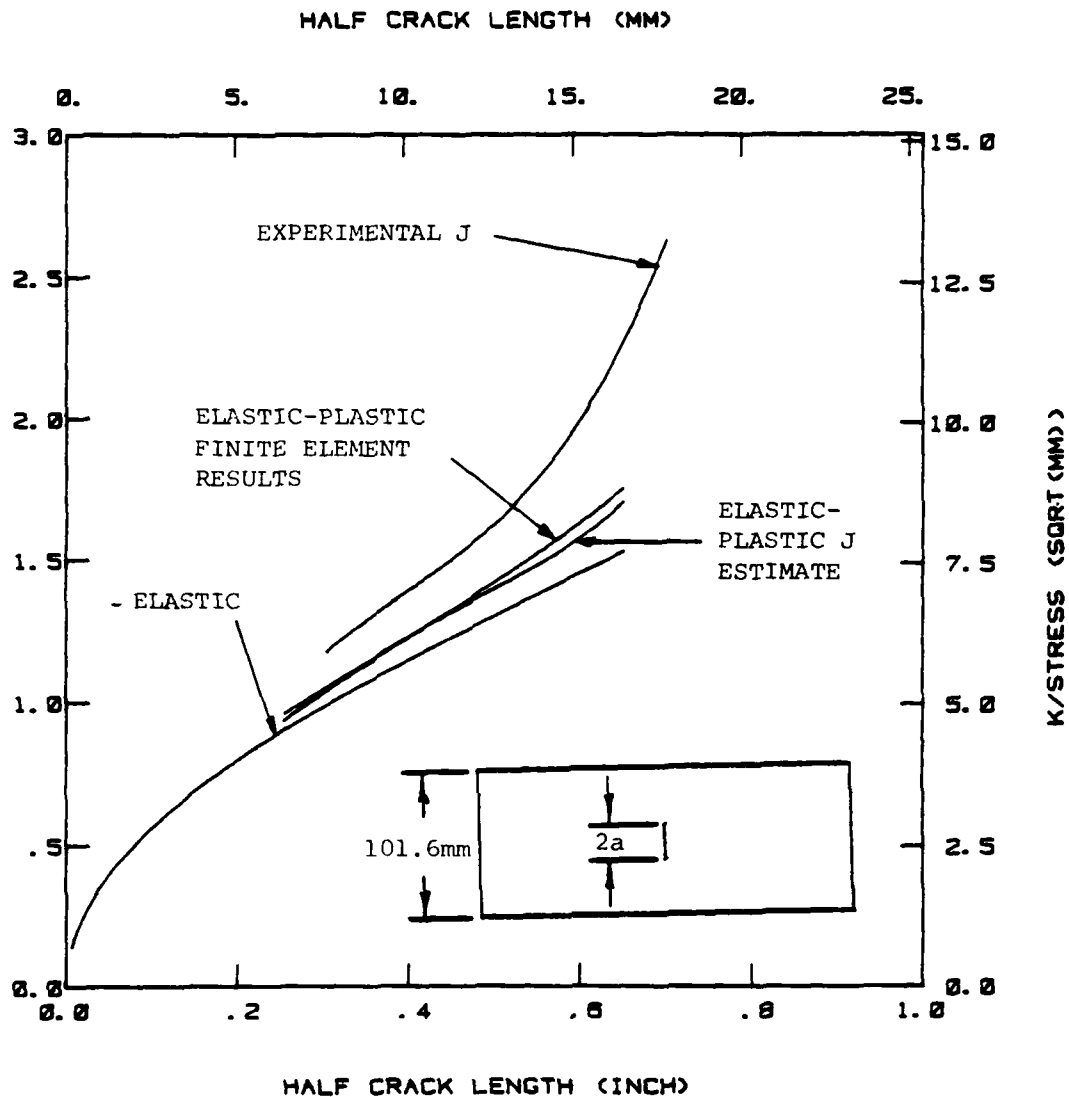
Figure 29. Experimental J-Integral Values Presented as a
Pseudo Stress-Intensity Factor for the Center
Cracked Panel (CCP) Specimen. Experimental J
and Elastic-Plastic J Values are Established
at a Maximum Load of 50.0 Kips (222.4KN).

47

CRACK LENGTH (MM)
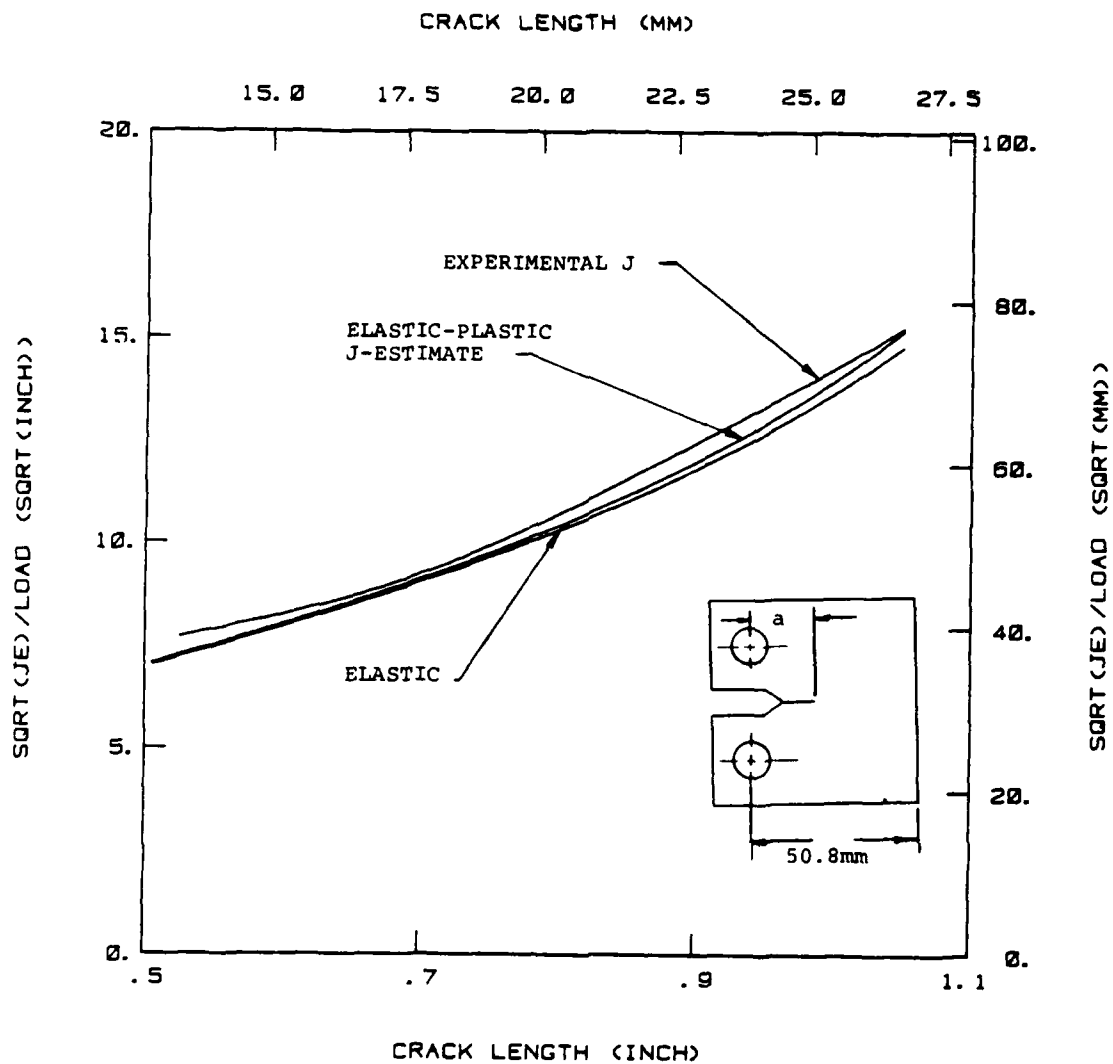
Figure 30. Experimental J-Integral Values Presented as a Pseudo Stress-Intensity Factor for the Compact (CT) Specimen. Experimental J and Elastic-Plastic J Results are Based on a Maximum Load of 1.69 Kips (7.5 KN).

CRACK LENGTH (MM)
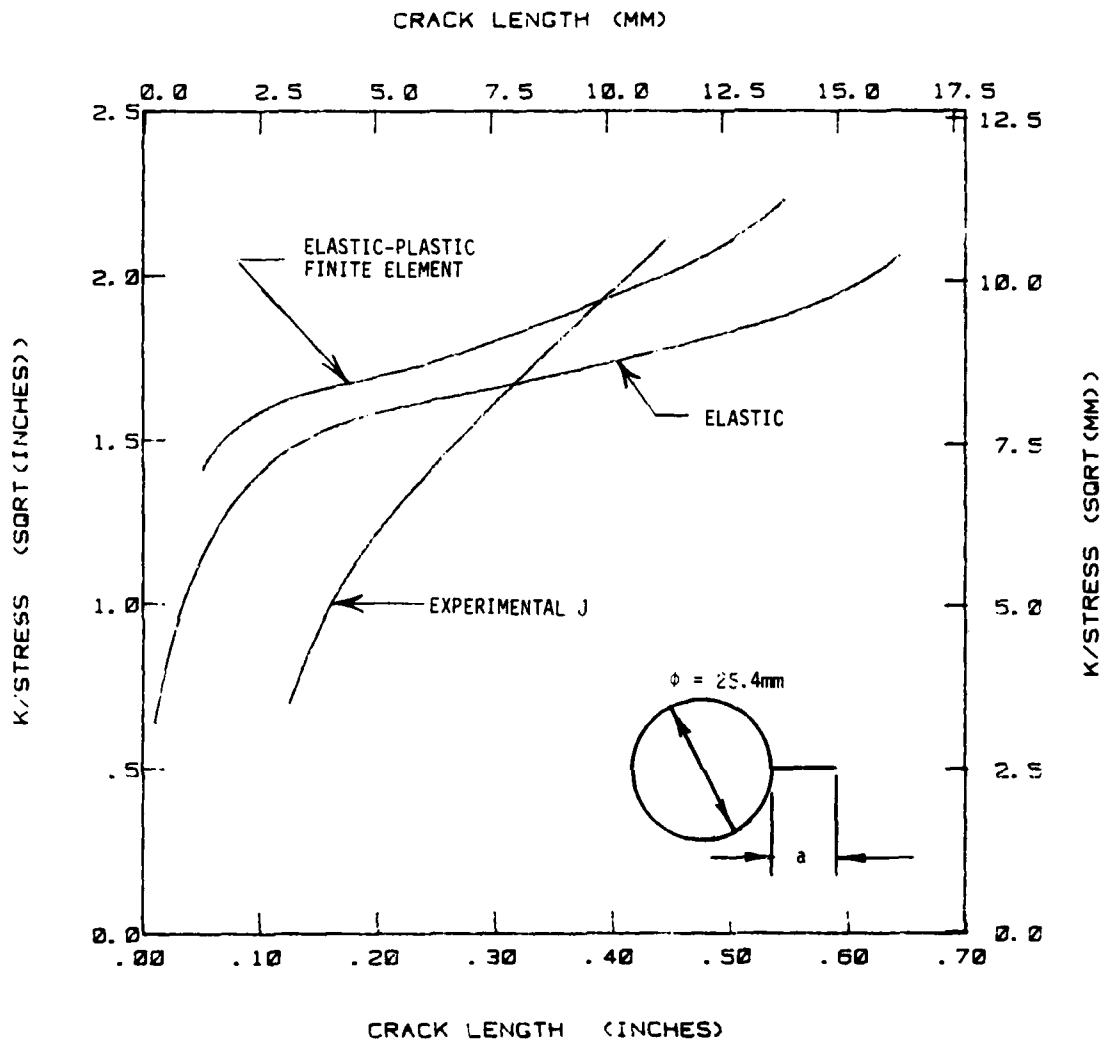
Figure 31. Experimental J-Integral Values Presented as A Pseudo Stress-Intensity Factor for the Radial Hole Crack (RHC) Specimen. Experimental and Elastic-Plastic J Results are Based on a Maximum Load of 33 Kips (146.8 KN).

SECTION 4
RESULTS AND DISCUSSION

As indicated in Section 1, the effort was focused on evaluating several P* parameters for applicability to fatigue crack growth problems where large amounts of plasticity take place. This section outlines how the parameters developed in Section 3 describe fatigue crack growth rate (FCGR) behavior and predict crack growth lives.

4.1 PARAMETER CORRELATIONS

4.1.1 Prediction Procedure

There are two basic criteria that a crack driving parameter (P*) must satisfy. These are: (a) the parameter P* must be able to correlate FCGR data via Equation 1

$$\frac{da}{dN} = f(P*) \qquad \text{(1 Repeated)}$$

such that the correlation is independent of structural geometry and stress level, and (b) the parameter P* must allow for sufficiently accurate estimates of crack growth lives (N_p) to be made from the inverse of Equation 1, i.e.,

$$N_p = \int_{a_O}^{a_f} \frac{da}{f(P*)} \qquad (20)$$

where a_O and a_f are the initial and final crack lengths in the interval, respectively.

Relative to this program, baseline data are provided by the CCP and CT specimen geometries and the verification data were provided by the RHC specimen geometries. Fatigue crack growth rate (FCGR) data were generated using the seven point incremental polynominal method suggested by ASTM Standard E647 [7];

50

these FCGR data were correlated to the various parameters evaluated at the mean crack length associated with each seven point (data) interval. For purposes of evaluation, two crack growth rate plots of the type shown in Figure 32 were prepared. When the mean trend baseline curve is found to describe both the baseline data (two geometries, multiple stress levels) and the verification data (one geometry, multiple stress levels), the parameter P* satisfies the basic similitude conditions for a crack tip driving parameter.

When the mean trend fatigue crack growth rate curve appears to describe the data, the life predictions given by Equation 20 are reasonably accurate. The application of Equation 20 in making blind predictions of crack growth life behavior is, however, a better discriminator of parameter correlation than the growth rate correlation since it is difficult to distinguish relatively small differences in behavior on a FCGR data plot. In making blind predictions, one tests the complete methodology associated with a fracture mechanics approach based on the given parameter. This methodology is illustrated for a numerical analysis of Equation 20 in Figure 33.

The remaining numbered paragraphs of this subsection present the FCGR data correlations as in Figure 32 and life predictions for RHC test results (if the growth rate correlations are reasonable) for the parameters given in Section 3.

4.1.2 Stress-Intensity Factor (K) Correlations

In this paragraph, the linear elastic fracture mechanics parameter K_{max}, the maximum stress-intensity factor in the fatigue cycle, is evaluated for its ability to correlate fatigue cracking behavior where large amounts of plasticity occur. In this case, the parameter $P^* = K_{max}$, where K_{max} is evaluated from the expression

$$K_{max} = \sigma_{max} \left(\frac{K}{\sigma} \right) \tag{21}$$

o RHC Data
— CCP and CT Curve

$$\frac{da}{dN} = f(P*)$$

P*

(b) Verification Data and Baseline Curve

o CCP and CT Data
— CCP and CT Curve

$$\frac{da}{dN} = f(P*)$$

P*
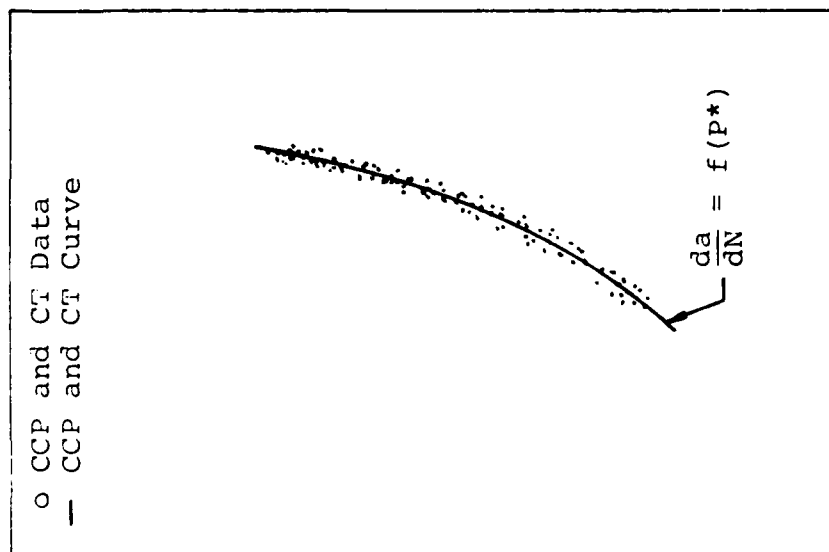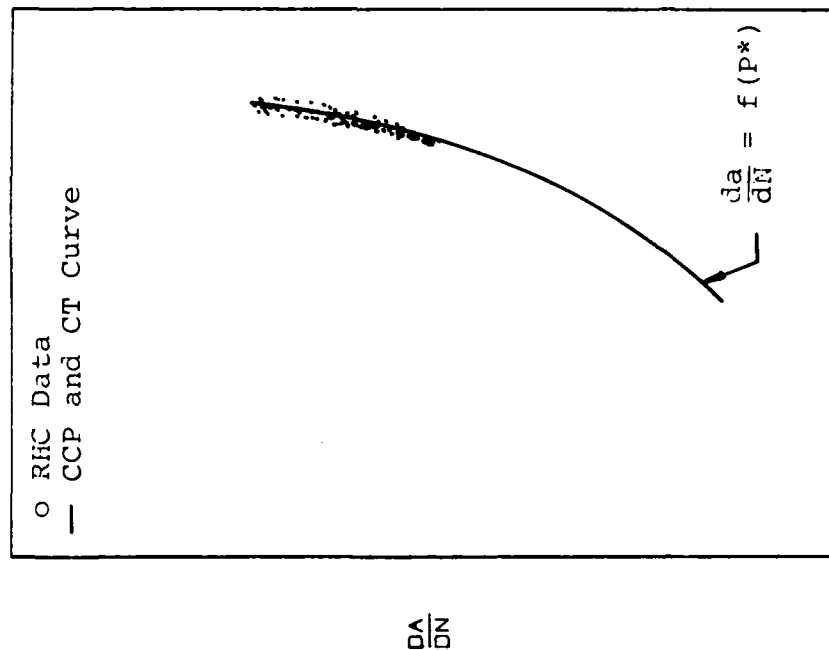
(a) Baseline Data and Curve

Figure 32. Fatigue Crack Growth Rate Verification Scheme.

52

N_P (predicted)

N_A (actual)

$\frac{da}{dN}$

N

a_f

a

a_o

$$a = a_o + \sum \frac{da}{dN}$$

Life Prediction Ratio

$$\left(\frac{N_P}{N_A}\right) > 1$$

non-conservative

$$\frac{da}{dN} = f(P*)$$

$\frac{da}{dN}$

P*

P*

crack length

$\sigma(t)$

$\frac{a}{\uparrow}$
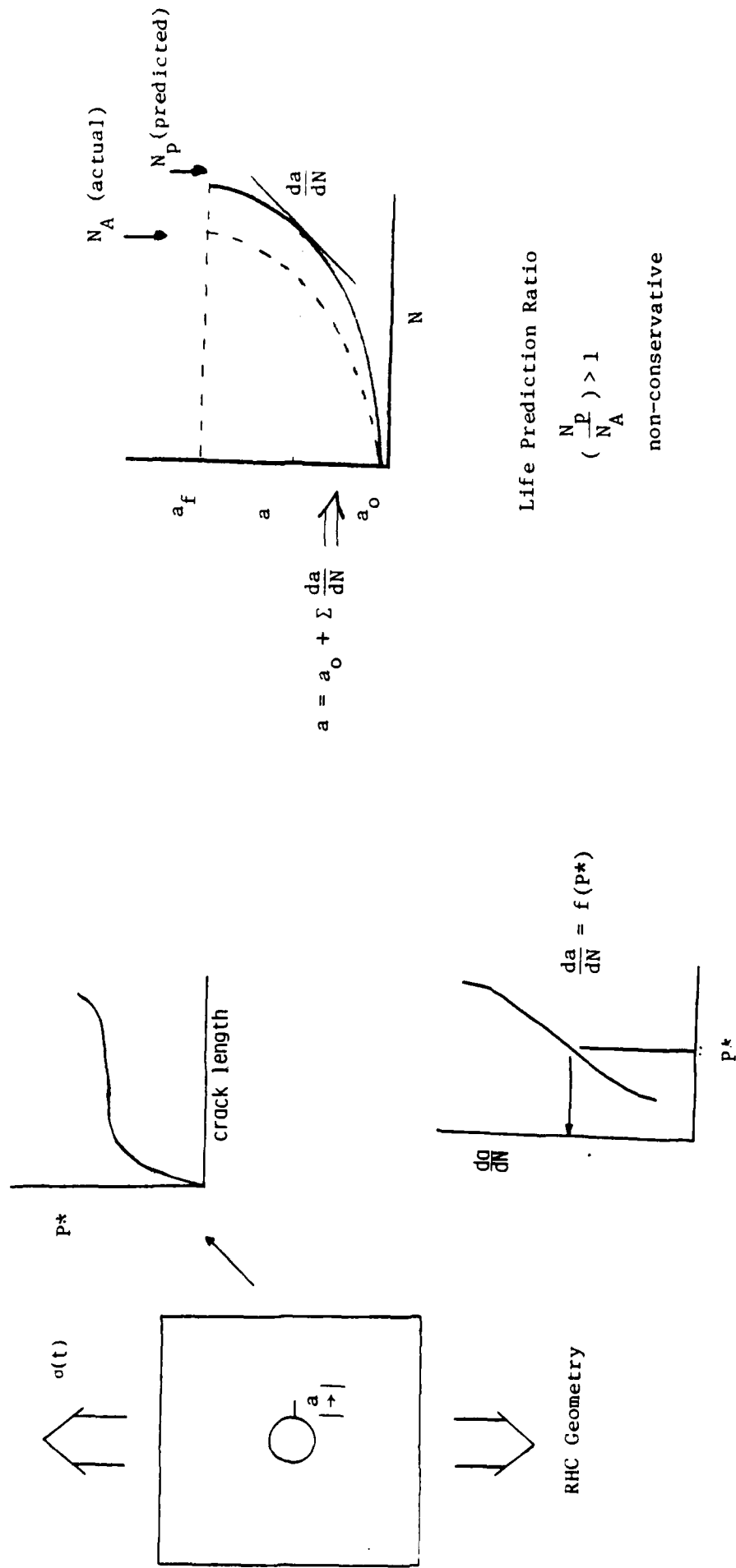
RHC Geometry

Figure 33. Verification Crack Growth Life Prediction Scheme.

53

where σ_{max} is the maximum stress in the fatigue cycle and (K/σ) is the stress-intensity factor coefficient for the given geometry of interest. We note that (K/σ) does not incorporate any influence of plasticity and is only dependent on geometry. Stress-intensity factor coefficients for the CCP, CT and RHC structural geometries were derived from Equations 3,4 and 6, respectively.

The results obtained from comparing the crack growth rate data correlated on the basis of $P^* = K_{max}$ are described in Figure 34. The curve in Figure 34 is a power law relationship given by

$$\frac{da}{dN} = 4.31 \times 10^{-11} \; K_{max}^{4.03} \tag{22}$$

where da/dN and K_{max} are expressed in units of inches/cycle and ksi$\sqrt{in.}$, respectively. Since this mean trend curve appears to describe the fatigue crack growth rate behavior, Equation 22 was used in conjunction with Equation 21 to develop the life predictions listed in Table 2 for the five RHC tests. Two of the five experimental crack growth life curves are presented in Figure 35 along with the predicted curves

The results of the elastic analysis were somewhat surprising, given the considerable plasticity noted as gross specimen deformation during some tests (See Figure 3). As indicated by Figure 35, the predicted crack growth behavior parallelled the actual behavior; this was so for all the tests considered. The life predictions provided in Table 2 indicate that the elastic parameter will lead to unconservative predictions as might be expected from Figure 34b where the Equation 22 is shown to be slightly lower than the observed RHC fatigue crack growth rate data.

54

(b) Verification Data and Baseline Curve

(a) Baseline Data and Curve
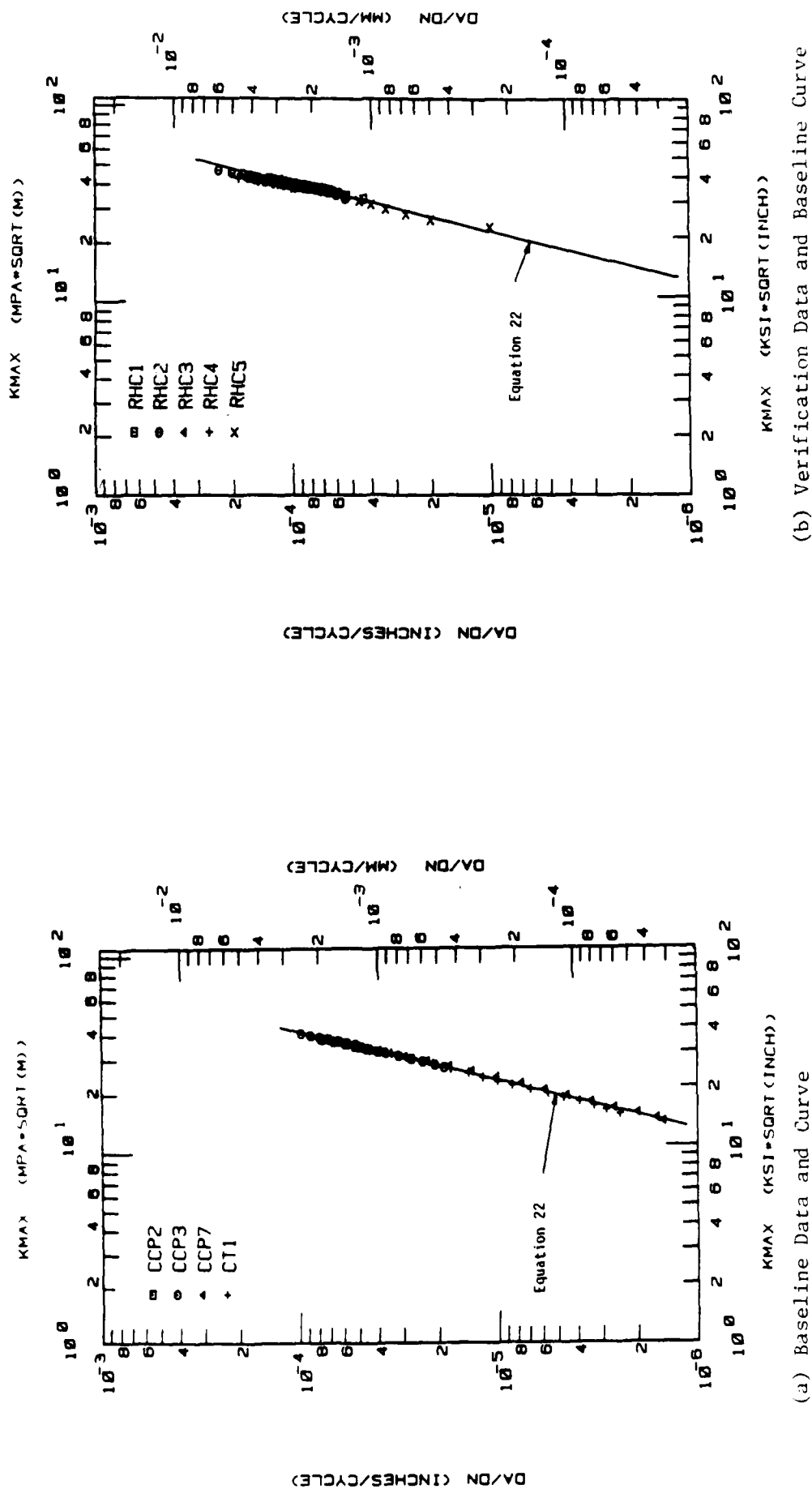
Figure 34. Fatigue Crack Growth Rate Data Described as a Function of the Maximum Stress-Intensity Factor in the Fatigue Cycle.

TABLE 2

LIFE PREDICTIONS BASED ON THE ELASTIC PARAMETER K

Specimen ID	a_o (mm)	a_f (mm)	N_i Predicted	N/A Actual	(N_p/N_A)*
RHC1	0.89	13.77	7940	7441	1.06
RHC2	0.86	13.79	8010	6241	1.28
RHC3	1.14	9.32	3870	2661	1.45
RHC4	1.57	9.42	3340	2501	1.34
RHC5	0.20	15.39	14500	12600	1.15

* $(N_p/N_A) > 1$ implies Non-conservative Predictions

56

a.   2000.   4000.   6000.   8000.   10000.

(a) Results for RHC1 (Low Stress)

CYCLES

a.   1000.   2000.   3000.   4000.   5000.
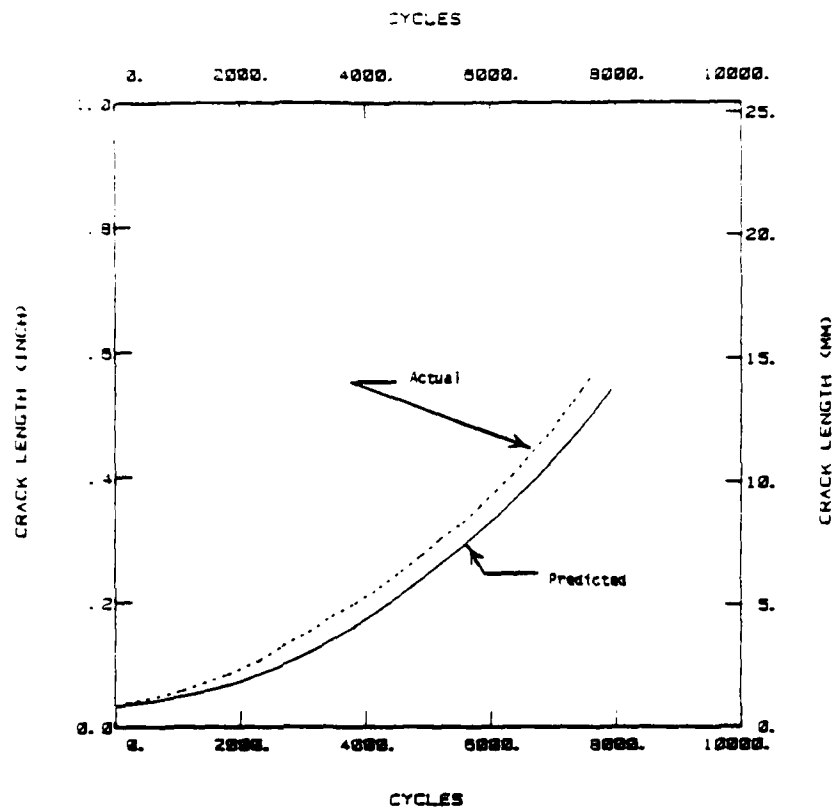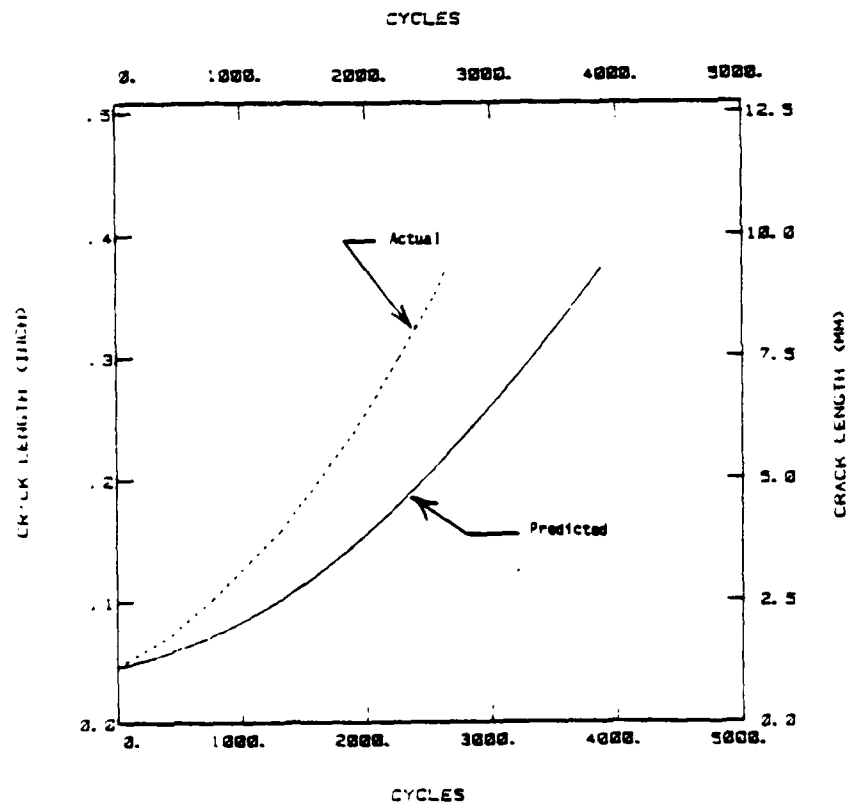
(b) Results for RHC3 (High Stress)

Figure 35.   Experimental Fatigue Crack Growth Behavior Compared to
That Predicted Based on K_{max} Parameter.

57

4.1.3 Numerical Elastic-Plastic Parameter Correlations

In this paragraph, the numerical elastic-plastic parameter $P^* = \sqrt{J_{max} \cdot E}$ is evaluated for its ability to correlate fatigue cracking behavior under conditions approaching gross plasticity. The parameter $\sqrt{J_{max} \cdot E}$ is equivalent to the K_{max} parameter where elastic conditions dominate. For load levels that exceed those associated with small-scale yielding, the J_{max} parameter senses the amount of potential energy available for crack growth (assuming nonlinear elasticity). The parameter $\sqrt{J_{max} E}$ can be thought of as a pseudo maximum stress-intensity factor (obtained via Equation 5) that incorporates the influence of nonlinear behavior.

The J_{max} values associated with a given geometry and crack-length must be evaluated for the maximum load (stress) applied in the fatigue cycle. Paragraphs 3.2.1 and 3.2.2 provide the details of the numerical procedures used to obtain these values of J_{max} using finite element based line integral results and the Shih estimation scheme, respectively. After comparing the results for the center-cracked panel based on both the finite element and estimation schemes, it was decided that the numerical results could be used interchangeably.

The numerical values of J_{max} for the CCP, CT, and RHC geometries were based on finite element results, the estimation scheme, and finite element results, respectively. The specific J_{max} values are shown in Figures 13, 18, and 14, for the maximum load (stress) conditions for the CCP, CT, and RHC geometries, respectively.

The results obtained from comparing the crack growth rate data correlated on the basis of $P^* = \sqrt{J_{max} E}$ are described in Figure 36. The curve in Figure 36 is a power law given by

$$\frac{dc}{dN} = 1.75 \times 10^{-10} \left(\sqrt{J_{max} \cdot E} \right)^{3.56} \tag{23}$$
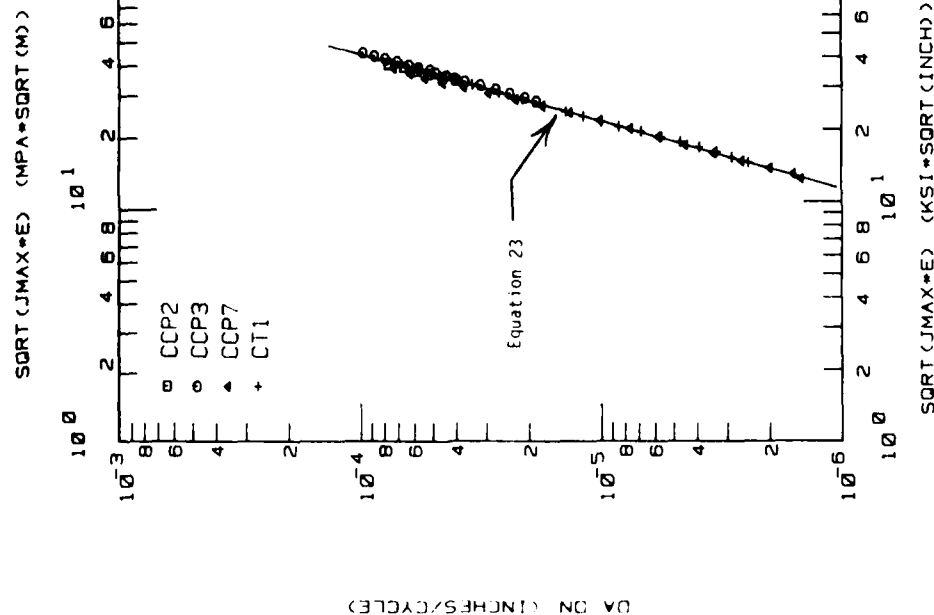
(b) Verification Data and Baseline Curve
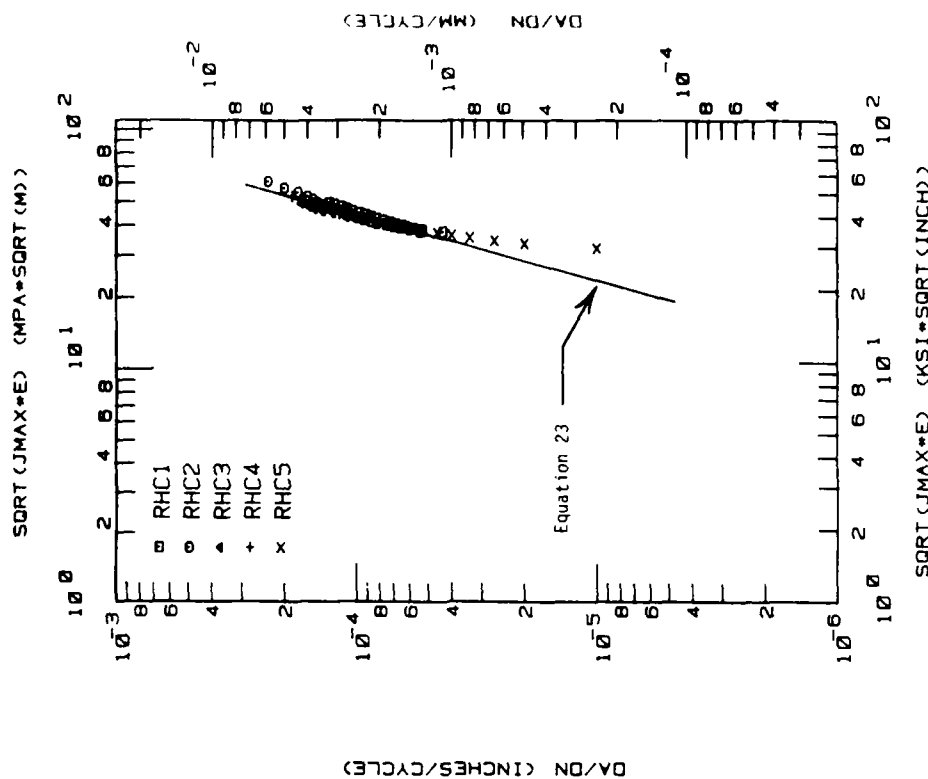
(a) Baseline Data and Curve.

Figure 36. Fatigue Crack Growth Rate Data Described as a Function of the Maximum Pseudo Stress-Intensity Factor, Based on J_{max} and Derived from Numerical Results (Finite Element and Estimation Scheme).

where da/dN and $\sqrt{J_{max}}$,E are expressed in units of inches per cycle
and ksi in, respectively. Except for the lower growth rates
associated with one of the radial hole cracked tests (RHC5), the
mean trend baseline curve given by Equation 23 provided a reasonable
description of the radial hole cracked growth rate data. When
Equation 23 was used in conjunction with Equation 21, the life
predictions listed in Table 3 were obtained. Figure 37 describes
the crack growth behavior (actual versus predicted) for two radial
hole cracked tests. As can be seen by comparing Table 3 and
Figure 37 with Table 2 and Figure 35, the $\sqrt{J_{max}E}$ parameter predicted
crack growth lives and behavior to a slightly better degree than
the corresponding elastic stress-intensity factor. Conversely,
by comparing the crack growth rate correlations for the two para-
meters (Figure 34 and 36), it appears that the elastic stress-
intensity factor parameter provides a better correlation. There
will be more discussion on comparisons and correlations subsequently
in subsection 4.2.

4.1.4   Experimental Elastic-Plastic Parameter Correlations

In this paragraph, the experimental elastic-plastic
parameter $P* = \sqrt{J_{max}}.E$ is evaluated for its ability to correlate
fatigue cracking behavior under conditions approaching gross
plasticity. From an analytical standpoint, the numerical and
experimental results of J_{max} should be equivalent; but, based on the
work presented in paragraph 3.2.3, we note that they are not.
The J_{max} values associated with a given geometry and crack length
were evaluated for the maximum load (stress) applied in the fatigue
cycle; these were presented in Figures 29, 30, and 31 for the CCP,
CT, and RHC geometries, respectively.

The results obtained from comparing the crack growth
rate data correlated on the basis of $P* = \sqrt{J_{max}E}$ are described in
Figure 38. The curve in Figure 38 is a power law given by

$$\frac{da}{dN} = 1.03\times10^{-9} \ (\ \sqrt{J_{max}E})^{2.93} \qquad (24)$$

TABLE 3

LIFE PREDICTIONS BASED ON THE ELASTIC-PLASTIC PARAMETER $\sqrt{J_{max} \cdot E}$

Specimen ID	a_o (mm)	a_f (mm)	N_p Predicted	N_A Actual	N_p/N_A
RHC1	0.89	13.77	6500	7441	0.88
RHC2	0.86	13.79	6540	6241	1.05
RHC3	1.14	9.32	2940	2661	1.10
RHC4	1.57	9.42	2690	2501	1.08
RHC5	0.20	15.39	8410	12600	0.67
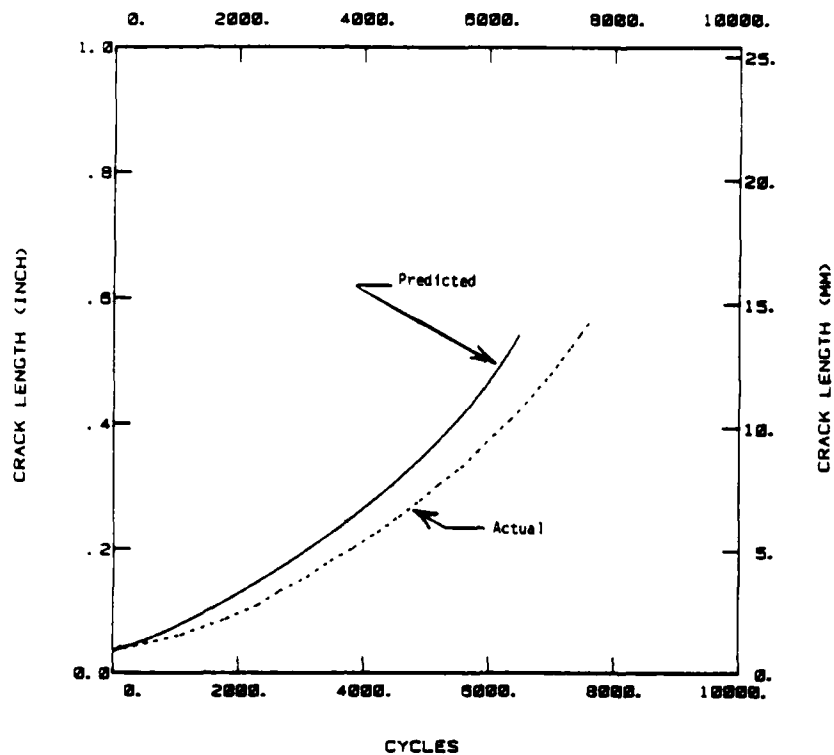
(a) Results for RHC1 (Low Stress)
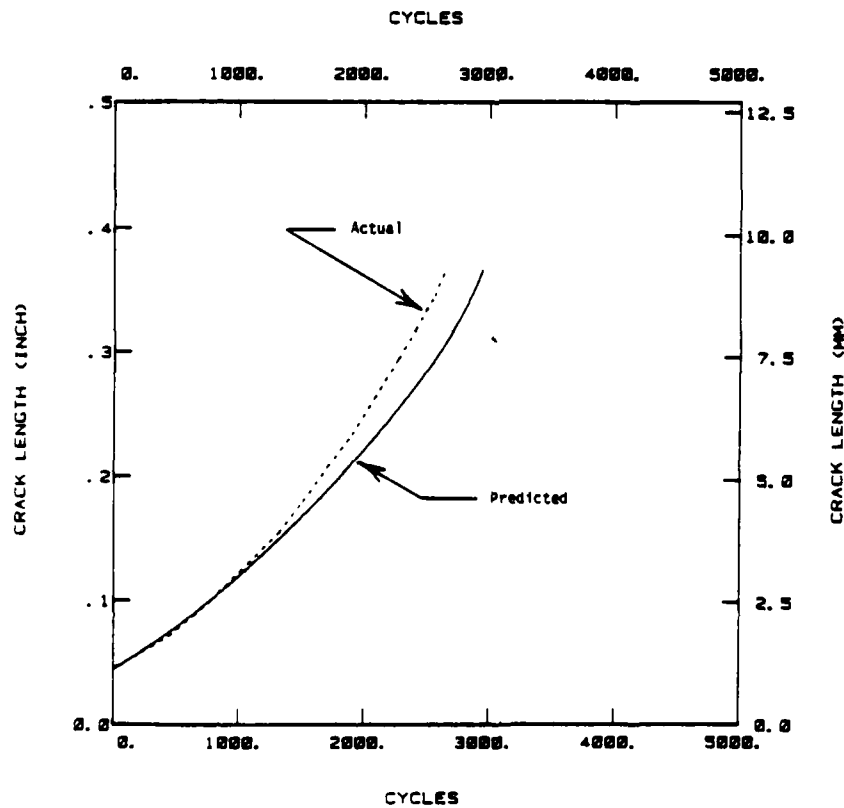
(b) Results for RHC3 (High Stress)

Figure 37. Experimental Fatigue Crack Growth Behavior Compared to that Predicted Based on Numerical $\sqrt{J_{max} E}$ Parameter.
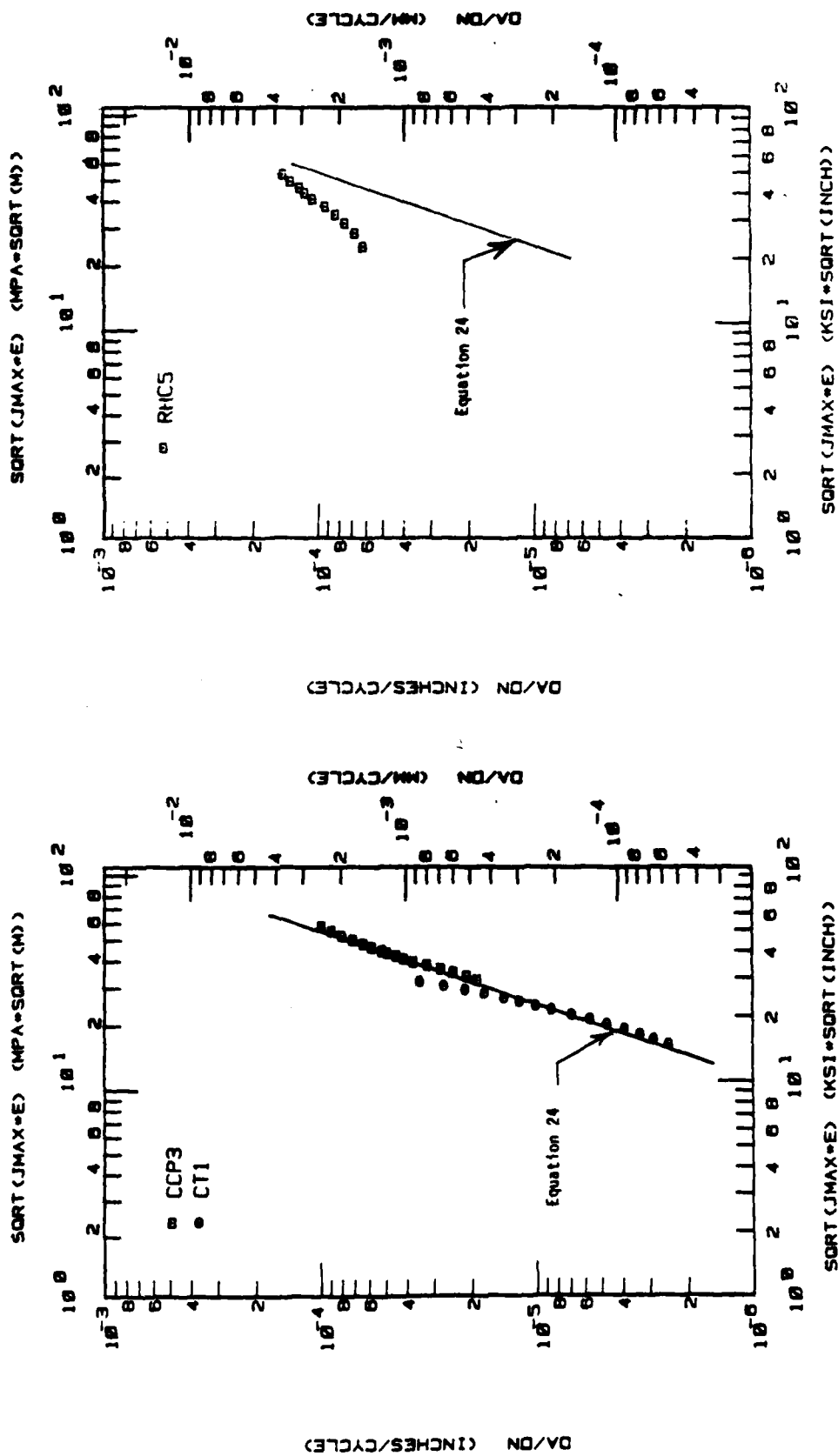
(b) Verification Data and Baseline Curve.

(a) Baseline Data and Curve.

Figure 38. Fatigue Crack Growth Rate Data Described as a Function of the Maximum Pseudo Stress-Intensity Factor, Based on J_{max} and Derived from Experimental Load-Displacement Results.

where da/dN and $\sqrt{J_{max}E}$) are expressed in units of inches/cycle and ksi $\sqrt{in}$, respectively.

While Equation 24 provides an adequate description of the baseline data shown in Figure 38a, it does not describe the trend in the RHC test crack growth rate data at all. Only one RHC test (RHC-5) yielded load-displacement data which was considered sufficiently valid for J-integral analysis, i.e., the displacements were measured either directly across the hole at a 4.0 inch gage length. Because the experimental crack growth rates were so poorly correlated, no attempt to calculate life was made.

4.2   DISCUSSION OF RESULTS

The various elastic and elastic-plastic parameters considered in the previous subsection were all able to correlate the baseline fatigue crack growth rate behavior associated with center crack panel and compact geometries. Except for the experimental elastic-plastic parameter, the parameters were also found to provide adequate predictions of the behavior exhibited by the radial hole crack geometry. This subsection further considers the results in a comparative sense and then describes some of the authors' concerns as they developed the results.

4.2.1   Comparisons of Growth Rate Correlations

The pseudo stress-intensity factor parameter $\sqrt{J_{max} \cdot E}$ can be used to provide the means for evaluating the effects that increased amounts of plasticity have on the crack growth rate. As subsection 3.2 illustrated the elastic-plastic $\sqrt{J_{max} \cdot E}$ values were slightly higher than the elastic value of the maximum stress-intensity factor K_{max}. In evaluating crack grwoth rates, it is seen in Figure 39 that the increasing amount of plasticity associated with the $\sqrt{J_{max}E}$ parameter causes the baseline curve to shift (rotate) at the higher levels of the parameter. Thus, one would expect that a fatigue crack growth rate baseline based on linear elastic fracture mechanics would provide conservative life estimates for structures experiencing elastic-plastic strains during fatigue cycling. Figure 40 illustrates this where
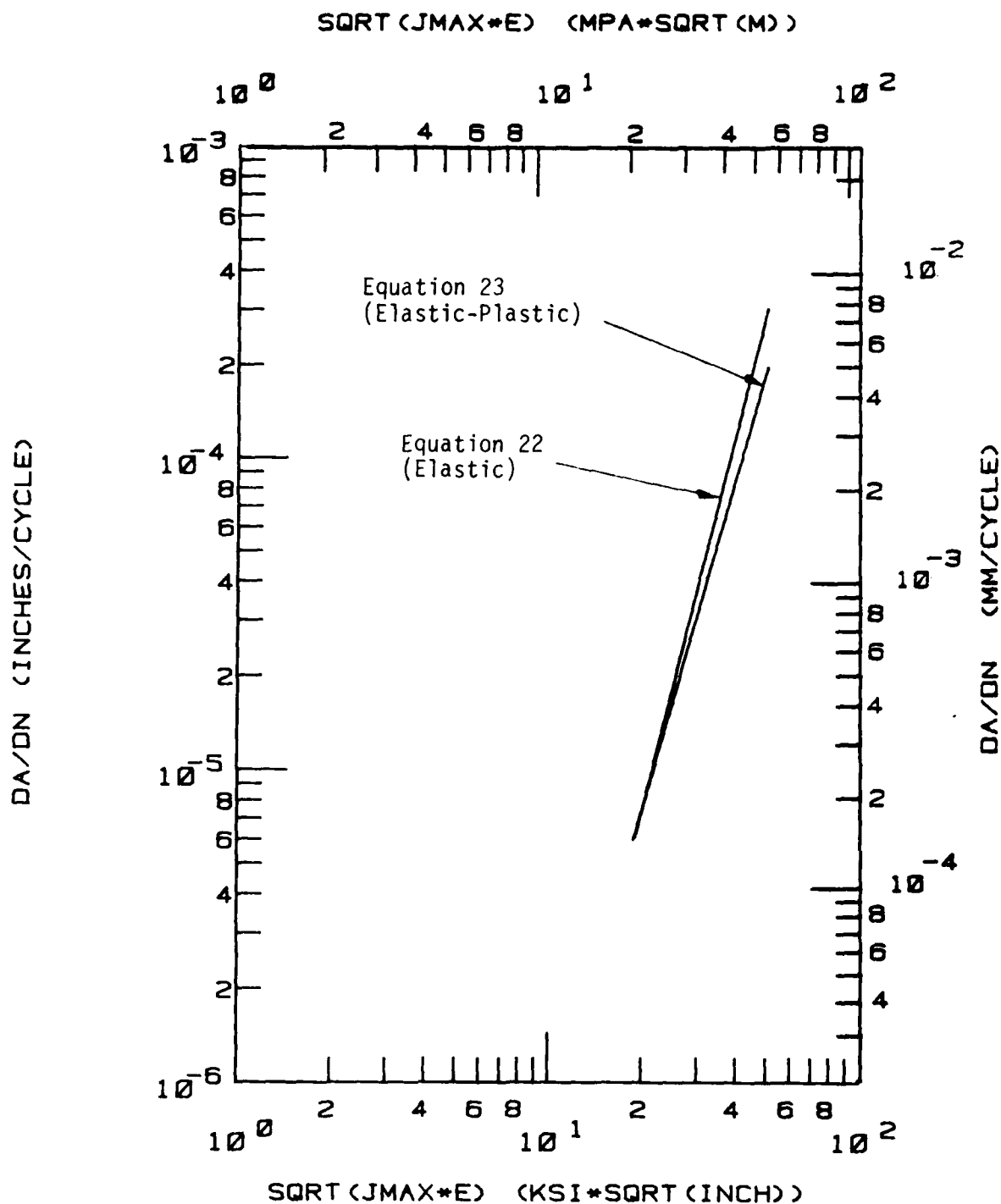
Figure 39. Comparison of the Elastic and (Numerical) Elastic-
Plastic Parametric Correlations of the Baseline
Fatigue Crack Growth Rate Data.

65
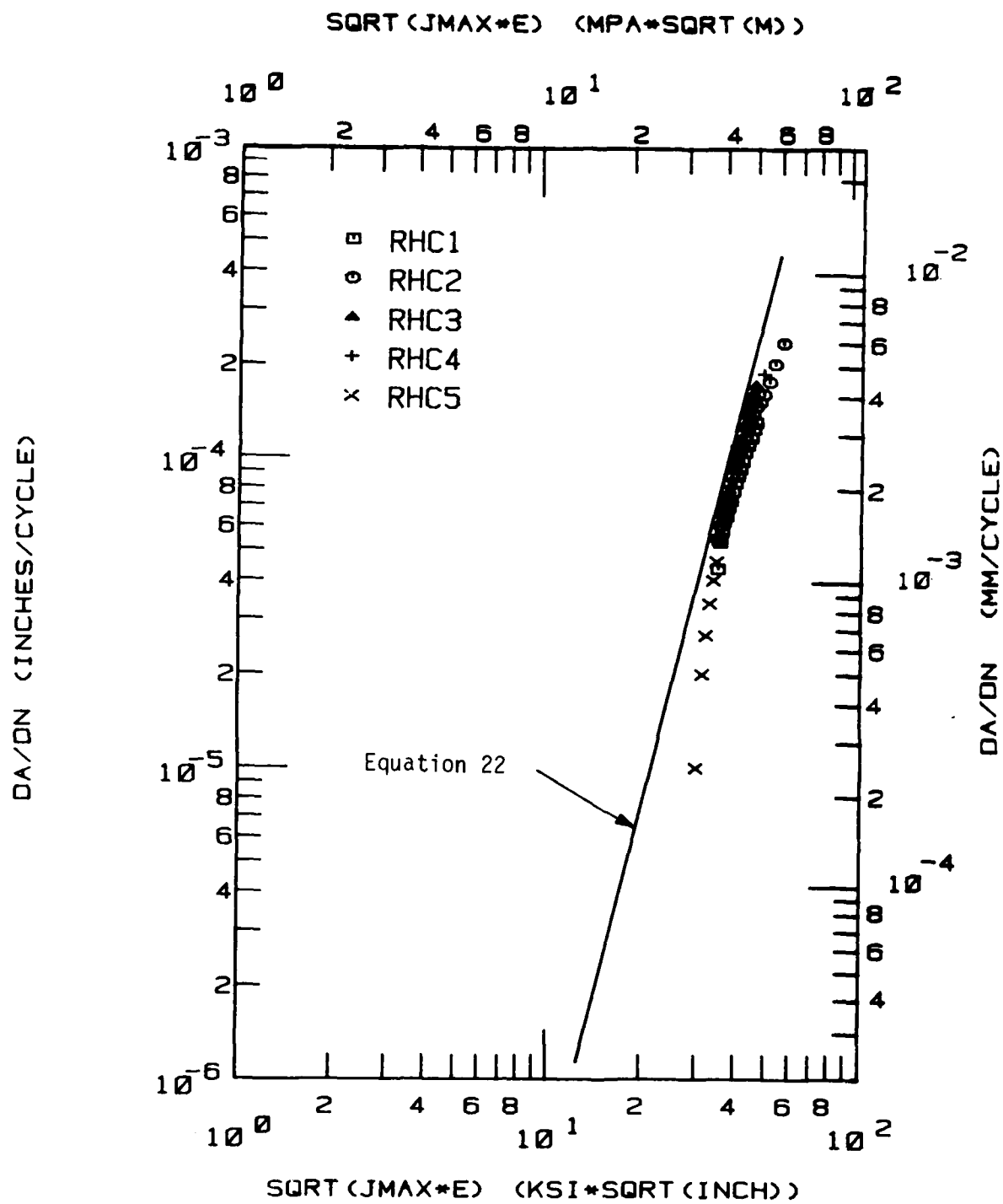
Figure 40. Elastic Baseline Crack Growth Rate Curve Compared to RHC Data Correlated Using Numerical Elastic-Plastic Parameters.

the elastic baseline (Equation 22) is compared to the RHC fatigue
crack growth rate data correlated using the numerical elastic-
plastic $\sqrt{J_{max}E}$ parameter. Table 4 provides the corresponding
life predictions based on this approach. Just how conservative this
approach is relative to life can be determined by comparing the
life prediction ratios in Table 4 to those in Table 3.

An approach based on an elastic baseline and on an
elastic-plastic parameter for the structure was previously
suggested by Ratwani et al.[26] for a structural airframe problem.
Ratwani et al. studied the crack growth behavior at large semi-
circular notches subjected to a substantial amount of localized
plasticity and developed a predictive crack growth life analysis
based on a J-integral approach. While the application of the J-
integral approach was in itself not new, they provided a systematic
approach to developing the structural parameter J via analysis
and estimating crack growth rate through

$$\frac{da}{dN} = f \ (K_{max}^{T}, R).$$
(25)

which was derived using long crack data collected under nominally
elastic conditions. For the structural geometry of interest, the
parameter of K_{max}^{T} was obtained from

$$K_{max}^{T} = K_{max} \left(\frac{J_T}{J_{e\ell}}\right)^{\frac{1}{2}}$$
(26)

where K_{max} is the maximum stress-intensity factor obtained in the
traditional way and where the terms J_T AND $J_{e\ell}$ represent the J-
integral values obtained from a finite element analysis of the
structure assuming elastic-plastic and elastic material behavior,
respectively. Figure 41 provides an evaluation of the Ratwani
et al. $(J_T/J_{e\ell})^{\frac{1}{2}}$ factor for a crack growing from a 0.50 inch
radius semi-circular notch in 7075-T7351. Using their approach,
reasonable estimates of the variable amplitude fatigue life data
were obtained whereas a purely elastic based approach (elastic
baseline and elastic structural parameter) resulted in very non-
conservative life predictions.

67

TABLE 4

LIFE PREDICTIONS USING THE ELASTIC BASELINE DATA AND
THE ELASTIC-PLASTIC PARAMETER $\sqrt{J_\varepsilon}$

Specimen ID	a_o (mm)	a_f (mm)	N_p Predicted	N/A Actual	(N_p/N_A)
RHC1	0.89	13.77	4790	7441	0.64
RHC2	0.86	13.79	4830	6241	0.77
RHC3	1.14	9.32	2070	2661	0.78
RHC4	1.57	9.42	1390	2501	0.76
RHC5	0.20	15.39	6030	12600	0.48

CRACK LENGTH (MM)
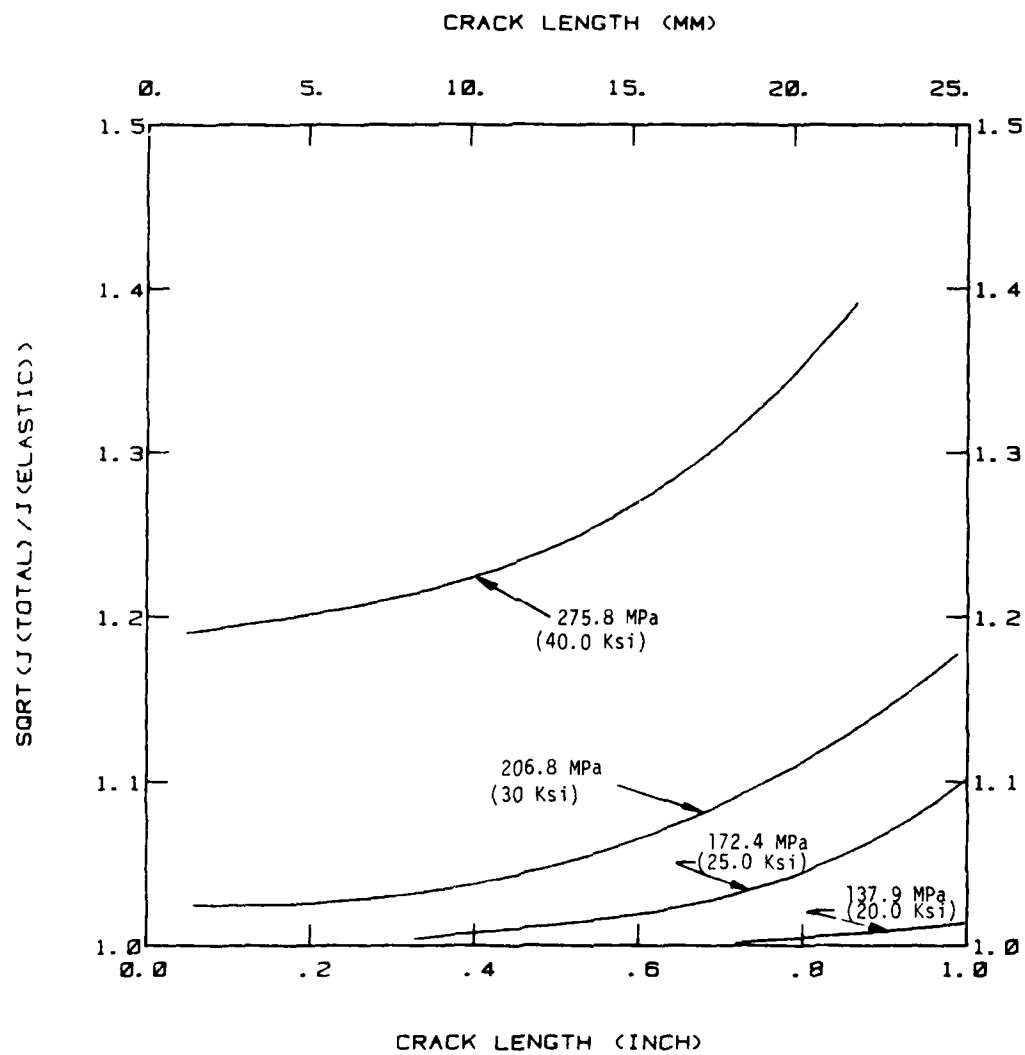
Figure 41.   Plastic Correction Factor for 7075-T7351 Aluminum
with a Semi-Circular (0.50 Inch Radius) Notch,
Derived from Reference 26.

69

One of the strongest enticements for using the Ratwani, et al. approach is that one can use the current constant amplitude data base as the starting point for a life analysis. However, if one has to compute the J-integral values for every geometry and every material of interest via a finite element procedure, the initial enticement is quickly lost. Shih and his co-workers have noticed this particular drawback and have developed procedures to obtain estimates of J_T for various crack geometries. These estimates are expressed in functional forms that allow one to generalize the finite element results obtained for one material. General Electric recently prepared a report for the Electric Power Research Institute that summarized their work on this technique[15]. We have followed the work of Shih and his co-workers since we believe that their methodology is applicable to the subcritical crack growth problem. During an earlier phase of our evaluation, a report was issued which described this approach to estimating the J-integral and other related field parameters[23].

4.2.2 Concerns and Assumptions

During the course of this investigation there were a series of assumptions made relative to the modeling of the material behavior. This paragraph reviews and discusses the assumptions and some of the authors' concerns.

4.2.2.1 Choice of Material

The ETP copper was chosen for the study because it exhibited almost elastic perfectly plastic stress-strain behavior. It was anticipated that this material would exhibit substantial cyclic plasticity throughout the fatigue crack growth test. In particular, we were anticipating that large cyclic plastic zones would be created at the edge of the hole in the RHC specimens. A preliminary set of finite element calculations based on the monotonic stress-strain behavior showed (See Figures 42 and 43) that a substantial amount of plasticity would occur at the hole (uncracked configuration).
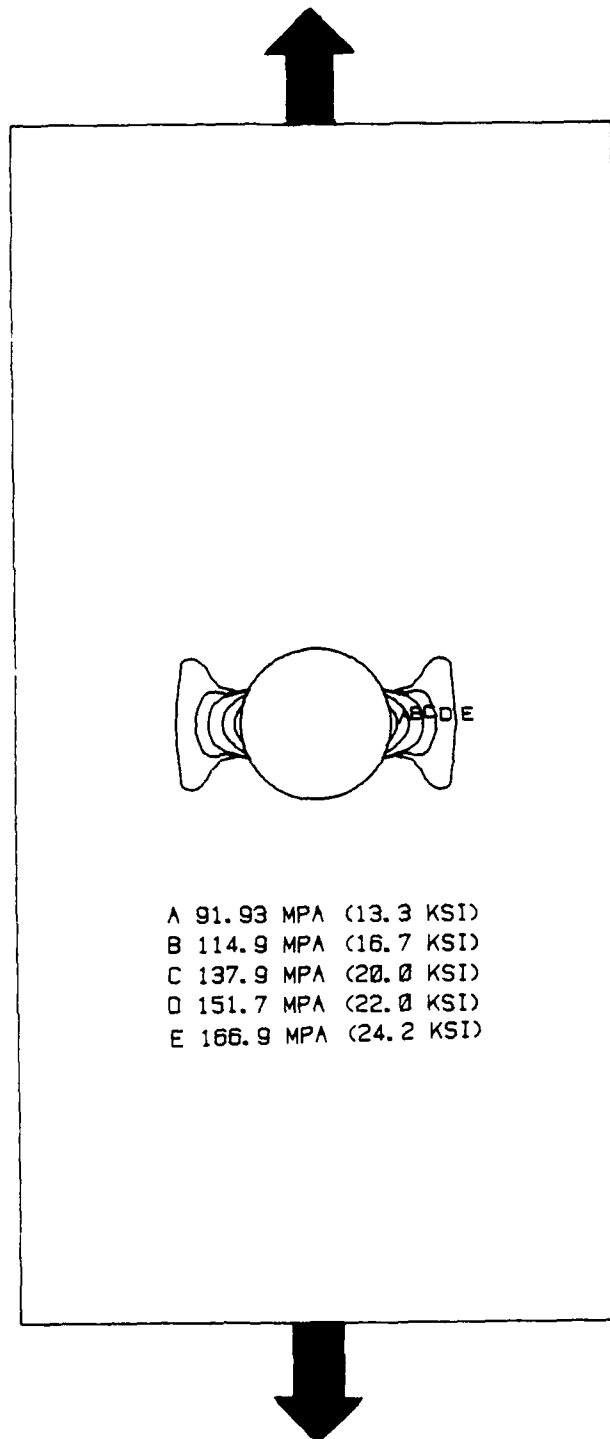
Figure 42. Extent of Plastic Zone Size for a 1-inch
            Diameter Hole in a 4-inch Wide Copper Plate
            Subjected to the Loading Indicated (Based on
            Monotonic Loading).

71
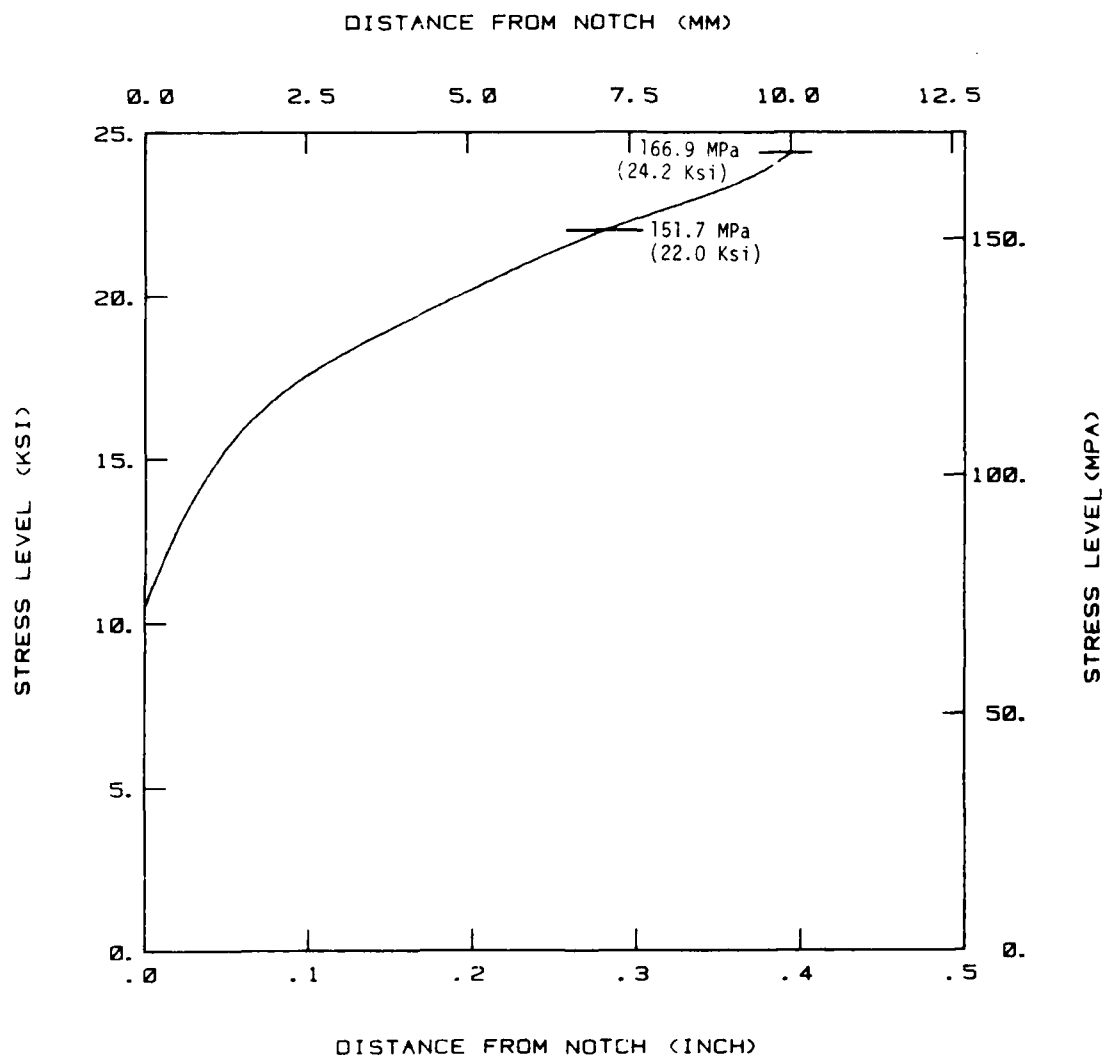
Figure 43. Extent of Plastic Zone Size Along the Expected
Path of the Crack (Based on Monotonic Loading).

During the course of experiments, we noted that the material exhibited linear load-displacement behavior for the most part with the exception of test start-up and for crack length conditions approaching critical levels.

In fact, when experiments were performed to monitor the strains at the notch during first and subsequent cyclic loading, we noted that significant reduction of notch strain occurred. The results of this test are shown in Figure 44 for a strain gage located 1.27mm (0.05 inch) from the hole edge. As expected, the cyclic strains were much smaller than the monotonic strains because of the redistribution of stresses following first yielding. The finite element calculations simulated the monotonic strains to within 5 percent of the experimental results but substantially overestimated the strains during cycling.

Despite this overestimation of cyclic plastic strains, the life predictions obtained from the finite element based elastic- $\sqrt{J_{max}E}$ were good. (Refer to Table 3 for a summary of the life prediction results.) By incorporating the residual stress behavior into the calculations of J_{max}, the correlation parameter would give a mean trend curve that is bounded by the elastic and elastic-plastic correlations shown in Figure 39.

One additional difficulty worth noting is that due to the toughness of the copper relative to the yield strength, failures occurred by net section yielding rather than by a fracture criteria. This made it difficult to obtain crack growth rate data in the region above 10^{-4} inch/cycle in the center crack panel specimens.

STRAIN (MM/MM)
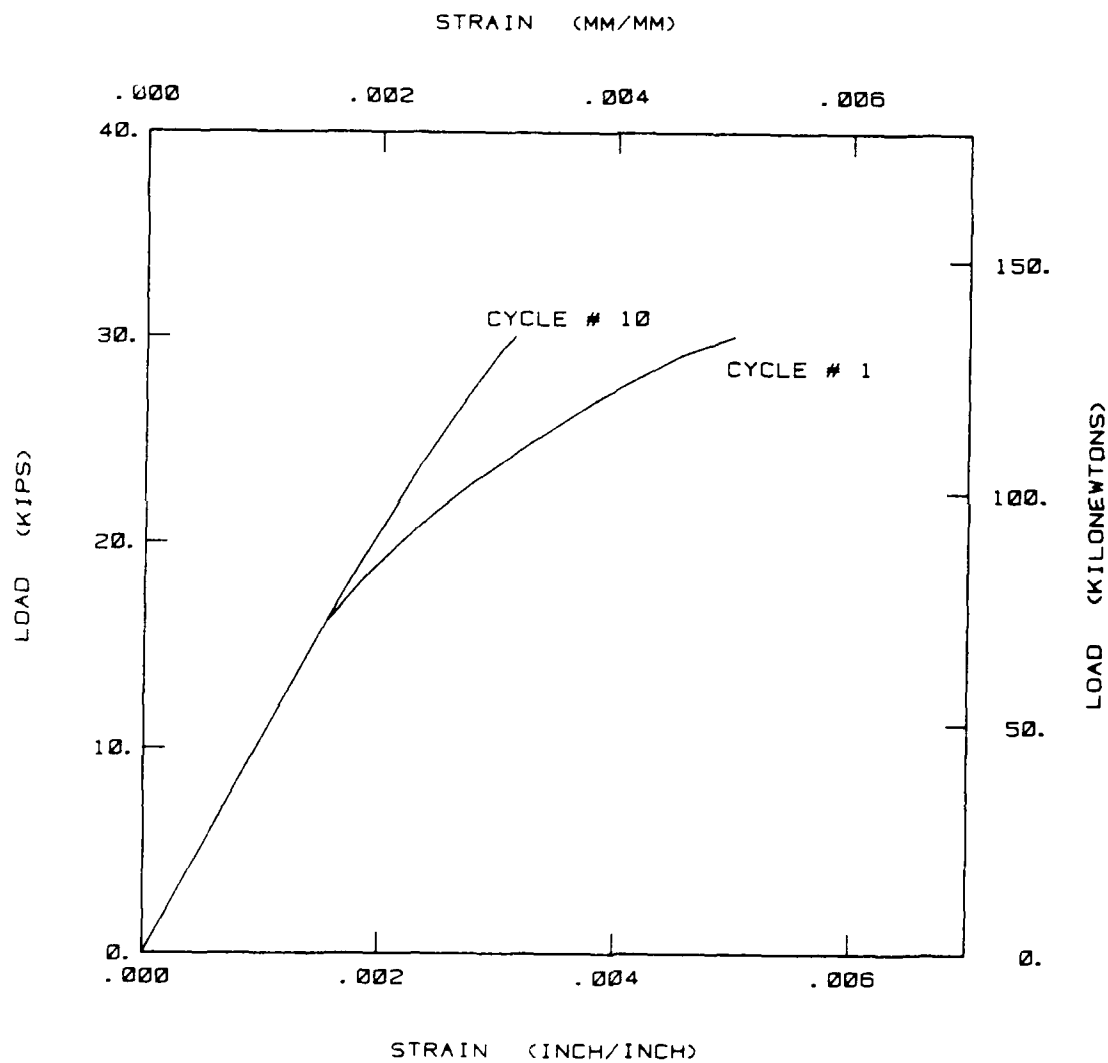
Figure 44. Surface Strains at a Distance of 0.05 Inch (1.27 mm) from the Hole Edge. Strains were Measured with Conventional Foil Strain Gages.

4.2.2.2 Choice of J as a Driving Force

There is one basic, but overriding, assumption made relative to using the J-integral as the crack driving force. This assumption is that the J-integral calculations primarily measure the change in the potential energy of deformation as a function of crack length. As long as the material remains primarily elastic, the assumption is valid. Our concerns are that the load-displacement behavior measured during the cyclic crack extension senses recoverable as well as non-recoverable energy associated with crack extension. Equation 13 was initially based on nonlinear elastic material behavior, and thus only senses the change in recoverable (or stored) energy during the crack extension process. Our concerns were heightened as a result of the RHC test results.

In the RHC tests, there was a non-recoverable cyclic plastic deformation process occurring on both sides of the hole while only the radial crack was extending. We believe that this is the major part of the reason why the crack growth correlations failed for the experimental $\sqrt{J_{max} \cdot E}$ parameter. Since the experimental method measured non-recoverable (cyclic plasticity) work associated with the uncracked side of the hole, and this non-recoverable work was not associated with the cracking process, it identified a potential problem associated with measurements of non-recoverable work in general. Not withstanding the previous arguments of Paris [30], Rice [31] and Parks [32] based on steady state crack movements, we are concerned about incorporating the non-recoverable work in the calculations of the driving force without a clear understanding of their contribution to the cracking process.

The above remarks are made even though it has been shown here and elsewhere [1, 27-29] that incorporating nonlinear inelastic material behavior for J-integral calculation will provide good crack growth rate correlation when the inelastic behavior is directly associated with the crack tip region as in CT and CCP geometries. While the numerical line integral results were also shown to correlate the RHC geometry cracking rates, it would

be advisable to further investigate the specific contribution that the cyclic non-recoverable work processes have on the fatigue crack growth behavior.

4.3   RECOMMENDATIONS

The following recommendations for additional study are out-growths of difficulties encountered in the present study.

1.   Additional experimental J-parameter data should be collected using pin-loaded specimens. This would eliminate potential nonsymmetric loading conditions and provide unambiguous points to measure load point deflection. Any materials chosen for subsequent studies should include consideration of the ratio of toughness to yield strength and cyclic properties.

2.   Most of the available elastic-plastic fracture mechanics parameters are in some way related to the localized stress-strain field at the tip of the crack. The magnitude of elastic-plastic parameters in terms of the remote loading and geometrical conditions are heavily influenced by the material properties (described by constitutive models). For application, it will be necessary to generate convenient handbook procedures for calculating the parameters, in the manner suggested by Reference 15.

3.   Improved characterization of the fatigue cracking process should be obtained by detailed analytical crack tip studies where various crack tip criteria for crack extension are evaluated. These analytical growth studies should be compared with corresponding fatigue crack growth rate data.

SECTION 5
CONCLUSIONS

The following conclusions have been drawn from analysis of the test data and results from other investigations cited herein:

1. The maximum stress-intensity factor, based on a linear elastic fracture mechanics approach was observed to correlate fatigue crack growth rate behavior reasonably well. Life predictions of the radial hole cracked (RHC) geometry were slightly nonconservative based on crack growth rate data obtained from center cracked panel (CCP) and compact (CT) specimen geometries.

2. The pseudo maximum stress-intensity factor parameter ($\sqrt{J_{max} \cdot E}$) based on finite element calculations and on the Shih et al. estimation scheme provided a good correlation of the crack growth rate behavior and improved life estimates of the RHC test geometries.

3. The experimentally based pseudo maximum stress-intensity factor parameter $\sqrt{J_{max} \cdot E}$ correlated the crack growth rate behavior of the CCP and CT geometries but not of the RHC test specimens. No life predictions were made here. The inability of this parameter to correlate the fatigue crack growth rate behavior from the RHC geometry is probably due to the measured inelastic behavior occurring on the non-cracked side of the hole.

4. Coupling an elastically based crack growth rate description with an elastic plastic (pseudo elastic) parameter evaluated for a given structure will result in conservative fatigue crack growth life predictions.

77

SECTION 6

REFERENCES

1. Dowling, N. E., and Begley, J. A., "Fatigue Crack Growth During Gross Plasticity and the J-Integral," Mechanics of Crack Growth, ASTM STP 590, American Society for Testing and Materials, 1976, pp. 82-103.

2. Rice, J. R., "A Path Independent Integral and the Approximate Analysis of Strain Concentration by Notches and Cracks," J. Applied Mech., Vol. 35, 1968, pp. 379-386.

3. Rice, R. R., "Fracture - An Advanced Treatise, Vol. II, Mathematical Fundamentals," Academic Press, New York, 1968, pp. 191-311.

4. Weerasooriya, T., Gallagher, J. P., and Rhee, H. C., "A Review of Nonlinear Fracture Mechanics Relative to Fatigue," AFML-TR-79-4196, Materials Laboratory, Air Force Wright Aeronautical Laboratories, Wright-Patterson AFB, OH, Dec., 1979.

5. Meyers, G. J., "Fracture Mechanics Criteria for Turbine Engine Hot Section Components - Final Report," NASA CR-167896, NASA-Lewis Research Center, Cleveland, OH, May 1982.

6. Trantina, G. G., and deLorenzi, H. G., "Elastic-Plastic Fracture Mechanics of Small Cracks." AMMRC-MS-82-4, Proceedings of the Army Symposium on Solid Mechanics, 1982 - Critical Mechanics Problems in Systems Design, AMMRC, Watertown, MA, Sept. 1982, pp. 203-214.

7. ASTM Standard E647-81, "Standard Test Method for Constant-Load-Amplitude Fatigue Crack Growth Rates Above 10^{-8} m/Cycle, ASTM Annual Book of Standards, Part 10, 1982, pp. 772-790.

8. ASTM Standard E399-81, "Standard Test Method for Plane-Strain Fracture Toughness of Metallic Materials," ASTM Annual Book of Standards, Part 10, 1982, pp. 592-622.

9. Brockman, R. A., "MAGNA Computer Program User's Manual," UDR-TR-80-107, November 1980.

10. Rajendran, A. M., "Introduction of Constant Triangle Elements and J-Integral Calculation Routines into MAGNA Program to Facilitate Solutions of Crack Problems," UDR-TM-82-21, July 1982.

11. Bowie, O. L., Journal of Mathematics and Physics, Vol. 35, 1956, pp. 60-71.

12. Grandt, A. ᴿ., Jr., "Stress Intensity Factors for Some Through Cracked Fastener Holes," Int. J. of Fracture, 1974.

13. Shih, C. C. and Kumar, V., "Estimation Techniques for the Prediction of Elastic-Plastic Fracture of Structural Components of Nuclear Systems," First Semiannual Report, July 1978 - January 1979 for EPRI Contract RP 1237-1, General Electric Company, Schenectady, N.Y., June 1, 1979.

14. Shih, C. F. and Hutchinson, J. S., "Fully Plastic Solutions and Large Scale Yielding Estimates for Plane Stress Crack Programs," J. of Engineering Materials and Technology, 1976, Vol. 98, pp. 289-295.

15. Kumar, V., German, M. D. and Shih, C. F., "Estimation of Technique for the Prediction of Elastic-Plastic Fracture of Structural Components of Nuclear Systems," Combined Second and Third Semiannual Report, Feb. 1979 to Jan. 1980 for EPRI, General Electric Company, SRD-8-094.

16. Rajendran, A. M., "Model Problems to Check the Validity of Constant Strain Triangle and J-Integral Routines in MAGNA," UDR-TM-83-08, University of Dayton Research Institute, Dayton, OH, January 1983.

17. Yamada, Y. and Yoshimura, N., "Plastic Stress-Strain Matrix and its Application for the Solution of Elastic-Plastic Problems by the Finite Element Method," Int. J. Mech. Sci., Vol. 10, 1968, pp. 343-354.

18. Ashbaugh, N. E. and Ahmad, J., "Finite Element Analysis of Some Full-and Partial-Ring Crack-Propagation Test Specimens," AFWAL-TR-82-4015, Materials Laboratory, Air Force Wright Aeronautical Laboratories, Wright-Patterson AFB, OH, March 1982.

19. Goldman, N. L. and Hutchinson, J. W., "Fully Plastic Crack Problems: The Center-Cracked Strip under Plane Strain." Int. J. Solids Structures, 1975, Vol. 11, pp. 575-591.

20. Hutchinson, J. W., Needleman, A., and Shih, C. F., "Fully Plastic Crack Problems in Bending and Tension," Fracture Mechanics, ed. N. Perrons, et al., University of Virginia, 1978, pp. 515-527.

21. Hutchinson, J. W., "Plastic Stress and Strain Fields at the Crack Tip," Journal of Mechanics and Physics of Solids, 1968, pp. 13-31, pp. 337-347.

22. Rice, J. R., and Rosengren, G. F., "Plane Strain Deformation Near a Crack Tip in Power-Law Hardening Material," Journal of Mechanics and Physics and Solids, 1968, pp. 1-12.

23. Weerasooriya, T. and Gallagher, J. P., "Determining Crack Tip Field Parameters for Elastic-Plastic Materials Via an Estimation Scheme," AFWAL-TR-81-4044, July 1981.

24. Sadananda, K. and Shahinian, P., "A Fracture Mechanics Approach to High Temperature Fatigue Crack Growth in Udimet 700," Engineering Fracture Mechanics, Vol. 11, pp. 73-84.

25. Hudak, S. J., Jr., Saxena, A., Bucci, R. J., and Malcom, R.C., "Development of Standard Methods of Testing and Analyzing Fatigue Crack Growth Rate Data (Third Semi-Annual Report)," Westinghouse Report on AFML Contract F33615-75-C-5064, Westinghouse Research Laboratories, Pittsburgh, PA 10 March 1977.

26. Ratwani, M. M., Wilhem, D. P., Carter, J. P., Kan, H. P., and Kaplan, M., "Fatigue Crack Growth at Stress Concentrations Subjected to Strains Beyond Elastic Range," J. of Aircraft, Vol. 18, No. 3, March 1981, pp. 206-212.

27. Vardar, O., "Fatigue Crack Propagation Beyond General Yield," J. of Engineering Materials and Technology, Vol. 104, No. 3, July 1982, pp.

28. Leis, B. N., "Fatigue Crack Propagation in an Inelastic Gradient Field," Proceedings Sixth SMIRT Conference, Paris, France, 1981, Vol. G, paper G8/5.

29. Hudak, S. J., Jr., "Small Crack Behavior and the Prediction of Fatigue Life," J. of Engineering Materials and Technology, Vol. 103, No. 1, January 1981, pp. 26-35.

30. Paris, P. C., "Fracture Mechanics in the Elastic-Plastic Regime," Flow Growth and Fracture, ASTM STP 631, American Society for Testing and Materials, 1977, pp. 3-27.

31. Rice, J.R., "Elastic-Plastic Fracture Mechanics," The Mechanics of Fracture, F. Erdogan, Applied Mechanics Division, American Society of Mechanical Engineers, Vol. 19, 1976, pp. 23-53.

32. Parks, D. M., "Reversed Plasticity from Unloading," Remarks presented at Conference on Elastic-Plastic Mechanics held at Washington University, St. Louis Mo., 31 May-2 June 1978.

APPENDIX A

CRACK GROWTH DATA

CRACK GROWTH DATA

THE FOLLOWING CRACK GROWTH DATA WERE COLLECTED FROM TESTS OF ETP COPPER
SAMPLES AT ROOM TEMPERATURE AND IN LABORATORY AIR.   THE FOLLOWING DATA APPLY
TO ALL SAMPLES OF THE TYPE LISTED

CCP

    WIDTH= 4.00 INCHES
    LENGTH= 22.0 INCHES
    CRACK LENGTHS LISTED ARE HALF CRACK LENGTHS CALCULATED BY DIVIDING
    THE TOTAL CRACK LENGTH BY 2.

RCH

    WIDTH= 4.00 INCHES
    THICKNESS= .375 INCHES
    LENGTH= 22.0 INCHES
    HOLE DIAMETER= 1.00 INCHES
    CRACK LENGTHS LISTED ARE MEASURED FROM THE EDGE OF THE HOLE TO THE
    CRACK TIP.

CT

    WIDTH= 2.00 INCHES
    THICKNESS= .500 INCHES
    CRACK LENGTHS LISTED ARE MEASURED FROM THE LOAD LINE TO THE CRACK TIP.

1

SPECIMEN ID= CCP2   # POINTS= 12   GROSS SECTION STRESS= 21.3 KSI
THICKNESS= .500 INCHES

CYCLES	A(INCH)
0.	.4970
871.	.5280
1371.	.5360
2051.	.5630
2701.	.5940
3522.	.6380
4061.	.6640
4431.	.6860
4791.	.7120
5081.	.7360
5291.	.7580
5531.	.7850

SPECIMEN ID= CCP3   # POINTS= 22   GROSS SECTION STRESS= 25.0 KSI
THICKNESS= .500 INCHES

CYCLES	A(INCH)
0.	.2610
290.	.2670
1600.	.2850
2190.	.2960
3340.	.3210
4635.	.3450
5510.	.3690
6305.	.3950
7190.	.4240
7730.	.4500
8140.	.4660
8700.	.4740
8700.	.4930
9080.	.5130
9410.	.5330
9720.	.5540
9951.	.5730
10250.	.5960
10560.	.6230
14751.	.6460
10945.	.6670
11088.	.6880

83

```
SPECIMEN ID= CCP7    # POINTS= 24    GROSS SECTION STRESS= 18.7 KSI
THICKNESS= .375 INCHES
  CYCLES      A(INCH)
  95000.      .1280
 100000.      .1390
 105000.      .1460
 110000.      .1500
 120000.      .1630
 130000.      .1780
 140000.      .2030
 150000.      .2320
 160000.      .2720
 170000.      .3280
 175000.      .3630
 180000.      .4110
 185000.      .4700
 189000.      .5350
 192000.      .6040
 194000.      .6630
 195000.      .7000
 196000.      .7460
 197000.      .7980
 197500.      .8280
 198000.      .8610
 198500.      .8990
 199000.      .9460
 199500.     1.0060
```

1

SPECIMEN ID= CT1   # POINTS= 21   APPLIED LOAD= 1.689 KIPS

CYCLES	A(INCH)
5957.	.5380
36150.	.5890
47630.	.6120
70210.	.6660
84410.	.7020
93770.	.7340
102540.	.7650
114610.	.8170
119810.	.8450
125050.	.8780
128320.	.9080
133000.	.9520
136000.	.9740
137451.	1.0020
138900.	1.0290
140837.	1.0670
142385.	1.1050
143810.	1.1480
144800.	1.1910
145516.	1.2310
146004.	1.2700

1

SPECIMEN ID= RCH1   # POINTS= 23   GROSS SECTION STRESS= 22.0 KSI

CYCLES	A(INCH)
0.	.0350
1070.	.0600
1790.	.0860
2294.	.1080
2650.	.1310
3071.	.1530
3445.	.1790
3811.	.2000
4201.	.2250
4551.	.2500
4881.	.2760
5181.	.3020
5541.	.3290
5811.	.3540
6051.	.3790
6321.	.4040
6551.	.4290
6761.	.4540
6961.	.4760
7141.	.5010
7302.	.5220
7441.	.5420
7581.	.5610

SPECIMEN ID= RCH2   # POINTS= 27   GROSS SECTION STRESS= 22.0 KSI

CYCLES	A(INCH)
0.	.0340
591.	.0570
1151.	.0810
1641.	.1080
2101.	.1400
2521.	.1610
2861.	.1870
3211.	.2120
3541.	.2390
3831.	.2630
4121.	.2880
4361.	.3140
4631.	.3400
4901.	.3680
5131.	.3930
5371.	.4220
5571.	.4470
5741.	.4730
5921.	.5010
6091.	.5220
6241.	.5430
6381.	.5710
6481.	.5850
6631.	.6180
6723.	.6440
6861.	.6790
6971.	.7250

86

1
```
SPECIMEN ID= CT1        # POINTS= 21     APPLIED LOAD= 1.689 KIPS
   CYCLES      A(INCH)
    5957.       .5380
   36150.       .5890
   47630.       .6120
   70210.       .6660
   84410.       .7020
   93770.       .7340
  102540.       .7650
  114610.       .8170
  119810.       .8450
  125053.       .8780
  128320.       .9080
  133000.       .9520
  135000.       .9740
  137051.      1.0020
  138900.      1.0290
  140837.      1.0670
  142385.      1.1050
  143810.      1.1480
  144800.      1.1910
  145516.      1.2310
  146004.      1.2700
```

85

```
SPECIMEN ID= RCH3     # POINTS= 13    GROSS SECTION STRESS= 24.2 KSI
    CYCLES      A(INCH)
     21.         .0450
    451.         .0710
    781.         .0990
   1081.         .1290
   1331.         .1540
   1521.         .1790
   1721.         .2070
   1911.         .2330
   2091.         .2620
   2281.         .2940
   2421.         .3180
   2571.         .3450
   2661.         .3670
SPECIMEN ID= RCH4     # POINTS= 14    GROSS SECTION STRESS= 24.2 KSI
    CYCLES      A(INCH)
      0.         .0620
     31.         .0640
    371.         .0910
    801.         .1290
   1031.         .1560
   1311.         .1930
   1511.         .2200
   1721.         .2490
   1911.         .2790
   2111.         .3120
   2221.         .3280
   2341.         .3490
   2431.         .3710
   2501.         .3960
SPECIMEN ID= RCH5     # POINTS= 24    GROSS SECTION STRESS= 22.0 KSI
   1000.         .0080
   5000.         .0170
   6070.         .0290
   6570.         .0355
   6970.         .0430
   7370.         .0565
   7770.         .0640
   8100.         .0790
   8400.         .0935
   8700.         .1105
   9000.         .1245
   9500.         .1545
  10000.         .1895
  10500.         .2185
  11000.         .2610
  11300.         .2915
  11600.         .3175
  11900.         .3515
  12200.         .3895
  12500.         .4310
  12800.         .4655
  13100.         .5065
  13400.         .5655
  13600.         .6060
```

87

APPENDIX B

LOAD-DEFLECTION PRESENTED FOR GIVEN CRACK LENGTHS

LOAD-DEFLECTION DATA

THE FOLLOWING DATA WERE COLLECTED FROM TESTS ON ETP COPPER.   DETAILS
OF THE TEST CONDITIONS ARE DESCRIBED IN APPENDIX A.

RCH-5
****
```
 CURVE #1   A= 0.1245 INCHES
 DEFL.    LOAD
(INCH)   (POUNDS)
 .0         0.
 .00104 2915.
 .00237 6655.
 .0037 10395.
 .00511 14195.
 .00687 19195.
 .00871 24195.
 .01055 29170.
 .01079 29645.
 CURVE #2   A= 0.1545 INCHES
 DEFL.    LOAD
(INCH)   (POUNDS)
 .0         0.
 .00146 4120.
 .00324 9125.
 .00502 14130.
 .00687 19135.
 .00873 24140.
 .01066 29145.
 .01084 29605.
 CURVE #3   A= 0.1895 INCHES
 DEFL.    LOAD
(INCH)   (POUNDS)
 .0         0.
 .00141 4090.
 .00322 9080.
 .00506 14100.
 .00686 19090.
 .00876 24080.
 .01087 29590.
 CURVE #4   A= 0.2185 INCHES
 DEFL.    LOAD
(INCH)   (POUNDS)
 .0         0.
 .0015 4085.
 .00323 9070.
 .00504 14125.
 .00692 19100.
 .0088 24110.
 .01097 29575.
 CURVE #5   A= 0.261 INCHES
 DEFL.    LOAD
(INCH)   (POUNDS)
 .0         0.
 .00148 4045.
 .00326 9060.
 .00504 14040.
 .00697 19065.
 .00883 24065.
 .01096 29550.
```

90

```
CURVE #6   A= 0.2915 INCHES
DEFL.    LOAD
(INCH)   (POUNDS)
.0          0.
.00149  4055.
.00328  9060.
.00516  14065.
.00693  19070.
.00891  24075.
.01106  29550.
CURVE #7   A= 0.3175 INCHES
DEFL.    LOAD
(INCH)   (POUNDS)
.0          0.
.00139  3995.
.00318  9015.
.0051   14045.
.00692  19000.
.00884  24020.
.01106  29520.
CURVE #8   A= 0.3515 INCHES
DEFL.    LOAD
(INCH)   (POUNDS)
.0          0.
.00146  4025.
.00324  9020.
.0051   14015.
.00692  19010.
.00893  24045.
.0109   29015.
.01111  29510.
CURVE #9   A= 0.3895 INCHES
DEFL.    LOAD
(INCH)   (POUNDS)
.0          0.
.00148  4005.
.00332  9040.
.00515  14035.
.00706  19030.
.00903  24025.
.01124  29495.
CURVE #10   A= 0.431 INCHES
DEFL.    LOAD
(INCH)   (POUNDS)
.0          0.
.00143  4045.
.00333  9070.
.00516  14065.
.00705  19060.
.00906  24055.
.0113   29535.
```

```
CURVE #11   A= 0.4655 INCHES
DEFL.      LOAD
(INCH)     (POUNDS)
.0          0.
.00148  4035.
.00331  9020.
.00525  14030.
.00713  19040.
.00916  24050.
.0115  29515.
CURVE #12   A= 0.5065 INCHES
DEFL.      LOAD
(INCH)     (POUNDS)
.0          0.
.00148  4080.
.00338  9095.
.0052  14110.
.00721  19125.
.00922  24105.
.01161  29595.
CURVE #13   A=0.5655 INCHES
DEFL.      LOAD
(INCH)     (POUNDS)
.0          0.
.00157  4135.
.00346  9145.
.00543  14155.
.00737  19140.
.00944  24160.
.01195  29695.
CURVE #14   A=0.606 INCHES
DEFL.      LOAD
(INCH)     (POUNDS)
.0          0.
.00158  4155.
.00351  9185.
.00548  14195.
.0075  19205.
.00958  24185.
.01221  29655.
```

CT-1
****
 CURVE #1 A= 0.508 INCHES
 DEFL.   LOAD
 (INCH)   (POUNDS)
 .00000   0.
 .00011   46.
 .00023   92.
 .00034   178.
 .00047   184.
 .00055   230.
 .00066   277.
 .00078   323.
 .00089   369.
 .00099   415.
 .00110   461.
 .00123   507.
 .00136   553.
 .00146   599.
 .00159   645.
 .00172   691.
 .00181   737.
 .00193   783.
 .00207   830.
 .00216   876.
 .00231   922.
 .00241   968.
 .00254   1014.
 .00267   1060.
 .00280   1106.
 .00290   1152.
 .00302   1198.
 .00315   1244.
 .00328   1290.
 .00341   1336.
 .00354   1383.
 .00365   1429.
 .00377   1475.
 .00388   1519.

```
CURVE #2   A= 0.589 INCHES
DEFL.      LOAD
(INCH)     (POUNDS)
.00000        0.
.00011       48.
.00024       96.
.00037      144.
.00050      192.
.00064      240.
.00076      288.
.00089      336.
.00102      384.
.00117      432.
.00129      481.
.00141      529.
.00155      577.
.00167      625.
.00180      673.
.00193      721.
.00208      769.
.00220      817.
.00235      865.
.00248      913.
.00260      961.
.00275     1009.
.00296     1057.
.00299     1105.
.00313     1153.
.00326     1201.
.00340     1249.
.00353     1297.
.00367     1345.
.00383     1393.
.00397     1442.
.00410     1490.
.00420     1520.
```

94

```
CURVE #3   A= 0.612 INCHES
 DEFL.    LOAD
(INCH)   (POUNDS)
.00000        0.
.00011       46.
.00024       91.
.00037      137.
.00050      182.
.00063      228.
.00076      273.
.00089      319.
.00102      364.
.00115      410.
.00128      455.
.00141      501.
.00153      546.
.00166      592.
.00179      637.
.00192      683.
.00205      728.
.00218      774.
.00231      819.
.00244      865.
.00259      910.
.00271      956.
.00283     1001.
.00297     1047.
.00310     1093.
.00324     1138.
.00337     1184.
.00351     1229.
.00364     1275.
.00378     1320.
.00392     1366.
.00406     1411.
.00420     1457.
.00433     1502.
.00440     1520.
```

```
CURVE #4   AT 0.666 INCHES
   DEFL.     LOAD
 (INCH)    (POUNDS)
 .00000          0.
 .00014         50.
 .00030        101.
 .00046        151.
 .00062        201.
 .00078        251.
 .00094        302.
 .00110        352.
 .00126        402.
 .00142        453.
 .00158        503.
 .00174        553.
 .00190        604.
 .00206        654.
 .00220        704.
 .00237        754.
 .00251        805.
 .00267        855.
 .00284        905.
 .00300        956.
 .00317       1006.
 .00333       1056.
 .00350       1107.
 .00366       1157.
 .00383       1207.
 .00399       1257.
 .00416       1308.
 .00432       1358.
 .00449       1408.
 .00465       1459.
 .00482       1509.
 .00485       1519.
```

```
CURVE #5   A= 0.702 INCHES
DEFL.    LOAD
(INCH)   (POUNDS)
.00000        0.
.00017       51.
.00033      102.
.00049      153.
.00069      203.
.00084      254.
.00103      305.
.00121      356.
.00139      407.
.00157      458.
.00175    . 509.
.00189      559.
.00207      610.
.00225      661.
.00243      712.
.00261      763.
.00277      814.
.00293      865.
.00313      915.
.00330      966.
.00350     1017.
.00367     1068.
.00383     1119.
.00402     1170.
.00421     1221.
.00439     1272.
.00456     1322.
.00474     1373.
.00491     1424.
.00509     1475.
.00526     1520.
```

```
CURVE #6   A= 0.734 INCHES
  DEFL.     LOAD
 (INCH)    (POUNDS)
 .00000         0.
 .00016        47.
 .00033        93.
 .00050       140.
 .00066       186.
 .00083       233.
 .00101       279.
 .00118       326.
 .00135       372.
 .00152       419.
 .00169       465.
 .00186       512.
 .00203       558.
 .00220       605.
 .00237       651.
 .00254       698.
 .00271       744.
 .00288       791.
 .00305       837.
 .00322       884.
 .00339       930.
 .00356       977.
 .00373      1023.
 .00390      1070.
 .00407      1116.
 .00425      1163.
 .00444      1209.
 .00461      1256.
 .00478      1302.
 .00495      1349.
 .00512      1395.
 .00530      1442.
 .00549      1488.
 .00560      1520.
```

CURVE #7   A= 0.765 INCHES

DEFL. (INCH)	LOAD (POUNDS)
.00000	0.
.00024	61.
.00048	122.
.00072	183.
.00096	244.
.00120	305.
.00144	366.
.00168	427.
.00189	488.
.00214	549.
.00239	610.
.00262	671.
.00285	732.
.00308	793.
.00334	854.
.00358	915.
.00381	976.
.00406	1037.
.00429	1098.
.00455	1159.
.00479	1220.
.00504	1281.
.00528	1341.
.00553	1402.
.00578	1463.
.00604	1520.

CURVE #8   A= 0.817 INCHES

DEFL. (INCH)	LOAD (POUNDS)
.00000	0.
.00024	64.
.00053	127.
.00081	193.
.00109	260.
.00137	323.
.00165	391.
.00193	455.
.00221	521.
.00249	587.
.00277	653.
.00305	715.
.00333	777.
.00361	839.
.00389	904.
.00417	968.
.00445	1036.
.00473	1096.
.00501	1163.
.00529	1224.
.00557	1282.
.00585	1349.
.00613	1407.
.00641	1467.
.00663	1520.

99

```
CURVE #9   A= 0.845 INCHES
DEFL.    LOAD
(INCH)   (POUNDS)
.00000      0.
.00020     51.
.00039     92.
.00059    134.
.00078    175.
.00098    219.
.00117    262.
.00137    306.
.00156    346.
.00176    392.
.00195    437.
.00215    476.
.00234    515.
.00254    559.
.00273    601.
.00293    643.
.00312    689.
.00332    730.
.00351    770.
.00371    814.
.00390    856.
.00410    903.
.00429    937.
.00449    980.
.00468   1021.
.00488   1061.
.00507   1102.
.00527   1142.
.00546   1183.
.00566   1223.
.00585   1264.
.00605   1304.
.00624   1345.
.00644   1388.
.00663   1429.
.00683   1465.
.00702   1506.
.00709   1520.
```

```
CURVE #10   A= 0.878 INCHES
DEFL.    LOAD
(INCH)   (POUNDS)
.00000       0.
.00024      50.
.00047      98.
.00071     145.
.00094     192.
.00118     240.
.00141     285.
.00165     330.
.00188     380.
.00212     429.
.00235     474.
.00259     523.
.00282     571.
.00306     615.
.00329     664.
.00353     713.
.00376     755.
.00400     803.
.00423     850.
.00447     897.
.00470     944.
.00494     992.
.00517    1036.
.00541    1081.
.00564    1125.
.00588    1170.
.00611    1218.
.00635    1265.
.00658    1308.
.00682    1358.
.00705    1401.
.00729    1447.
.00752    1490.
.00767    1521.
```

```
CURVE #11   A= 0.908 INCHES
DEFL.    LOAD
(INCH)   (POUNDS)
.00000       0.
.00025      49.
.00049      95.
.00074     141.
.00098     188.
.00123     234.
.00147     280.
.00172     325.
.00196     373.
.00221     420.
.00245     469.
.00270     514.
.00294     559.
.00319     604.
.00343     652.
.00368     700.
.00392     745.
.00417     791.
.00441     837.
.00466     882.
.00490     928.
.00515     973.
.00539    1019.
.00564    1066.
.00588    1111.
.00613    1157.
.00637    1202.
.00662    1250.
.00686    1293.
.00711    1341.
.00735    1383.
.00760    1429.
.00784    1472.
.00811    1520.
```

CURVE #12   A= 0.952 INCHES

DEFL. (INCH)	LOAD (POUNDS)
.00000	0.
.00027	47.
.00054	94.
.00081	137.
.00108	183.
.00135	231.
.00162	272.
.00189	319.
.00216	367.
.00243	416.
.00270	465.
.00297	514.
.00324	558.
.00351	599.
.00378	646.
.00405	693.
.00432	742.
.00459	790.
.00489	837.
.00518	889.
.00548	941.
.00577	989.
.00607	1040.
.00636	1088.
.00666	1136.
.00695	1190.
.00725	1237.
.00754	1288.
.00784	1337.
.00813	1385.
.00843	1433.
.00872	1479.
.00897	1521.

CURVE #13   A= 0.974 INCHES

DEFL. (INCH)	LOAD (POUNDS)
.00000	0.
.00043	69.
.00086	138.
.00129	207.
.00172	276.
.00215	351.
.00258	421.
.00301	494.
.00344	563.
.00387	633.
.00430	702.
.00473	771.
.00516	842.
.00559	911.
.00602	980.
.00645	1049.
.00688	1118.
.00731	1187.
.00774	1256.
.00817	1322.
.00860	1389.
.00903	1455.
.00948	1520.

```
CURVE #14   A= 1.002 INCHES
DEFL.    LOAD
(INCH)   (POUNDS)
.00000        0.
.00039       58.
.00077      114.
.00116      174.
.00154      234.
.00193      292.
.00231      352.
.00270      413.
.00308      470.
.00347      529.
.00385      589.
.00424      648.
.00462      708.
.00501      763.
.00539      823.
.00578      883.
.00616      941.
.00655      998.
.00693     1058.
.00732     1115.
.00770     1169.
.00809     1228.
.00847     1286.
.00886     1341.
.00924     1397.
.00963     1452.
.01001     1508.
.01010     1521.
```

```
CURVE #15   A= 1.029 INCHES
  DEFL.     LOAD
 (INCH)    (POUNDS)
 .00000       0.
 .00036       54.
 .00073      105.
 .00110      157.
 .00149      209.
 .00182      259.
 .00216      308.
 .00249      354.
 .00283      404.
 .00316      451.
 .00350      501.
 .00383      550.
 .00417      597.
 .00450      647.
 .00484      694.
 .00517      742.
 .00551      789.
 .00584      834.
 .00618      885.
 .00651      929.
 .00685      976.
 .00718     1024.
 .00752     1071.
 .00785     1118.
 .00819     1163.
 .00852     1211.
 .00886     1256.
 .00919     1301.
 .00953     1347.
 .00986     1392.
 .01020     1437.
 .01053     1481.
 .01082     1520.
```

```
CURVE #16   A= 1.067 INCHES
DEFL.    LOAD
(INCH)   (POUNDS)
.00000       0.
.00037      48.
.00074      95.
.00111     143.
.00148     191.
.00185     240.
.00222     288.
.00259     337.
.00296     385.
.00333     434.
.00370     483.
.00407     533.
.00444     580.
.00481     630.
.00518     676.
.00555     727.
.00592     773.
.00629     823.
.00666     872.
.00703     916.
.00740     966.
.00777    1014.
.00814    1060.
.00851    1107.
.00888    1153.
.00925    1199.
.00962    1246.
.00999    1292.
.01036    1336.
.01073    1380.
.01110    1426.
.01147    1470.
.01189    1520.
```

```
CURVE #17   A= 1.105 INCHES
DEFL.     LOAD
(INCH)    (POUNDS)
.00000          0.
.00045         52.
.00089        105.
.00134        157.
.00178        207.
.00223        262.
.00267        315.
.00312        368.
.00356        422.
.00401        476.
.00445        529.
.00490        583.
.00534        635.
.00579        689.
.00623        743.
.00668        796.
.00712        847.
.00757        899.
.00801        950.
.00846       1002.
.00890       1055.
.00935       1104.
.00979       1156.
.01024       1205.
.01068       1257.
.01113       1305.
.01157       1355.
.01202       1406.
.01246       1454.
.01291       1502.
.01305       1520.
```

```
CURVE #18   A= 1.148 INCHES
 DEFL.    LOAD
(INCH)   (POUNDS)
.00000         0.
.00046        47.
.00091        94.
.00137       142.
.00182       189.
.00228       238.
.00273       286.
.00319       335.
.00364       384.
.00410       433.
.00455       481.
.00501       528.
.00546       578.
.00592       624.
 00637       675.
.00683       723.
. 0728       769.
.00774       819.
.00819       869.
.00865       913.
.00910       959.
.00956      1005.
.01001      1052.
.01047      1098.
.01092      1144.
.01138      1190.
.01183      1234.
.01229      1281.
.01274      1327.
.01320      1372.
.01365      1414.
.01411      1458.
.01456      1504.
.01474      1520.
```

```
CURVE #19   A= 1.191 INCHES
 DEFL.    LOAD
(INCH)   (POUNDS)
.00000         0.
.00059        54.
.00118       108.
.00177       164.
.00236       219.
.00295       275.
.00354       330.
.00413       388.
.00472       443.
.00531       500.
.00590       557.
.00649       611.
.00708       669.
.00767       725.
.00826       777.
.00885       834.
.00944       889.
.01003       943.
.01062       996.
.01121      1050.
.01180      1101.
.01239      1156.
.01298      1205.
.01357      1260.
.01416      1310.
.01475      1362.
.01534      1412.
.01593      1464.
.01663      1521.
```

```
CURVE #20   A= 1.231 INCHES
 DEFL.     LOAD
(INCH)    (POUNDS)
.00000         0.
.00059        49.
.00117        97.
.00176       146.
.00234       176.
.00293       247.
.00351       294.
.00410       345.
.00468       394.
.00527       444.
.00585       494.
.00644       544.
.00702       594.
.00761       643.
.00819       692.
.00878       742.
.00936       790.
.00995       838.
.01053       887.
.01112       933.
.01170       981.
.01229      1029.
.01287      1075.
.01346      1121.
.01404      1167.
.01463      1212.
.01521      1260.
.01580      1304.
.01638      1348.
.01697      1391.
.01755      1436.
.01814      1478.
.01875      1521.
```

CCP-3
****
CURVE #1   A= 0.261 INCHES
DEFL.   LOAD
(INCH)   (POUNDS)
 .0   0.
 .000555 4980.
 .0011475 9960.
 .001755 15005.
 .002385 20050.
 .0029975 25050.
 .0036325 30050.
 .00429   35050.
 .0049475 40050.
 .00565   45025.
CURVE #2   A= 0.285 INCHES
DEFL.   LOAD
(INCH)   (POUNDS)
 .0   0.
 .0005525 4935.
 .0011625 9960.
 .001755   14935.
 .0023725 19910.
 .0029975 24960.
 .0036425 29965.
 .004305   34970.
 .00494   39975.
 .0056475 44980.
CURVE #3   A= 0.296 INCHES
DEFL.   LOAD
(INCH)   (POUNDS)
 .0   0.
 .000058   4990.
 .0011185 10030.
 .00179   15020.
 .002415   20010.
 .00304   25000.
 .0036665 29990.
 .004325   34980.
 .004985   40020.
 .0056825 45060.
CURVE #4   A= 0.321 INCHES
DEFL.   LOAD
(INCH)   (POUNDS)
 .0   0.
 .00058   5015.
 .0011825 10030.
 .0018075 15045.
 .002425   20010.
 .0030425 24975.
 .0036975 29995.
 .0043525 35015.
 .00502   40035.
 .0057325 45055.

111

```
CURVE #5  A= 0.345 INCHES
DEFL.    LOAD
(INCH)   (POUNDS)
 .0          0.
 .0000595 4995.
 .00121 9990.
 .0018325 15010.
 .002475 20030.
 .0031175 25050.
 .00376 30005.
 .00442 34960.
 .00511 39980.
 .005815 45000.
CURVE #6  A= 0.369 INCHES
DEFL.    LOAD
(INCH)   (POUNDS)
 .0          0.
 .0006 5010.
 .00123 10020.
 .00186 15030.
 .00249 20040.
 .00315 25050.
 .00381 30060.
 .00447 35070.
 .00516 40080.
 .0058875 45090.
CURVE #7  A= 0.395 INCHES
DEFL.    LOAD
(INCH)   (POUNDS)
 .0          0.
 .00006025 4975.
 .00124 10005.
 .00187 14990.
 .00252 19975.
 .00317 24960.
 .003845 29995.
 .0045425 35030.
 .0052175 40000.
 .0059675 44970.
CURVE #8  A= 0.424 INCHES
DEFL.    LOAD
(INCH)   (POUNDS)
 .0          0.
 .00063 5005.
 .00126 10010.
 .0019025 15015.
 .0025625 20020.
 .0032375 25025.
 .0039125 30030.
 .0046075 35035.
 .0053025 40040.
 .00606 45045.
```

```
CURVE #9   A= 0.450 INCHES
DEFL.    LOAD
(INCH)   (POUNDS)
.0           0.
.0006225 5000.
.001245 10000.
.0018975 15000.
.00257 20000.
.003225 25000.
.00391 30000.
.0046225 35000.
.005345 40000.
.0061175 45000.
CURVE #10  A= 0.466 INCHES
DEFL.    LOAD
(INCH)   (POUNDS)
.0           0.
.0006325 5030.
.0012875 10060.
.0019425 15050.
.002615 20040.
.0032875 25030.
.0039775 30020.
.004695 35010.
.0054125 40000.
.0061775 44990.
CURVE #11  A= 0.474 INCHES
DEFL.    LOAD
(INCH)   (POUNDS)
.0           0.
.00061 4995.
.0012725 9990.
.0019225 14985.
.0025925 19980.
.003285 24975.
.003975 30005.
.0046925 35035.
.0054325 40065.
.00619 45005.
CURVE #12  A= 0.493 INCHES
DEFL.    LOAD
(INCH)   (POUNDS)
.0           0.
.000645 5000.
.00129 10000.
.0019675 15000.
.002645 20000.
.00334 25000.
.004035 30000.
.00475 35000.
.005485 40000.
.0062625 45000.
```

113

```
CURVE #13   A= 0.513 INCHES
DEFL.    LOAD
(INCH)   (POUNDS)
.0         0.
.0006475 5030.
.0013225 10060.
.0019975 15090.
.0026825 20045.
.0033675 25035.
.0040825 30025.
.00481  35015.
.005555 40005.
.0063525 44995.
CURVE #14   A= 0.533 INCHES
DEFL.    LOAD
(INCH)   (POUNDS)
.0         0.
.000645 4995.
.0013275 9990.
.00199  14985.
.00269  19980.
.00339  24975.
.004105 29970.
.0048475 34965.
.00562  39960.
.006435 44960.
CURVE #15   A= 0.554 INCHES
0.554
(INCH)   (POUNDS)
.0         0.
.0006425 5055.
.0013125 10020.
.002005  14985.
.0026975 19950.
.0034125 24995.
.00417  30040.
.004915 35020.
.005695 40000.
.0065225 45045.
CURVE #16   A= 0.573 INCHES
DEFL.    LOAD
(INCH)   (POUNDS)
.0         0.
.00068249999999999 4980.
.0013325 9960.
.0020475 15020.
.002745 20000.
.0034675 24980.
.0042125 29960.
.0049575 34940.
.0057525 39950.
.0066175 44980.
```

114

```
CURVE #17  A= 0.596 INCHES
DEFL.    LOAD
(INCH)   (POUNDS)
 .0        0.
 .0006775 5070.
 .0013675 10015.
 .002085 15025.
 .0028025 20035.
 .00354 24995.
 .004285 30010.
 .005065 35025.
 .005875 40040.
 .0067525 45055.
CURVE #18  A= 0.623 INCHES
DEFL.    LOAD
(INCH)   (POUNDS)
 .0        0.
 .0006925 4995.
 .001385 9990.
 .0021225 14985.
 .00286 19980.
 .0035975 24975.
 .00437 29970.
 .00517 34965.
 .00599 39960.
 .0068675 44955.
CURVE #19  A= 0.646 INCHES
DEFL.    LOAD
(INCH)   (POUNDS)
 .0        0.
 .0006925 5025.
 .0014225 10050.
 .0021175 14975.
 .00288 19960.
 .003615 24945.
 .004415 29930.
 .005215 34980.
 .0060525 39970.
 .0069725 44960.
DEFL.    LOAD
```